NACA TN 3264

NATIONAL ADVISORY COMMITTEE FOR AERONAUTICS

TECHNICAL NOTE 3264

STUDY OF THE MOMENTUM DISTRIBUTION OF TURBULENT BOUNDARY LAYERS IN ADVERSE PRESSURE GRADIENTS

By Virgil A. Sandborn and Raymond J. Slogar

Lewis Flight Propulsion Laboratory
Cleveland, Ohio

NACA

Washington
January 1955

NATIONAL ADVISORY COMMITTEE FOR AERONAUTICS

TECHNICAL NOTE 3264

STUDY OF THE MOMENTUM DISTRIBUTION OF TURBULENT BOUNDARY LAYERS IN ADVERSE PRESSURE GRADIENTS

By Virgil A. Sandborn and Raymond J. Slogar

SUMMARY

Evaluation and analysis were made of the mean and turbulent terms of the equations of motion and the stress tensor at four stations in a turbulent boundary layer with a progressively increasing adverse pressure gradient.

Good agreement between the values of skin friction obtained by heat transfer - skin friction instrument measurements and by the evaluation of the Ludwieg-Tillmann empirical equation was found to exist. The evaluation of skin friction from the integrated momentum equation failed to agree with the results of other methods of obtaining skin friction.

Evaluation of the terms of the turbulent stress tensor indicates that the normal stresses $\rho\overline{v^2}$ and $\rho\overline{w^2}$ and the shear stress $-\rho\overline{uv}$ are of comparable magnitude, while the normal stress $\rho\overline{u^2}$ was found to be roughly four times as large near the wall. The angle between the principal axis of the turbulent stress tensor and the boundary appeared to be largely independent of x-distance or pressure gradient.

Evaluation of the x- and y-direction equations of motion shows that the rate of change normal to the wall of the mean square of the y-direction turbulent velocity in the y-direction equation when taken near the wall is as large as or larger than any term in the x-direction equation. The x- and y-momentum equations are, however, still independent.

INTRODUCTION

In recent years progress has been made in the measurement of the statistical properties of specialized turbulent shear flows. For the free turbulent shear flows in the wakes of circular cylinders and in free air jets, Townsend (ref. 1) and Corrsin (ref. 2), respectively, have evaluated from experiments the important statistical terms. The

most accurate investigations have been made in free turbulent shear flows, since the absence of solid boundaries greatly facilitates measurements. In fully developed turbulent flow in pipes and channels, which is the other extreme, Laufer (refs. 3 and 4) has presented extensive measurements. Laufer's results brought to light significant features of flows with solid boundaries; it was found that flow conditions in the close proximity of the wall were of major importance. For turbulent boundary layer flows, which represent an intermediate type of flow between fully free turbulent and channel flow, measurements are meager. The very recent work of Townsend (ref. 5) and Klebanoff at the National Bureau of Standards has made inroads into the understanding of the characteristics and structure of turbulent boundary layers with zero pressure gradient, with both investigators directing their attention toward the turbulent energy balance. The exacting investigations of Askenas, Riddell, and Rott at Cornell University in a zero pressure gradient boundary layer were unable to eliminate the apparent inconsistencies in the measured shear distributions. (The shear stress curves possessed a maximum away from the wall.) Preliminary experimental measurements with hot-wire equipment by Schubauer and Klebanoff (ref. 6) in boundary layers with adverse pressure gradients also resulted in inconsistencies in the shear distribution. (The shear stress curves indicated too high a value of skin friction.) Other experimenters have also been confronted with inconsistent wall shear stress evaluations.

The NACA Lewis laboratory is employing a 6- by 60-inch boundary layer channel in a long-range program to provide an insight into the phenomenon of turbulent boundary layer separation. The method of attack is to evaluate all mean and fluctuating quantities of interest (a) far upstream in the unseparated turbulent boundary layer, and (b) within the region of separation. A comparison of the two sets of data should then greatly assist in the study of the manner in which the boundary layer separates.

This report constitutes the first phase of part (a), in which all terms pertaining to momentum have been evaluated, such as the mean and turbulent shear stress and stress tensor, along with the time-averaged equations of motion. These terms are evaluated and analyzed for a flow with progressively increasing pressure gradient. Special effort was made to present a consistent set of measurements; however, wherever conflicting results were encountered, two or more independent sets of data are shown.

THEORETICAL BACKGROUND

Following the assumptions of Reynolds, the time-averaged Navier-Stokes equations of motion for an incompressible turbulent fluid motion may be written

$$\rho \frac{DU_i}{Dt} = \frac{\partial}{\partial x_j}\left(\mu \frac{\partial U_i}{\partial x_j} - \rho\overline{u_i u_j} - \delta_{ij}p\right) \tag{1}$$

where

$$(i,j = 1,2,3)$$

$$\delta_{ij} = 1 \quad \text{for} \quad i = j$$

$$\delta_{ij} = 0 \quad \text{for} \quad i \neq j$$

and

$$\frac{DU_i}{Dt} = \frac{\partial U_i}{\partial t} + U_j \frac{\partial U_i}{\partial x_j}$$

(A list of symbols will be found in appendix A.) The two basic groups of terms appearing in equation (1) are the inertia terms, which are those on the left side, and the stress terms, which appear in the parentheses on the right side.

For the particular boundary layer flow studied in this report, equation (1) may be simplified by assuming that the mean motion of the flow is two-dimensional; thus all gradients in the z-direction are zero. Although the turbulent motions are of a three-dimensional nature, both they and the mean flow are assumed symmetric relative to the xy-plane. From this condition of plane-symmetry, it follows that a reflection of the z-axis will require that $\overline{uw}$ and $\overline{vw}$ equal their respective negatives, which implies that both must vanish. This argument for the vanishing of $\overline{uw}$ and $\overline{vw}$ is patterned after the argument employed in isotropic turbulence, where the turbulence is spherically symmetric (ref. 7). Consequently, for the flow investigated, the steady-state equations of motion may be simplified to, for the x-direction,

$$U \frac{\partial U}{\partial x} + V \frac{\partial U}{\partial y} + \frac{\partial \overline{u^2}}{\partial x} + \frac{\partial \overline{uv}}{\partial y} = -\frac{1}{\rho}\frac{\partial p}{\partial x} + \nu\left(\frac{\partial^2 U}{\partial x^2} + \frac{\partial^2 U}{\partial y^2}\right) \tag{2}$$

and for the y-direction,

$$U \frac{\partial V}{\partial x} + V \frac{\partial V}{\partial y} + \frac{\partial \overline{v^2}}{\partial y} + \frac{\partial \overline{uv}}{\partial x} = -\frac{1}{\rho}\frac{\partial p}{\partial y} + \nu\left(\frac{\partial^2 V}{\partial x^2} + \frac{\partial^2 V}{\partial y^2}\right) \tag{3}$$

Previous measurements (ref. 6) of the terms in equations (2) and (3) have not been sufficiently accurate to discuss the equations adequately, but it is generally believed that certain of the terms may be neglected, thus further simplifying the equations.

The stress terms for plane-symmetry turbulent shear flow may be arranged as a symmetrical stress tensor.

$$\underset{\sim}{T} = \begin{Vmatrix} \tau_{xx} & \tau_{xy} & 0 \\ \tau_{xy} & \tau_{yy} & 0 \\ 0 & 0 & \tau_{zz} \end{Vmatrix} \tag{4}$$

where

$$\begin{aligned} \tau_{xx} &= -p + 2\mu \frac{\partial U}{\partial x} - \rho\overline{u^2} \\ \tau_{yy} &= -p + 2\mu \frac{\partial V}{\partial y} - \rho\overline{v^2} \\ \tau_{zz} &= -p - \rho\overline{w^2} \\ \tau_{xy} &= \mu\left(\frac{\partial U}{\partial y} + \frac{\partial V}{\partial x}\right) - \rho\overline{uv} \end{aligned} \tag{4b}$$

These terms are the flux of momentum in the flow and their derivatives yield the forces acting within the boundary layer. It will be convenient to further subdivide the stress tensor into two additive tensors, one composed of the stresses associated with viscosity and pressure and the other containing the turbulent contributions.

The specific object of this report was the experimental evaluation of the stress terms, the equations of motion, and other terms that are known to be important for the understanding of turbulent boundary layer flow.

TEST PROCEDURE AND RESULTS

Tunnel and test conditions. - The measurements reported herein were made in the turbulent boundary layer along the test wall of the Lewis 6- by 60-inch boundary layer channel. A schematic diagram of the tunnel is shown in figure 1, and a complete description of the channel, except for a modified inlet, appears in reference 8. All measurements were

taken with a constant Reynolds number per foot of 3.33×10^5, which corresponded to a free-stream velocity of approximately 58 feet per second, maintained at the entrance of the test section. The suction across the porous wall was sufficient to keep the boundary layer along the porous wall at a constant thickness (the same as reported in ref. 8 for the 25 in. water pressure drop case).

The four stations at which the momentum surveys were taken are shown in figure 1. They are approximately 18 inches apart, with the first located 72 inches from the inlet contraction. The boundary layer was approximately 1 inch thick at station 1 and increased to 3 inches at station 4.

Pressure measurements. - The static-pressure distribution along the test wall was obtained from wall static orifices (0.025-in.-diam.) located on lines 12 inches above and below the center line, as noted in figure 2. The actual pressures were recorded with a water micromanometer with a least count of 0.001 inch of water. The manometer was referenced to atmospheric pressure.

Mean velocity profiles were evaluated from measurements with the total-pressure probe shown in figure 3. The static pressure was obtained from wall orifices. The probe tip was of 0.040-inch-outside-diameter tubing with 0.004-inch-thick walls. The end was flattened to give a rectangular opening with an over-all height of 0.020 inch, thus allowing the center of the probe opening to be brought within 0.010 inch of the wall. The pressures were recorded using a ± 0.15 psi and a ± 0.05 psi full range strain-gage-type pressure transducer. The transducers are of the differential-pressure type consisting of a bellows and an unbonded strain gage. The output of the transducers was recorded on a 2 millivolt full-scale recording potentiometer, so that under steady conditions it was possible to detect pressure differences of the order of 0.01 and 0.004 pound per square foot, respectively, for the two instruments. The voltage balance and calibration circuits used to operate the transducers are shown in figure 4.

For each profile the probe was zeroed at the wall by an electrical contact and then actuated outward through the boundary layer with an actuator which could be set at any distance in the boundary layer with an error no greater than ± 0.001 inch.

It is of interest to point out a physical phenomenon which has been encountered in all turbulent boundary layer measurements made with both pressure transducers and manometers. Figure 5 shows inserts of the output signal of a pressure transducer connected to the total-pressure probe at different y-distances within the boundary layer of station 1. These records show large-amplitude fluctuations occurring near the bend

in the velocity profile, with greatly damped signals being noted near the wall. This fluctuation record should not be interpreted quantitatively, since the output of the system will be influenced by the natural frequency (250 cps) of the pressure transducer and by the frequency responce of the recording instruments, but it does give a qualitative idea of the behavior to be expected when total-pressure measurements of this type are made. The fluctuating signal was shunted out through a capacitance in order that mean pressure could be recorded. It was noted that the indicated mean pressures were higher than the approximate mean of the fluctuating signal.

The calculated mean velocity profiles are shown in figure 6. In all cases except the last station (station 4), the recording equipment could be sufficiently damped to obtain uniform velocity profiles. For station 4 it was necessary to obtain the points near the wall as the average of several points taken at different times for each y-distance because of the large fluctuations. Hot-wire velocity measurements were also included in the averaging of the points near the wall for station 4.

The mean velocity evaluated from hot-wire measurements has also been included in figure 6(b). Although the hot wires employed for fluctuation measurements are rather poor for mean velocity measurements because of calibration shifts caused by dust particles striking the wires, the selected results presented in figure 6(b) are in good agreement.

The correction suggested in reference 9 for the effect of turbulence on the total-pressure measurements has been evaluated and the corrected mean velocities at a few points are included in figure 6. The effect due to turbulence results in a maximum error for the mean velocity of roughly 2 percent which is for the region near the wall. The correction for the displacement of the effective center of the probe opening due to the velocity gradient across the mouth of the probe (ref. 10) was also included in the corrected points.

Flow deflection measurement. - The flow deflection angle measuring device is shown in figure 7. The instrument employs the standard two total-pressure tubes, each making an angle of 45° with the mean flow. It is a null-balance system, with a special actuation mechanism being employed to rotate the probes in the boundary layer. The accuracy of measuring the flow deflection was of the order of $\pm 0.1^{\circ}$. The angles measured between the mean flow and the test wall are shown in figure 8. The first station proved to have too small a variation in deflection angle in the boundary layer; thus no measurements could be obtained.

Heat transfer - skin friction measurements. - The technique of determining the local turbulent skin friction from a measure of the local heat transferred from a small locally heated insulated segment of the wall was developed in reference 11. For the present report a calibrated relation between the skin friction and the heat transfer was obtained in a fully developed turbulent channel flow, where the skin friction could be independently determined from the pressure gradient. A description of the instruments employed and the calibration technique used is given in reference 8.

Preliminary measurements (ref. 8) with the heat transfer - skin friction instruments gave only qualitative agreement with the Ludwieg-Tillmann predictions. However, it was found in the present work that the agreement was improved by taking several measures of the heat transfer at a station and averaging the results to minimize random errors inherent in the measure of such low voltages. The local measurements of skin friction obtained with the heat transfer - skin friction instrument are shown in figure 9.

The simplicity of operation of these heat transfer - skin friction instruments makes them a very practical tool for the type of boundary layer studies now under way.

Hot-wire anemometry measurements. - The hot-wire anemometer system employed for the measurement of turbulent fluctuations was the constant-temperature system described in detail in reference 12, with minor changes made to reduce as much as possible the noise level of the modified system so that it now compares favorably with the conventional constant-current systems. The constant-temperature system reduced the time required to record data to less than half that for constant-current systems, and direct comparisons show that the two systems give equally accurate measurements of the turbulence for the levels encountered.

A detailed description of the system and the theory of measurement of fluctuating velocities by constant-temperature hot-wire anemometer systems is presented in appendixes B and C.

The four particular types of hot-wire probes used for the measurements are shown in figure 3. The wires used were 0.0002-inch-diameter etched tungsten (shown as sample B, fig. 18, ref. 12). The wires were mounted by copper plating the ends, so that it is possible to soft-solder the wires to the probe prongs (see ref. 13). All wires had a 0.040-inch unplated center section, with the probe prongs being 0.050 inch apart. The x-probes have their wires mounted in parallel planes 0.010 inch apart, since this appeared to be the minimum distance for which practical mounting could be accomplished. The wire angles (45° and 30° with the direction of flow) were maintained within approximately $\pm 1^\circ$ with the use of a toolmaker's microscope.

In the operation of x-probes no attempts were made to match hot wires or in any way to rotate the probes to match wire sensitivities, as there is some question as to the accuracy of using such methods in simplifying data recording. All measurements with x-probes presented herein were made up of two or more independent readings of hot-wire outputs.

The y-distance for the hot-wire probes was determined in the same manner as that described for the total-pressure probe, with extreme caution being used to prevent more than a light contact with the wall. The construction of the probe limits the nearness to the wall for which intensities may be measured to the following approximate values: $\overline{u^2}$, 0.001 inch, $\overline{w^2}$, 0.010 inch, and $\overline{v^2}$, 0.025 inch. Also, the values of $\overline{w^2}$ near the wall are questionable, as the two x-wires are in planes 0.010 inch apart; however, measurements of $\overline{u^2}$ with the $\overline{w^2}$ probes close to the wall check favorably with those obtained with a single-wire probe, so that the error is believed small.

The turbulent intensity measurements for the four stations are presented in figures 10 to 12. All measurements were reduced to the statistical velocity fluctuations by using equations (B5), (C11), and (C12) in appendixes B and C. Stations 1 and 2 show little random variation in measurements of $\sqrt{\overline{u^2}}$, while stations 3 and 4 indicate some random scatter; therefore, check measurements are included for stations 3 and 4 (figs. 10(c) and (d)). A check of the consistency of the fluctuation measurements is included in figure 10(a), where the measurement of $\sqrt{\overline{u^2}}$ obtained by three independent hot-wire-probe types is shown. In all measurements of $\sqrt{\overline{v^2}}$ and $\sqrt{\overline{w^2}}$ presented, the maximum allowable random error in the calculated values of $\sqrt{\overline{u^2}}$ from the x-wires was required to be less than 10 percent; any profiles indicating greater disagreement were not included in the report.

The $\sqrt{\overline{u^2}}$ measurements at station 3 are somewhat questionable, since considerable difficulty was encountered in obtaining consistent measurements. A systematic disagreement was noted in the $\sqrt{\overline{u^2}}$ profiles from day to day, with checks indicating that two distinctly different types of $\sqrt{\overline{u^2}}$ profiles were equally likely. This duality of profiles will be discussed more fully in the section "Summary of velocity measurements."

The turbulent shear stress values obtained with a 45° x-probe are presented in figure 13. The measurements were reduced to stress values

by using equation (C6) in appendix C. In the course of these measurements it proved difficult to obtain consistent values of $\overline{uv}$ without a great deal of scatter, since the evaluation of $\overline{uv}$ requires working with the squares of the physical measurements of the hot-wire outputs, thus magnifying any error which might have been present in the actual measurements. Figure 14 shows a set of points of the squared output of each wire of a uv probe; the faired curves from plots similar to this were used to obtain the faired curves shown in figure 13. The data points in figure 13 correspond to the direct measured difference between the hot wires and exhibit random errors as great as 30 or 40 percent.

A consideration of the errors entering the measurement and calculation of the turbulent velocity fluctuations along with the cross checks made on the data indicates the maximum error for the measurements presented (other than $\overline{uv}$) is of the order of 10 percent.

DISCUSSION OF RESULTS

In order to obtain a picture of the momentum distribution through turbulent boundary layers, the terms of the modified Navier-Stokes equation for turbulent flow and of the turbulent stress tensor will be evaluated. However, to define the turbulent boundary layer flow investigated, terms not necessarily associated directly with momentum, such as the mean flow parameters, the turbulent velocities, and the wall shearing stress, must also be evaluated and discussed.

Mean flow parameters. - The mean flow parameters δ^*, θ, Re_θ, and H evaluated from the faired mean velocity profiles are presented in figures 15 and 16. Also included in the figures are points obtained when corrections for turbulence (ref. 9) and probe displacement (ref. 10) were applied to the data. The corrected values of θ also include momentum contributions due to the turbulent motion as derived in reference 14. Actually, the largest corrections to θ were due to probe corrections and only secondary corrections were realized from the turbulence. In all, it appears that no great error is incurred in θ by neglecting all corrections. The displacement thickness δ^* shows a slightly greater effect due to probe corrections, with a similar effect on the profile form parameter H.

Summary of velocity measurements. - Faired curves of the mean and turbulent velocities are shown in figure 17. The $\sqrt{\overline{v^2}}$ and $\sqrt{\overline{w^2}}$ components of velocity were found to be very nearly equal over most of the boundary layer. The difference exceeds the probable error of measurement only near the boundary. Except near the wall, $\sqrt{\overline{v^2}}$ and $\sqrt{\overline{w^2}}$ are seen to be roughly one-half $\sqrt{\overline{u^2}}$.

Some interesting points are noted in comparing the shapes of the turbulent velocity profiles. The boundary conditions imposed on $\sqrt{\overline{v^2}}$ by the wall affect the distribution of v a relatively long distance out into the boundary layer, since the $\sqrt{\overline{v^2}}$ curves begin to decrease before the rate of energy converted to turbulence from the mean flow has reached a maximum, as will be shown later (fig. 29). This decrease in the $\sqrt{\overline{v^2}}$ curve appears to affect the $\sqrt{\overline{u^2}}$ and $\sqrt{\overline{w^2}}$ curves in that inflection points in both curves appear to occur at about the same point. It is believed that the conditions imposed on $\sqrt{\overline{v^2}}$ by the wall may not require the fluctuating energy to be dissipated directly, but may rather result in a reorientation of $\sqrt{\overline{v^2}}$ energy in the other two directions. This concept of the shifting of the $\sqrt{\overline{v^2}}$ energy to the $\sqrt{\overline{u^2}}$ and $\sqrt{\overline{w^2}}$ components can be interpreted crudely as requiring that the axis of rotation of the turbulent eddies be turned more toward the perpendicular to the wall, as might be expected from the model proposed in reference 15. From this concept it appears that near the wall $\sqrt{\overline{v^2}}$, of the three turbulent components, is most directly related to the boundary conditions of the flow, with $\sqrt{\overline{u^2}}$ and $\sqrt{\overline{w^2}}$ in turn depending on $\sqrt{\overline{v^2}}$.

The variation of the $\sqrt{\overline{u^2}}$ profile with boundary layer development and pressure gradient also appears of interest. The general shapes of the $\sqrt{\overline{u^2}}$ curves for the first two stations (figs. 17(a) and (b)) are very similar to those observed by Laufer in a fully developed turbulent channel flow (ref. 3). The last station (fig. 17(d)), however, shows a decided change in the shape of the curve, with a corresponding change in the $\sqrt{\overline{w^2}}$ curve. In figure 17(c), the two possible $\sqrt{\overline{u^2}}$ profiles observed at station 3 for different runs are again shown. Of the two profiles, the solid line profile (1) agrees in form with profiles of the first two stations and the remaining profile agrees in form with that of the last station.

A comparison of the mean velocity profiles shows much the same result as the $\sqrt{\overline{u^2}}$ profiles, in that the first three stations show a rather universally developing profile and the last station shows the development toward an inflection in the profile. While the actual physical change in velocity profiles between stations 1 and 3 is slight, there is a great deal of change between the profiles at stations 3 and 4.

The previous observations can now be employed to attempt an explanation of the duality of measurements observed for station 3. In general, the observations of $\sqrt{\overline{u^2}}$ at station 3 fall into two distinct groups; one set agrees qualitatively with the profiles for the first two stations, and the second agrees with the observations for the last station. It therefore appears that the flow conditions were not completely reproduced from day to day, although no unexplained inconsistencies were noted for the other three stations. The fluctuation in setting up flow conditions could not have been large, as inlet conditions were nearly the same from day to day, with corrections being made for changes in atmospheric pressure and temperature (analysis shows the free-stream velocity was changed by a maximum of 0.7 percent as inlet conditions were varied from day to day). This has led to the conclusion that the change of velocity distribution to a profile as observed at station 4 must occur over a very short distance and is quite sensitive to flow conditions. The impression is that the profile changes abruptly from one type of distribution to another. Reference 16 contains some interesting information on equilibrium profiles in turbulent boundary layers, which appears to indicate similar results.

Evaluation of wall shearing stress. - Several methods are now available for the evaluation of the wall shearing stress; hence it was desirable to study the methods and attempt to place the necessary limitations on each. Figure 9 is a summary of the results of the several methods employed. The empirical equation of Ludwieg and Tillmann (ref. 17)

$$C_f = 0.246 \times 10^{-0.678H} R_\theta^{-0.268} \tag{5}$$

and the empirical flat-plate equation of Falkner (ref. 18)

$$C_f = \frac{0.01306}{(Re_\theta)^{1/6}} \tag{6}$$

are compared with the values obtained from the heat-transfer measurements. As was found in the previous work (ref. 8), the heat-transfer measurements and the Ludwieg-Tillmann relation are in good agreement. Secondly, the Falkner equation gives very good agreement for the first two stations and an error of less than 15 percent for station 3. The agreement of Falkner's equation for the first two stations might have been expected, since figure 16 shows H to have remained nearly constant, while the last two stations show rather marked increases in H.

The evaluation of skin friction by use of the von Kármán integral momentum relation is also included in figure 9. The suggestions of each of references 14, 19, and 20 were considered in the evaluation of skin friction for the flows investigated in this report. Unfortunately, these

suggestions give negligible contributions over the values obtained when all turbulence contributions are neglected. The resulting values of C_f obtained using the form suggested for θ_t in reference 14 and using the wall pressure as suggested in reference 19 are shown in figure 9.

It is evident that the suggested corrections have not been sufficient to allow the integrated momentum relation to predict skin friction in pressure gradients, and it appears necessary to look elsewhere for the answer. Another possibility that has been suggested is the lack of two-dimensionality of the mean flow. One of the chief aims in selecting the dimensions of the 6- by 60-inch channel was to eliminate any end effects on the flow along the center. Velocity profile and static pressure surveys show no marked variation in the center region, so that the flow was assumed to be two-dimensional in nature. However, the work of Clauser (ref. 16) in a tunnel at The Johns Hopkins University, which produces flow similar to that of the 6- by 60-inch channel, gave a strong indication of lateral spreading of the flow which resulted in an additional loss of momentum not included in the two-dimensional momentum equation.

It thus appears that for adverse pressure gradients the two-dimensional integral momentum relation is not adequate for evaluating skin friction. Moreover, most practical applications will involve even further deviation from two-dimensionality than those existing in the wind tunnel.

The large discrepancies shown in figure 9 may also be due to the fact that the evaluation of skin friction from the momentum equation involves obtaining small differences of large quantities that are derivatives of experimental curves.

Although lateral flow can cause large errors in skin friction calculated from the integral momentum equation, this flow is still so small that the actual skin friction and other physical features of the basic flow are not appreciably affected.

Shear stress distribution across boundary layer. - To obtain the total stress distribution across the boundary layer it is necessary to combine the turbulent and viscous contributions. Figure 18 shows the contribution of each of the shear stresses near the wall. Outside the region plotted, the viscous contribution will be negligible.

Although it was impossible to measure the turbulent stresses closer than 0.025 inch from the wall, the trends indicate reasonable agreement with the Ludwieg-Tillmann values. Some indication of the distribution near the wall might be found, as suggested in reference 6, by evaluating the streamwise momentum equation at the wall. This yields the initial slope of the total shear curve as

$$\frac{\partial \tau}{\partial y} = \frac{\partial p}{\partial x} \qquad (7)$$

A line of this slope is included in figure 18 at the wall value predicted by the Ludwieg-Tillmann equation.

There is also a limited amount of information available from figure 18 regarding actual shear and velocity distributions very close to the wall. The laminar sublayer has been assumed to be characterized by a linear velocity profile and vanishing turbulent shear stress for some small but finite distance out from the wall. Although actual data points do not extend deep into the sublayer, the trends indicated by the $\mu \frac{\partial U}{\partial y}$ curves (fig. 18) suggest a parabolic rather than a linear velocity distribution (i.e., $\frac{\partial^2 U}{\partial y^2}$ constant). Equation (2) evaluated at the wall

$$- \rho \frac{\partial \overline{uv}}{\partial y} + \mu \frac{\partial^2 U}{\partial y^2} = \frac{\partial \tau}{\partial y} = \frac{\partial p}{\partial x} \tag{8}$$

indicates that the assumption of a laminar sublayer with the conditions of a linear velocity profile could be consistent with the equation of motion only for a zero pressure gradient. The assumption often made that turbulent shear stress becomes unimportant for values of yU_τ/ν less than about 30 also appears inconsistent with the curves of figure 18, since the viscous shear stress terms indicate they reach the total shear stress value only very near the wall. It is noted that in the region next to the wall the total shear (viscous plus turbulent) changes very little compared with the large changes in the separate viscous and turbulent shear stress curves. It might be more useful, therefore, to speak of a sublayer in which $\frac{\partial \tau}{\partial y} = \frac{\partial p_w}{\partial x}$ rather than of a "laminar" sublayer with linear velocity profile and zero turbulent shear stress.

Attempts to predict the shear distribution through the turbulent boundary layer have been largely empirical in nature. Reference 21 tries to reduce the prediction of shear distribution to a power series representation, but can obtain at most only a finite number of terms, since the evaluation depends entirely on limited boundary conditions. Reference 22 resorts to the boundary conditions and the equations of motion for a fully developed turbulent channel flow to predict a special power series for the velocity profile (which in turn is used to evaluate the shear profile). The power series of reference 22 results in good agreement for the special one-dimensional flow investigated. Both methods must be classified as empirical, although reference 22 does rely on the equation of motion to give the final form of the shear distribution.

A third method for predicting the shear distribution near the wall from mean velocity measurements is presented in reference 23. Although

this method must be limited to the vicinity of the wall, it appears to be of a general form applicable to any type of turbulent boundary layer flow.

Starting with the assumption that the mean velocity profile near the wall can be represented by the universal profile predicted from similarity relations

$$\frac{U}{U_\tau} = f\left(\frac{yU_\tau}{\nu}\right) \tag{9}$$

which has been verified by many investigators in the past and is again verified in this report (fig. 19), the equations of motion and continuity are integrated.

Equation (9) is used in the continuity equation and the boundary condition $V = 0$ at $y = 0$ is applied in reference 23 to obtain the following relation for V:

$$\frac{V}{U_\tau} = -\frac{\mu}{\tau_W}\frac{dU_\tau}{dx}\frac{yU_\tau}{\nu}\frac{U}{U_\tau} \tag{10}$$

The momentum equation was integrated, using equation (9), which with the boundary condition $\tau = \tau_W$ at $y = 0$ gives an expression for the shear distribution

$$\frac{\tau}{\tau_W} = 1 + \frac{y}{\tau_W}\frac{dp}{dx} + \frac{\mu}{\tau_W}\frac{dU_\tau}{dx}\int_0^{\frac{yU_\tau}{\nu}}\left(\frac{U}{U_\tau}\right)^2 d\frac{yU_\tau}{\nu} \tag{11}$$

where dp/dx has been assumed independent of y. These equations for τ and V depend only on the assumption of the existence of a relation as expressed by equation (9), with no specific relation required between U/U_τ and yU_τ/ν.

Comparisons of the total shear stress as calculated from equation (11) with the measured distribution are included in figure 18, where the Ludwieg-Tillmann values of wall shear stress were used. The experimental total shear stress curves are within 10 percent (except at station 3) of those predicted by equation (11), but at some stations the trends with y differ as the wall is approached.

Figure 20 shows the total shear stress distribution for each station. Such distributions are needed for accurate calculations of turbulent boundary layer development, where the integral relations of the equations of motion are employed (ref. 24). In the absence of such

distributions, Granville (ref. 25) developed an expression for the integrated shear distribution through the boundary layer (this being the specific information needed to evaluate the relations of ref. 24) for a zero pressure gradient flow ψ_0. Evaluation of the shear distributions for adverse pressure gradients given in reference 6 led Granville to conclude that the effect of pressure gradient was negligible, namely $\psi = \psi_0$.

Comparison of the values of ψ, evaluated from the total stress curves of figure 20, with the equation and the measurements of reference 6 given by Granville, is shown in figure 21. A systematic variation in the measured shear integrals of this report with the zero pressure gradient values of ψ_0 is seen. However, the value at station 1, which is in a region of nearly zero pressure gradient, appears to agree well with the predictions. The variation indicates a definite effect of pressure gradient on ψ, which disagrees with the conclusion of Granville. It was noted, however, that the variation obtained herein was of no greater magnitude than the scatter appearing in the values of ψ evaluated by Granville from reference 6.

Evaluation of mean V velocity. - Evaluation of the momentum terms in the boundary layer requires knowledge of the distribution of the component V (normal to the wall) of the mean velocity. The V component is usually very small in the boundary layer, but it will appear in the momentum equation either as a derivative across the boundary layer or multiplied by some large quantity. Unlike the U component, the V component is not constant outside the boundary layer in a region of adverse pressure gradient. This result follows from the continuity equation together with the boundary condition $V = 0$ at $y = 0$, which leads to

$$V = \int_0^y - \frac{\partial U}{\partial x} \, dy \tag{12}$$

The two-dimensional continuity equation in the form of equation (12) was used to determine the values of V through the boundary layer. This form implies two-dimensional flow and thus neglects any lateral flow of the type suggested in reference 16. The mean V distributions obtained are shown as the solid curves in figure 22.

A second method of evaluating the V velocities was from the flow deflection angles. The values of V calculated from the angles are included as the symbols in figure 22. Unfortunately, the two methods of evaluating V do not give comparable results except near the wall. Because of the small magnitude involved in the determination of V, either method may be subject to considerable inaccuracy; therefore it

was impossible to conclude which values best represent the actual quantities. The values of V obtained from the continuity equation were employed for the analysis in the following sections, since a complete set of measurements of the flow deflection angles was not obtained.

Equation (10) may also be used to evaluate the mean V component near the wall. The three methods have been compared in this region in figure 23, where the universal velocity profile was found to be valid.

Stress tensor. - As noted in the section THEORETICAL BACKGROUND, one of the basic groups of terms encountered in a momentum study of viscous shear flows is the stresses. These terms form the components of a stress tensor (eq. (4)), which is composed of two additive tensors - pressure-viscous and turbulent terms. The terms of the turbulent stress tensor are of chief interest, since only limited information is available on their distributions through the shear regions.

The terms of the turbulent stress tensor for the flow investigated can be written

$$\underset{\approx}{T_T} = \rho \begin{Vmatrix} \overline{u^2} & \overline{uv} & 0 \\ \overline{uv} & \overline{v^2} & 0 \\ 0 & 0 & \overline{w^2} \end{Vmatrix} \tag{13}$$

The measured values are plotted in figure 24. It may be seen that here again the normal stress $\rho\overline{u^2}$ is by far the largest term and also that the other three terms are of equal magnitude, except near the wall. As the pressure gradient increases, $\rho\overline{v^2}$ and $-\rho\overline{uv}$ approach the same value throughout the boundary layer. This equality of $-\rho\overline{uv}$ and $\rho\overline{v^2}$ was one of the basic ideas underlying Prandtl's hypothesis of the mixing length theory (ref. 26)

$$\overline{uv} = -\ell^2\left(\frac{dU}{dy}\right)\left|\frac{dU}{dy}\right| \tag{14}$$

Although the mixing length theory is now generally considered to be inadequately founded, the assumption $\overline{uv} = \overline{v^2}$ is nearly correct.

Also included in figure 24 are the stress terms due to the mean flow. Of these mean terms, it was found that the pressure contribution p/τ_w (see legend of fig. 24) to the normal stresses is by far the largest, but this pressure contribution represents only the potential level of the system and, as concerns the actual forces, only the derivatives of the stress are of importance.

A second factor of interest in regard to the stress tensor is the direction along which the maximum stress acts. For the turbulent stress tensor the angle β between the principal axis and the x-direction is given by the equation (ref. 27)

$$\tan 2\beta = \frac{2\overline{uv}}{\overline{u^2} - \overline{v^2}} \tag{15}$$

The values calculated for β are shown in figure 25. Only the points near the wall can be evaluated accurately because equation (15) is extremely sensitive to the measured values in the outer edge of the boundary layer, since $\overline{u^2} \rightarrow \overline{v^2}$ and $\overline{uv} \rightarrow 0$. Disregarding the points for $y > 1$ inch (and excluding station 3), β was nearly constant for the different x-stations. As the wall was approached the angle decreased, so that the direction of principal stress was alined nearly parallel to the flow and the wall.

Evaluation of terms appearing in equations of motion. - Information is now available from the present measurements to evaluate the terms appearing in the x- and y-direction equations of motion, equations (2) and (3).

The terms of equations (2) and (3) have been evaluated from the faired data of this report and are shown in figure 26, where the individual terms are multiplied by θ/U_1^2 to give dimensionless values of rate of change of momentum. The term $\nu \frac{\partial^2 U}{\partial x^2}$ was found in all cases to be of the order of 1/1000 of $\nu \frac{\partial^2 U}{\partial y^2}$ and therefore was not included in the figures. Several theoretical investigators (refs. 14, 19, and 20) have speculated that $\frac{\partial \overline{u^2}}{\partial x}$ should be included in the equation, as it represents a contribution to the integral momentum equation; however, for the flows investigated, this term was found to be too small compared with the other terms of equation (2) to be plotted.

Curves of the experimental difference between the left and right sides of equation (2) are also included in figure 26. This difference, which should be zero, is attributed largely to uncertainty in the term $U \frac{\partial U}{\partial x}$, which was quite sensitive to curve fairing. Only the balance at station 3 appears to show a large discrepancy, larger than the experimental error in $U \frac{\partial U}{\partial x}$. This discrepancy is thought to be due to the possible existence of two types of equilibrium profile during the measurements of shearing stress and mean velocity.

The results of the evaluation of the terms of equation (3) appeared at first to be rather unexpected. The usual assumption made in boundary layer studies is that this equation may be neglected completely, and so it might be, except for the turbulent transfer velocity $\overline{v^2}$. All the mean flow terms of equation (3) are small and might well be neglected, but the term $\frac{\partial \overline{v^2}}{\partial y}$ was found to be as large, if not larger, than any of the terms appearing in the x-direction equation of motion. At first there appeared to be a discrepancy in the terms evaluated for equation (3), as no other term appeared capable of canceling the large $\frac{\partial \overline{v^2}}{\partial y}$ term. A re-examination revealed that a small uncertainty in the measured values of static pressure would result in a relatively large value of $\frac{1}{\rho}\frac{\partial p}{\partial y}$. If now it is assumed that the only terms of appreciable magnitude in equation (3) are $\frac{\partial \overline{v^2}}{\partial y}$ and $\frac{1}{\rho}\frac{\partial p}{\partial y}$, equation (3) may be integrated to give

$$\rho\overline{v^2} = p_w - p \tag{16}$$

since $\rho\overline{v^2} = 0$ and $p = p_w$ at $y = 0$.

The magnitude of change in static pressure can be estimated from equation (16). A check of the data shows the maximum value of $\rho\overline{v^2}$ measured was approximately 0.008 pound per square foot (fig. 11), which results in an absolute static-pressure variation of roughly 0.0004 percent. During the course of measurements, some static-pressure surveys were made, with indications being that any variation in static pressure was of the same order of magnitude as the uncertainty in the measurement. The variation in static pressure as given by equation (16) was found to fall within the region of uncertainty of the measurements.

For fully developed incompressible turbulent channel flow the y-momentum equation (3) is known to reduce exactly to equation (16) (ref. 22), and for the present case of turbulent boundary layer flow, the same reduction appears to be a good approximation. This last conclusion is also reached in reference 28. Comparison of the x-derivative of equation (16) with equation (2) shows that any coupling between the two equations must reside in the value of $\frac{\partial \overline{v^2}}{\partial x}$; experimentally, this coupling was found to be negligible $\left(\frac{\partial \overline{v^2}}{\partial x} \ll \frac{1}{\rho}\frac{\partial p}{\partial x}\right)$. Thus, the x- and y-momentum equations (2) and (3) are concluded to be independent for the flow investigated despite the presence of comparably large terms in both.

Evaluation of energy terms available from measurements. - The analysis of this report has been directed primarily toward the evaluation of the terms important in the study of the momentum distribution of the flow; however, a brief analysis of the distribution of the kinetic energy of the turbulent motion has been made.

The distributions of the local turbulent kinetic energy per unit mass

$$E_{local} = \frac{\overline{u^2} + \overline{v^2} + \overline{w^2}}{2} \tag{17}$$

are presented in figure 27. Of more interest is the average energy contained in the turbulent motion, which is written nondimensionally as

$$E_{total} = \frac{1}{\delta^* U_1^2} \int_0^{\delta} E_{local}\, dy \tag{18}$$

The resulting values of E_{total} are shown plotted in figure 28. Starting with the turbulent energy equation (first moment of the momentum equation), the author of reference 29 was able to arrive at an integral equation from which the value of E_{total} might be estimated. The analysis of reference 29 was made for fully developed flow in pipes and channels, with the resulting evaluation giving the equation

$$E_{total} \propto Re^{-3/8}\left(Re^{-1/8} - 2.0\right) \tag{19}$$

which gave reasonable correlation with the fully developed channel flow of reference 3. Equation (19) was fitted at the first x-station and the resulting curve is included in figure 28. Thus it would appear that the predictions of reference 29 developed for the one-dimensional fully developed turbulent flows are not incompatible with the turbulent energy in the boundary layer flows with arbitrary pressure gradients investigated.

The rate of removal of kinetic energy per unit volume from the mean flow by the turbulent stresses is (ref. 6)

$$\rho\left[\overline{u^2}\frac{dU}{dx} + \overline{v^2}\frac{\partial V}{\partial y} + \overline{uv}\left(\frac{\partial V}{\partial x} + \frac{\partial U}{\partial y}\right)\right]$$

The distribution of this term through the boundary layers investigated is presented in figure 29. This energy derived from the mean flow goes directly into the production of turbulent motion. The term $\overline{uv}\frac{\partial U}{\partial y}$, which is equivalent to $\tau\frac{\partial U}{\partial y}$, was by far the largest term over most of the boundary layer.

CONCLUSIONS

Analysis of measurements in turbulent boundary layers with adverse pressure gradients has led to the following conclusions:

Measurements show that the turbulent velocities $\sqrt{\overline{v^2}}$ and $\sqrt{\overline{w^2}}$ are nearly equal over most of the boundary layer, except near the wall, and that they are roughly one-half of the longitudinal velocity fluctuation $\sqrt{\overline{u^2}}$.

The shape of the $\sqrt{\overline{u^2}}$ curve was found to change with increasing pressure gradient. Measurements indicate that two possible distributions could exist, depending on flow conditions. A change with pressure gradient was noted for the mean velocity profiles.

At all pressure gradients good agreement was obtained for the values of skin friction determined from the Ludwieg-Tillmann relation and those measured with the heat transfer - skin friction instrument. At the low pressure gradients the agreement extended, in addition, to the Falkner flat-plate equation.

Use of the measured distributions of turbulent shear stress $-\rho\overline{uv}$ and viscous shear stress $\mu \frac{\partial U}{\partial y}$ to predict the wall shearing stress agrees roughly with the values obtained from heat-transfer measurements or predicted by the Ludwieg-Tillmann equation.

Measurements indicate that it may be possible to assume a sublayer within which the total shear stress obeys the relation $\frac{\partial \tau}{\partial y} = \frac{\partial p_W}{\partial x}$, where τ is the total shear stress and p_W is the static pressure at the wall.

The universal relation $\frac{U}{U_\tau}$ against $\frac{yU_\tau}{\nu}$ (where U is the local mean velocity, U_τ is the shear stress velocity, and ν is the kinematic viscosity) that has been observed by many workers was found to hold near the wall, and the total shear stress distributions predicted by use of this universal relation were found to agree qualitatively with the distributions obtained from the measurements.

The variation of the integrated shear distribution through the turbulent boundary layer suggested by Granville for zero pressure gradient does not appear to hold for the adverse pressure gradients investigated herein, although for the one station where the pressure gradient was nearly zero the agreement was good.

Evaluation of the terms of the turbulent stress tensor indicates that the normal stresses $\rho\overline{v^2}$ and $\rho\overline{w^2}$ and the shear stress $-\rho\overline{uv}$ are of the same order of magnitude, with $\rho\overline{v^2}$ and $-\rho\overline{uv}$ being nearly equal over the whole region for the largest pressure gradient.

The angle between the principal axis of the turbulent stress tensor and the x-direction was found to be nearly constant with x-distance and independent of pressure gradient. The angle also shows that the direction of principal stress near the wall tends to be alined nearly parallel to the wall.

Evaluation of the terms in the x-direction equation of motion indicates the equation may be written to sufficient accuracy as

$$U\frac{\partial U}{\partial x} + V\frac{\partial U}{\partial y} + \frac{\partial \overline{uv}}{\partial y} = -\frac{1}{\rho}\frac{\partial p}{\partial x} + \nu\frac{\partial^2 U}{\partial y^2}$$

where V is the mean velocity component normal to the boundary, ρ is the air density, and p is the static pressure. All other terms are small for the flows investigated.

Evaluation of the terms in the y-direction equation of motion indicates the term $\frac{\partial \overline{v^2}}{\partial y}$ to be as large as or larger than any of the terms in the x-direction equation. A sufficient approximation to the y-direction equation of motion appears to be

$$\frac{\partial \overline{v^2}}{\partial y} = -\frac{1}{\rho}\frac{\partial p}{\partial y}$$

or

$$\rho\overline{v^2} = p_w - p$$

for the flows investigated. The x- and y-equations of motion are independent if $\frac{\partial \overline{v^2}}{\partial x} << \frac{1}{\rho}\frac{\partial p}{\partial x}$, which is true for the cases investigated.

Lewis Flight Propulsion Laboratory
National Advisory Committee for Aeronautics
Cleveland, Ohio, August 10, 1954

APPENDIX A

SYMBOLS

The following symbols are found in this report:

A	constant, depending on physical quantities of hot wire
B	constant, depending on physical quantities of hot wire
C_f	local wall shear stress coefficient, $\frac{\tau_W}{1/2\ \rho U_1^2}$
c_f	shearing stress coefficient, $\frac{\tau}{1/2\ \rho U_1^2}$
E_{local}	local turbulent kinetic energy per unit mass
E_{total}	average energy contained in turbulent motion
e	voltage output of hot wire
Δe	fluctuation voltage output of hot wire due to mass-flow fluctuation
H	mean-velocity-profile form parameter, δ^*/θ
i	current flowing through hot wire
l	mixing length
p	static pressure
p_r	reference static pressure
p_W	static pressure at wall
R	operating resistance of hot wire
R_α	resistance of hot wire at flow temperature
Re	Reynolds number based on a convenient length; for this report, $\frac{\rho U_1 \delta^*}{\mu}$
Re_θ	Reynolds number based on momentum thickness, $\frac{\rho U_1 \theta}{\mu}$

S	hot-wire sensitivity
$\underset{\approx}{T}$	stress tensor
$\underset{\approx}{T}_T$	turbulent stress tensor
U,V	local mean velocity in x- and y-directions
U_1	mean velocity of free stream where viscous effects are neglected
U_τ	shear stress velocity, $\sqrt{\frac{\tau_w}{\rho}}$
V_i	instantaneous resultant mean plus turbulent velocities
u,v,w	instantaneous turbulent velocities in x-, y-, and z-directions
$\overline{u^2},\overline{v^2},\overline{w^2}$	mean squares of turbulent velocity fluctuations in x-, y-, and z-directions
$\overline{uv}$	Reynolds turbulent shear stress in xy-plane
$\overline{uw}$	Reynolds turbulent shear stress in xz-plane
$\overline{vw}$	Reynolds turbulent shear stress in yz-plane
x	direction parallel to test wall and in general direction of mean flow
y	direction normal to test wall and approximately normal to mean flow
z	direction normal to mean flow and parallel to test wall
α	angle in xy-plane resultant mean flow makes with wall
β	angle between principal axis of turbulent stress tensor and x-direction
δ	boundary layer thickness
δ^*	displacement thickness, representative of mass-flow deficiency, $\int_0^\infty \left(1 - \frac{U}{U_1}\right) dy$
δ_{ij}	Kronecker delta symbol

θ momentum thickness, representative of mean-flow momentum deficiency, $\int_0^\infty \frac{U}{U_1}\left(1 - \frac{U}{U_1}\right)dy$; corrected for turbulence,

$$\int_0^\delta \frac{U}{U_1}\left[1 - \frac{U}{U_1}\left(1 - \frac{\tau_{xx}}{\rho U^2} + \frac{\tau_{yy}}{\rho U^2}\right)\right]dy$$

μ viscosity of air

ν kinematic viscosity of air, μ/ρ

ρ density of air

Σ instantaneous angle between x-direction and instantaneous velocity vector

τ local shear stress

τ_w local shear stress at wall in x-direction

τ_{xx}, τ_{yy}, τ_{zz} normal stress terms, defined in eq. (4b)

τ_{xy} shear stress term, $\mu\left(\frac{\partial U}{\partial y} + \frac{\partial V}{\partial x}\right) - \rho\overline{uv}$

φ angle between x-direction and hot wires

ψ integrated shear distribution, $\int_0^{\delta/\delta^*} 2c_f \, d\left(\frac{y}{\delta^*}\right)$

ψ_0 integrated shear distribution for zero pressure gradient

APPENDIX B

THEORY OF CONSTANT-TEMPERATURE HOT-WIRE ANEMOMETRY MEASUREMENTS

The constant-temperature hot-wire anemometer is a system designed to eliminate the problem of thermal inertia encountered in the more common constant-current hot-wire anemometer systems. The use of the d-c feedback amplifier system employed in the measurements of this report to correct for any change in the wire operating temperature was suggested in reference 30.

The constant-temperature system employs the d-c amplifier as a servomechanism to sense the unbalance of a Wheatstone bridge, of which the wire is one arm, and by continuously varying the feedback voltage the bridge is kept in balance. If the wire is the only variable resistance in the bridge, the feedback voltage will serve to keep the wire resistance and likewise the wire temperature constant; thus the problem of thermal lag of the wire is eliminated since the change in wire temperature is negligible. A measure of the fluctuating feedback voltage is an indication of the fluctuating mass flow over the wire.

The refinements of the constant-temperature system of this report over that appearing in reference 12 are the shock mounting of the amplifiers and the replacing of the electronic tube rectifiers of the amplifier power supply by selenium rectifiers. Both changes were made to eliminate as much amplifier background noise as possible. The selenium rectifiers also helped to relieve a problem in amplifier cooling, which in turn helped to eliminate noise.

The output of the system was read on the average-square computers described and evaluated in reference 12. The sum and difference circuit was also the one described in reference 12 in connection with the double-correlation instrument. The sum circuit gave accurate results, but as will always be the case the difference circuit was affected by the circuit noise level. If the same sine wave of 1 volt was fed into the two inputs and subtracted through the circuit, a difference null of approximately 5 percent of the input signal was obtained. The actual error encountered because of the difference null was negligible except near or in the free-stream turbulence, and fortunately here the contribution of the sum and difference terms (see appendix C) to the total velocity fluctuation term was negligible.

The use of a d-c amplifier requires that the bridge of the constant-temperature hot-wire anemometer system operate at a slight unbalance; otherwise the amplifier would oscillate. The unbalance of the bridge was maintained constant at 3 microamps by use of a microammeter. This unbalance results in a slight systematic error in the fluctuating feedback voltage output. However, the data were not corrected as the random scatter in the measurements was found to overshadow the smaller systematic error.

The empirical relation between heat loss and mass flow for small cylinders electrically heated may be written

$$\frac{i^2R}{R - R_\alpha} = A + \beta\sqrt{\rho U} \tag{B1}$$

where i is the operating current of the hot wire, R is the operating resistance of the hot wire, R_α is the wire resistance at some reference temperature (usually that of the surrounding air stream), ρU is the mass flow past the wire, and A and B are empirical constants which must be determined for each wire. Equation (B1) has been referred to as King's equation (ref. 31) since he first arrived at the form from a theoretical analysis of the heat loss from small circular cylinders in potential flows. However, the equation is justified from empirical results, since King's analysis did not take into account viscous effects on the heat transfer.

Replacing the curve of i against U as predicted by equation (B1) by its tangent at any point makes possible the prediction of the instantaneous heat loss from small wires. Schubauer and Klebanoff (ref. 32) indicate that the heat loss is a function of the component of mass flow normal to the wire; thus equation (B1) can be generally written

$$\frac{i^2R}{R - R_\alpha} = A + B\sqrt{\rho V_i \sin \Sigma} \tag{B2}$$

where V_i is the total instantaneous velocity and Σ is the instantaneous angle between V_i and the wire. Differentiating equation (B2) with respect to the velocity vector, where the wire resistance is held constant and only the wire current varies, gives (incompressible flow)

$$\frac{2iR\ di}{R - R_\alpha} = \frac{B}{2}\frac{\rho}{\sqrt{\rho V_i \sin \Sigma}}(\sin \Sigma\ dV_i + V_i \cos \Sigma\ d\Sigma) \tag{B3}$$

This equation will be true for small fluctuations, where only the linear terms of the fluctuations are retained. In order to rearrange equation (B3) into a form where hot-wire measurements can be analyzed, the following approximations are made: (1) For small changes in Δe, the fluctuating voltage, let $R\ di = de = \Delta e$. (2) Assume the instantaneous velocity V_i is made up of a mean component U which makes an angle Φ

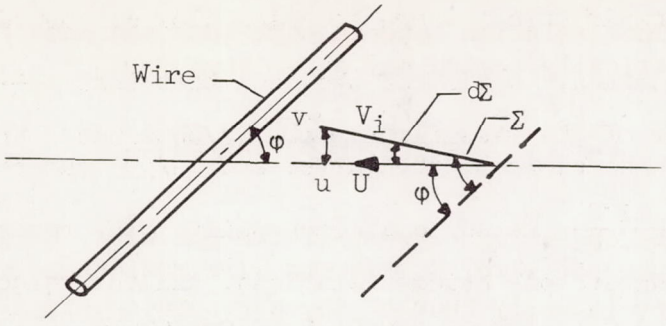

Sketch 1

with the wire (see sketch 1) plus the turbulent fluctuation components u and v. For this derivation V_i is taken as coplanar with U and the wire. With the restriction that u and v are very small compared with U, it follows from sketch 1 that

$$(a)\ dV_i \simeq u$$

$$(b)\ d\Sigma \simeq \pm \frac{v}{V_i}$$

$$(c)\ V_i \sin \Sigma \simeq U \sin \varphi$$

$$(d)\ \Sigma \simeq \varphi$$

Equation (B3) can now be written

$$u \sin \varphi \pm v \cos \varphi = \frac{4i\sqrt{\rho U \sin \varphi}}{\rho B(R-R_\alpha)} \Delta e \qquad (B4)$$

Equation (B4) is the general equation relating the fluctuating voltage due to the d-c amplifier feedback Δe to the turbulent velocity fluctuations occurring across the hot wire. This derivation parallels that given in reference 32 for the constant-current system. For the simplest case, that of a wire normal to the mean velocity U, equation (B4) reduces to

$$\sqrt{\overline{u^2}} = \frac{4i\sqrt{\rho U}}{\rho B(R-R_\alpha)} \sqrt{\overline{\Delta e^2}} \qquad (B5)$$

The terms on the right side of equation (B5) are determined at each point where $\sqrt{\overline{u^2}}$ is measured. The current is determined by measuring the mean bridge current and then using a balanced Wheatstone bridge relation to calculate the current through the wire. The mass flow $\sqrt{\rho U}$ and B are obtained from a calibration curve for the wire. The wire

is placed in an air stream where the mass flow can be varied and determined by other means. A plot of the mean heat loss $\frac{i^2R}{(R - R_\alpha)}$ against the square root of the mass flow $\sqrt{\rho U}$ is obtained. From this plot B is obtained as the slope of the curve, and $\sqrt{\rho U}$ can be determined from the value of $\frac{i^2R}{R - R_\alpha}$ measured at each point. The resistance R can be obtained from Wheatstone bridge relations, and the value of R_α is usually measured directly by use of a potentiometer. The fluctuating voltage was measured in terms of its root mean square value by means of an electronic squaring circuit.

The evaluation of hot-wire data in several cases required corrections for changes in heat loss calibration in order that consistent results might be obtained. The initial procedure was to calibrate the wires in the free stream of the channel after a profile through the boundary layer was completed. This type of calibration resulted many times in discontinuous jumps observed in the calculated quantities. (The discontinuous jumps were apparently caused by dirt particles striking the wires.) It was found that consistent results could be obtained if the velocity profiles measured in the boundary layer with a total-pressure probe were also employed. From the measured mean velocity profile for a given station and free-stream velocity, a value of $\sqrt{\rho U}$ at each point in the boundary layer was determined. If now the heat loss of the wires at each point in the boundary layer is plotted against the predetermined $\sqrt{\rho U}$, a master calibration of the wires at each point is obtained. In general, it was found that changes in calibration resulted only in shifting the calibration curve, with the slope remaining nearly constant.

APPENDIX C

REDUCTION OF x-WIRE DATA

The general equation relating the voltage fluctuation output of the anemometer to the turbulent fluctuations was derived in appendix B.

$$u \sin \varphi \pm v \cos \varphi = \frac{4i\sqrt{\rho U \sin \varphi}}{\rho B (R-R_\alpha)} \Delta e \qquad (B4)$$

The term $\frac{4i\sqrt{\rho U \sin \varphi}}{\rho B(R-R_\alpha)}$ is the sensitivity factor S of the wire, since it depends only on the mean quantities; thus the equation can be written

$$u \sin \varphi \pm v \cos \varphi = S \Delta e \qquad (C1)$$

If two wires are placed in the flow so that the mean velocity U makes an angle φ with each, as shown in sketch 2, it may be seen that

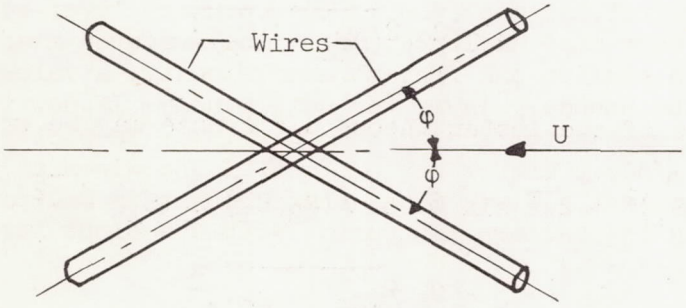

Sketch 2

equation (C1) gives the following equations for the two wires:

$$u \sin \varphi + v \cos \varphi = S_1 \Delta e_1 \qquad (C2)$$

and

$$u \sin \varphi - v \cos \varphi = S_2 \Delta e_2 \qquad (C3)$$

The mean squares of equations (C2) and (C3) are

$$\overline{u^2} \sin^2 \varphi + 2\overline{uv} \sin \varphi \cos \varphi + \overline{v^2} \cos^2 \varphi = S_1^2 \overline{\Delta e_1^2} \qquad (C4)$$

$$\overline{u^2} \sin^2 \varphi - 2\overline{uv} \sin \varphi \cos \varphi + \overline{v^2} \cos^2 \varphi = S_2^2 \overline{\Delta e_2^2} \qquad (C5)$$

Taking the difference of equations (C4) and (C5) yields

$$\overline{uv} = \frac{S_1^2\overline{\Delta e_1^2} - S_2^2\overline{\Delta e_2^2}}{4 \sin \varphi \cos \varphi} \tag{C6}$$

which is the relation used to determine the turbulent shearing stress $\rho\overline{uv}$.

The sum of equations (C4) and (C5) gives

$$\overline{u^2} \sin^2 \varphi + \overline{v^2} \cos^2 \varphi = \frac{S_1^2\overline{\Delta e_1^2} + S_2^2\overline{\Delta e_2^2}}{2} \tag{C7}$$

In order to obtain another equation between $\overline{u^2}$ and $\overline{v^2}$ it is necessary to obtain electrically the instantaneous sums and differences of the voltages of equations (C2) and (C3). The mean square of the instantaneous sum may be written

$$\overline{u^2} \sin^2\varphi(S_2+S_1)^2 + 2\overline{uv} \sin \varphi \cos \varphi (S_2-S_1)(S_2+S_1) + \overline{v^2} \cos^2\varphi(S_2-S_1)^2$$

$$= S_1^2S_2^2\overline{(\Delta e_1 + \Delta e_2)^2} \tag{C8}$$

The mean square of the instantaneous difference may be written

$$\overline{u^2} \sin^2\varphi(S_2-S_1)^2 + 2\overline{uv} \sin \varphi \cos \varphi (S_2-S_1)(S_2+S_1) + \overline{v^2} \cos^2\varphi(S_2+S_1)^2$$

$$= S_1^2S_2^2\overline{(\Delta e_1 - \Delta e_2)^2} \tag{C9}$$

The difference of equations (C8) and (C9) yields

$$\overline{u^2} \sin^2\varphi - \overline{v^2} \cos^2 \varphi = \frac{S_1S_2}{4}\left(\overline{\varepsilon_+^2} - \overline{\varepsilon_-^2}\right) \tag{C10}$$

where

$$\overline{\varepsilon_+^2} = \overline{(\Delta e_1 + \Delta e_2)^2}$$

$$\overline{\varepsilon_-^2} \quad \overline{(\Delta e_1 - \Delta e_2)^2}$$

Solving equations (C7) and (C10) for $\overline{u^2}$ and $\overline{v^2}$ gives

$$\overline{u^2} = \frac{1}{4\sin^2\varphi}\left[S_1^2\overline{\Delta e_1^2} + S_2^2\overline{\Delta e_2^2} + \frac{S_1S_2}{2}\left(\overline{\varepsilon_+^2} - \overline{\varepsilon_-^2}\right)\right] \qquad (C11)$$

and

$$\overline{v^2} = \frac{1}{4\cos^2\varphi}\left[S_1^2\overline{\Delta e_1^2} + S_2^2\overline{\Delta e_2^2} - \frac{S_1S_2}{2}\left(\overline{\varepsilon_+^2} - \overline{\varepsilon_-^2}\right)\right] \qquad (C12)$$

It should be noted that v can be replaced by w, depending on the wire orientation.

Figure 30 shows a block diagram of the instrumentation hookups used to obtain the turbulence measurements of this report.

REFERENCES

1. Townsend, A. A.: The Fully Developed Turbulent Wake of a Circular Cylinder. Australian Jour. Sci. Res., ser. A, vol. 2, no. 4, 1949, pp. 451-468.

2. Corrsin, Stanley: Investigation of Flow in an Axially Symmetrical Heated Jet of Air. NACA WR W-94, 1943. (Supersedes NACA ACR 3L23.)

3. Laufer, John: Investigation of Turbulent Flow in a Two-Dimensional Channel. NACA Rep. 1053, 1951. (Supersedes NACA TN 2123.)

4. Laufer, John: The Structure of Turbulence in Fully Developed Pipe Flow. NACA TN 2954, 1953.

5. Townsend, A. A.: The Structure of the Turbulent Boundary Layer. Proc. Cambridge Phil. Soc., vol. 47, pt. 2, 1950, pp. 375-395.

6. Schubauer, G. B., and Klebanoff, P. S.: Investigation of Separation of the Turbulent Boundary Layer. NACA Rep. 1030, 1951. (Supersedes NACA TN 2133.)

7. von Karman, T., and Howarth, Leslie: On the Statistical Theory of Isotropic Turbulence. Proc. Roy. Soc. (London), ser. A, vol. 164, Jan. 21, 1938, pp. 192-215.

8. Sandborn, Virgil A.: Preliminary Experimental Investigation of Low-Speed Turbulent Boundary Layers in Adverse Pressure Gradients. NACA TN 3031, 1953.

9. Goldstein, S.: A Note on the Measurement of Total Head and Static Pressure in a Turbulent Stream. Proc. Roy. Soc. (London), ser. A, vol. 155, 1936, pp. 570-575.

10. Young, A. D., and Maas, J. N.: The Behaviour of a Pitot Tube in a Transverse Total-Pressure Gradient. R. & M. No. 1770, British A.R.C., Sept. 9, 1936.

11. Ludwieg, H.: Instrument for Measuring the Wall Shearing Stress of Turbulent Boundary Layers. NACA TM 1284, 1950.

12. Laurence, James C., and Landes, L. Gene: Auxiliary Equipment and Techniques for Adapting the Constant-Temperature Hot-Wire Anemometer to Specific Problems in Air-Flow Measurements. NACA TN 2843, 1952.

13. Strehlow, Roger A.: A Method for Electroplating Fine Wires. CM-551, Univ. Wisconsin, June 27, 1949. (Navy BuOrd Contract NOrd 9938, Task WIS-1-E.)

14. Goldschmied, Fabio R.: Skin Friction of Incompressible Turbulent Boundary Layers Under Adverse Pressure Gradients. NACA TN 2431, 1951.

15. Munk, Max M.: On the Mechanism of Turbulent Fluid Motion. Novord Rep. 2298, Aeroballistic Res. Rep. No. 62, U.S. Naval Ord. Lab. (Maryland), Feb. 14, 1952. (Office Naval Res. Proj. NR 044-003.)

16. Clauser, Francis H.: Turbulent Boundary Layers in Adverse Pressure Gradients. Jour. Aero. Sci., vol. 21, no. 2, Feb. 1954, pp. 91-108.

17. Ludwieg, H., and Tillmann, W.: Investigations of the Wall-Shearing Stress in Turbulent Boundary Layers. NACA TM 1285, 1950.

18. Falkner, V. M.: A New Law for Calculating Drag. Aircraft Eng., vol. XV, no. 169, Mar. 1943, pp. 65-69.

19. Ross, Donald: Integration of the Reynolds Equations for Incompressible Turbulent Boundary Layers. Ord. Res. Lab., The Penn. State College, May 29, 1953. (Navy Dept., Bur. Ord. Contract NOrd 7958.)

20. Bidwell, Jerold M.: Application of the von Kármán Momentum Theorum to Turbulent Boundary Layers. NACA TN 2571, 1951.

21. Fediaevsky, K.: Turbulent Boundary Layers of an Airfoil. NACA TM 822, 1937.

22. Pai, S. I.: On Turbulent Flow Between Parallel Plates. Jour. Appl. Mech., vol. 20, no. 1, Mar. 1953, pp. 109-114.

23. Coles, D.: Measurements in the Boundary Layer on a Smooth Flat Plate in Supersonic Flow. Ph. D. Thesis, Calif. Inst. Tech., 1953.

24. Tetervin, Neal, and Lin, Chia Chiao: A General Integral Form of the Boundary-Layer Equation for Incompressible Flow with an Application to the Calculation of the Separation Point of Turbulent Boundary Layers. NACA Rep. 1046, 1951. (Supersedes NACA TN 2158.)

25. Granville, Paul S.: A Method for the Calculation of the Turbulent Boundary Layer in a Pressure Gradient. Rep. No. 752, Navy Dept., The David W. Taylor Model Basin, Wash. (D.C.), May 1951.

26. Goldstein, Sidney, ed.: Modern Developments in Fluid Dynamics. Clarendon Press (Oxford), 1938.

27. Dryden, Hugh L.: Some Recent Contributions to the Study of Transition and Turbulent Boundary Layers. NACA TN 1168, 1947.

28. Rotta, J.: On the Theory of the Turbulent Boundary Layer. NACA TM 1344, 1953.

29. Corrsin, Stanley: An Integral Relation from the Turbulent Energy Equation. Jour. Aero. Sci., vol. 18, no. 11, Nov. 1951, pp. 773-774.

30. Ossofsky, Eli: Constant-Temperature Operation of the Hot-Wire Anemometer at High Frequency. Rev. Sci. Instr., vol. 19, no. 12, Dec. 1948, pp. 881-889.

31. King, Louis Vessot: On the Convection of Heat from Small Cylinders in a Stream of Fluid: Determination of the Convection Constants of Small Platinum Wires with Applications to Hot-Wire Anemometry. Phil. Trans. Roy. Soc. (London), ser. A, vol. 214, no. 14, Nov. 1914, pp. 373-432.

32. Schubauer, G. B., and Klebanoff, P. S.: Theory and Application of Hot-Wire Instruments in the Investigation of Turbulent Boundary Layers. NACA WR W-86, 1946. (Supersedes NACA ACR 5K27.)

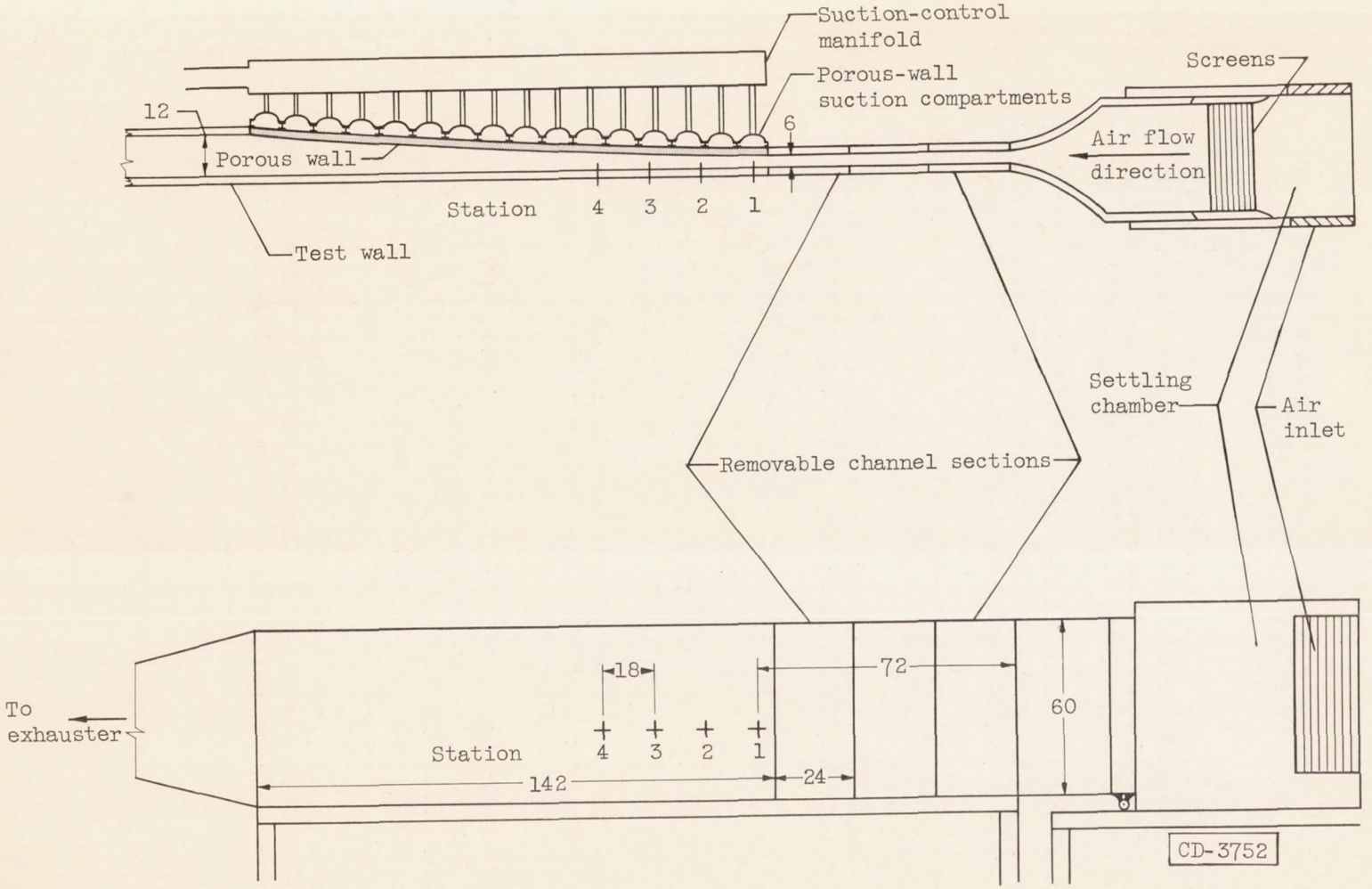

Figure 1. - Schematic diagram of 6- by 60-inch subsonic boundary-layer channel.

(All dimensions are in inches.)

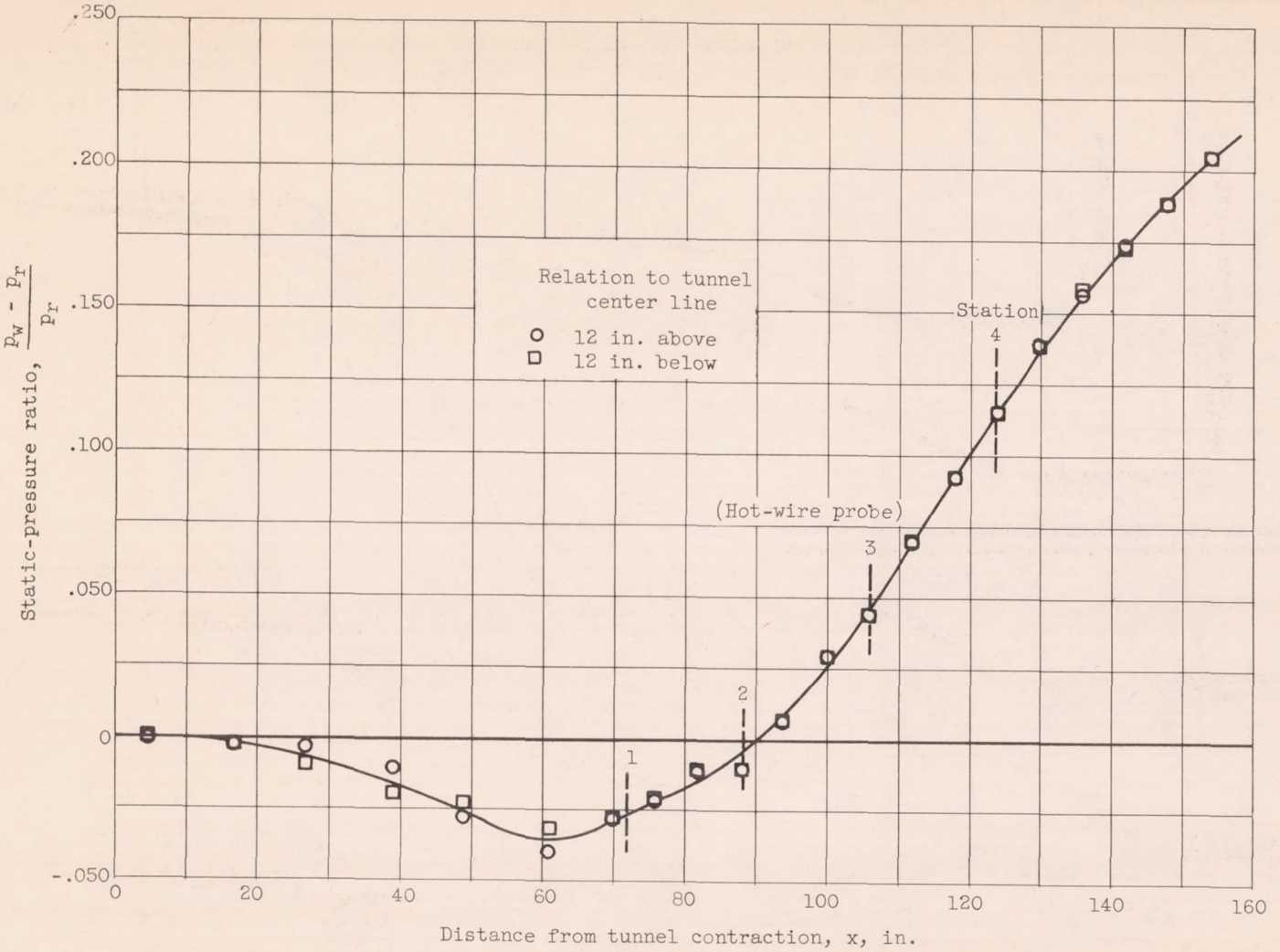

Figure 2. - Static-pressure distribution along tunnel wall. Reference static pressure p_r, 6.600 pounds per square foot (p_r = atmospheric pressure - tunnel static pressure at x = 0)(atmospheric barometric pressure, 29.21 in. Hg. at 81.5° F).

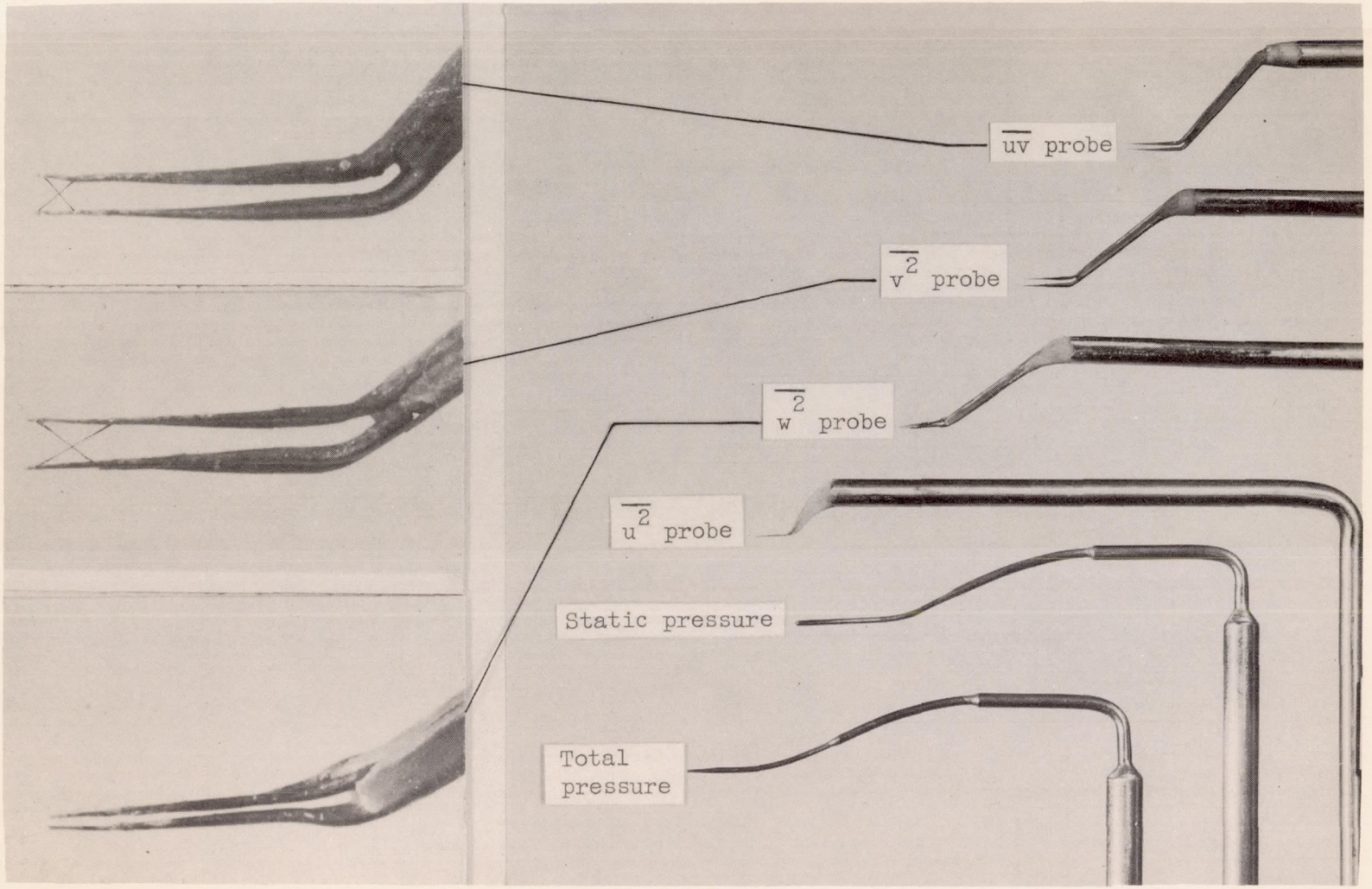

Figure 3. - Pressure and hot-wire boundary-layer probes.

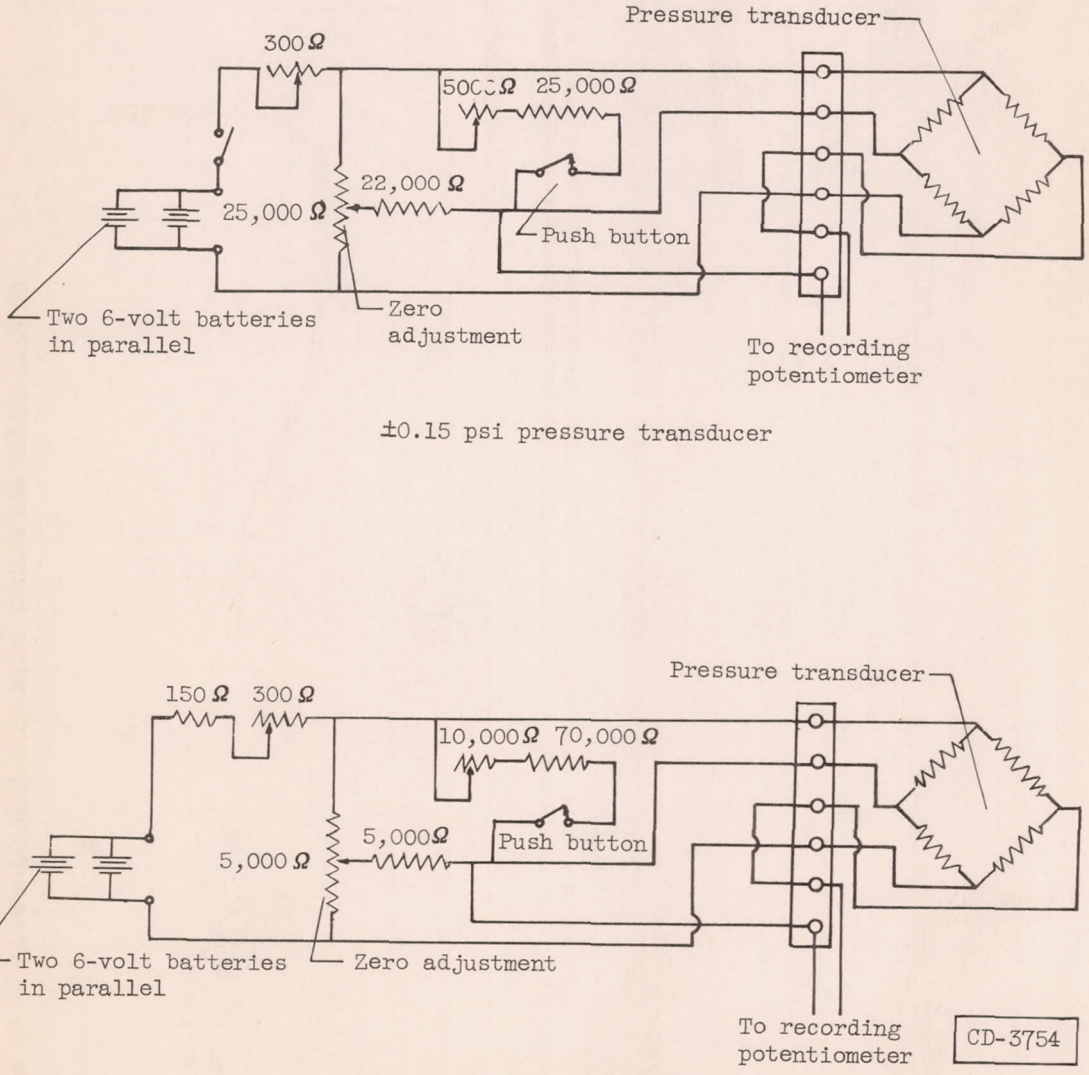

Figure 4. - Voltage control circuits for pressure transducers.

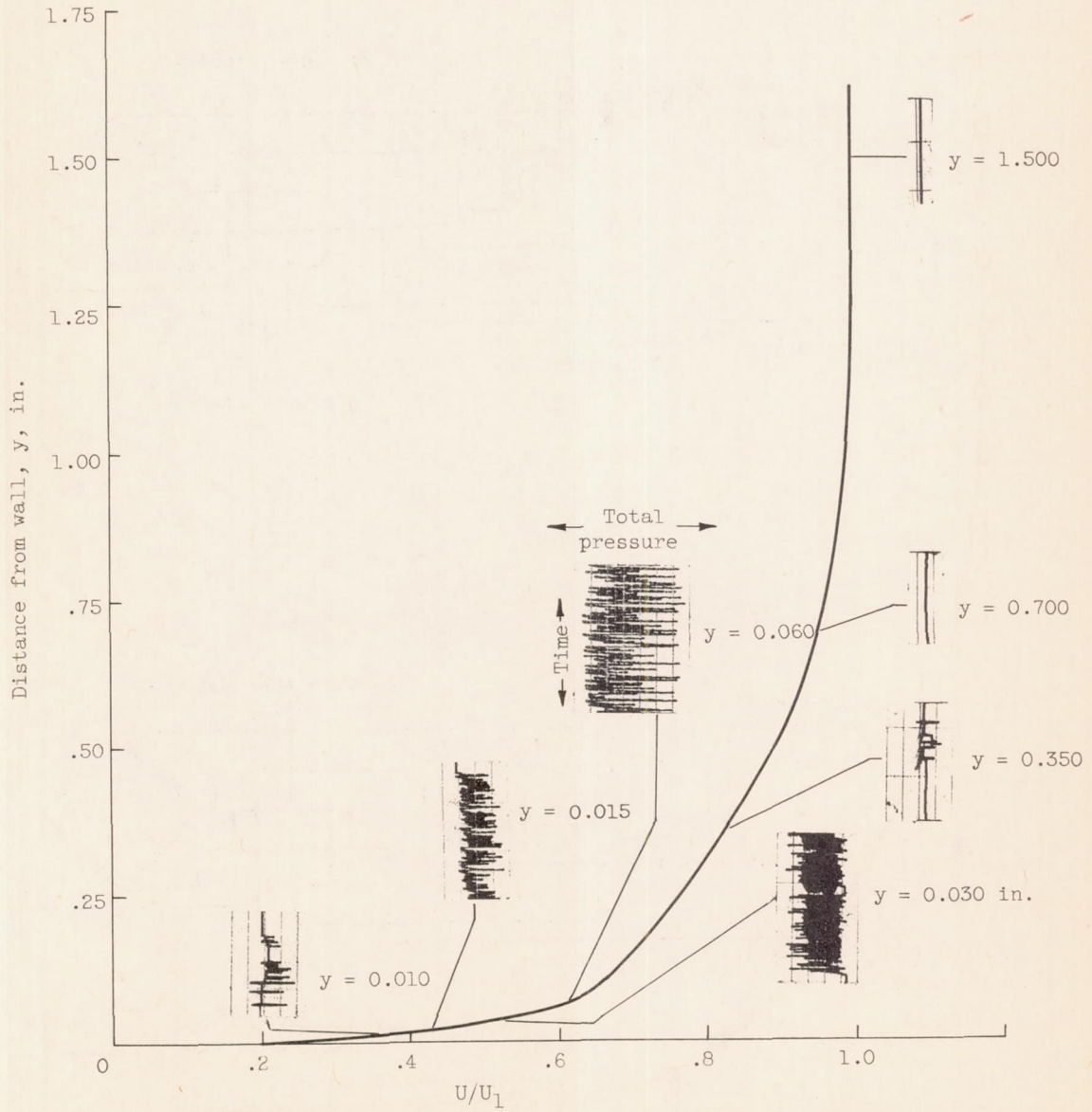

Figure 5. - Total-pressure variation observed through boundary layer at station 1. Each division on time scale equals approximately 10 seconds; smallest division on pressure chart is approximately 0.120 pound per square foot.

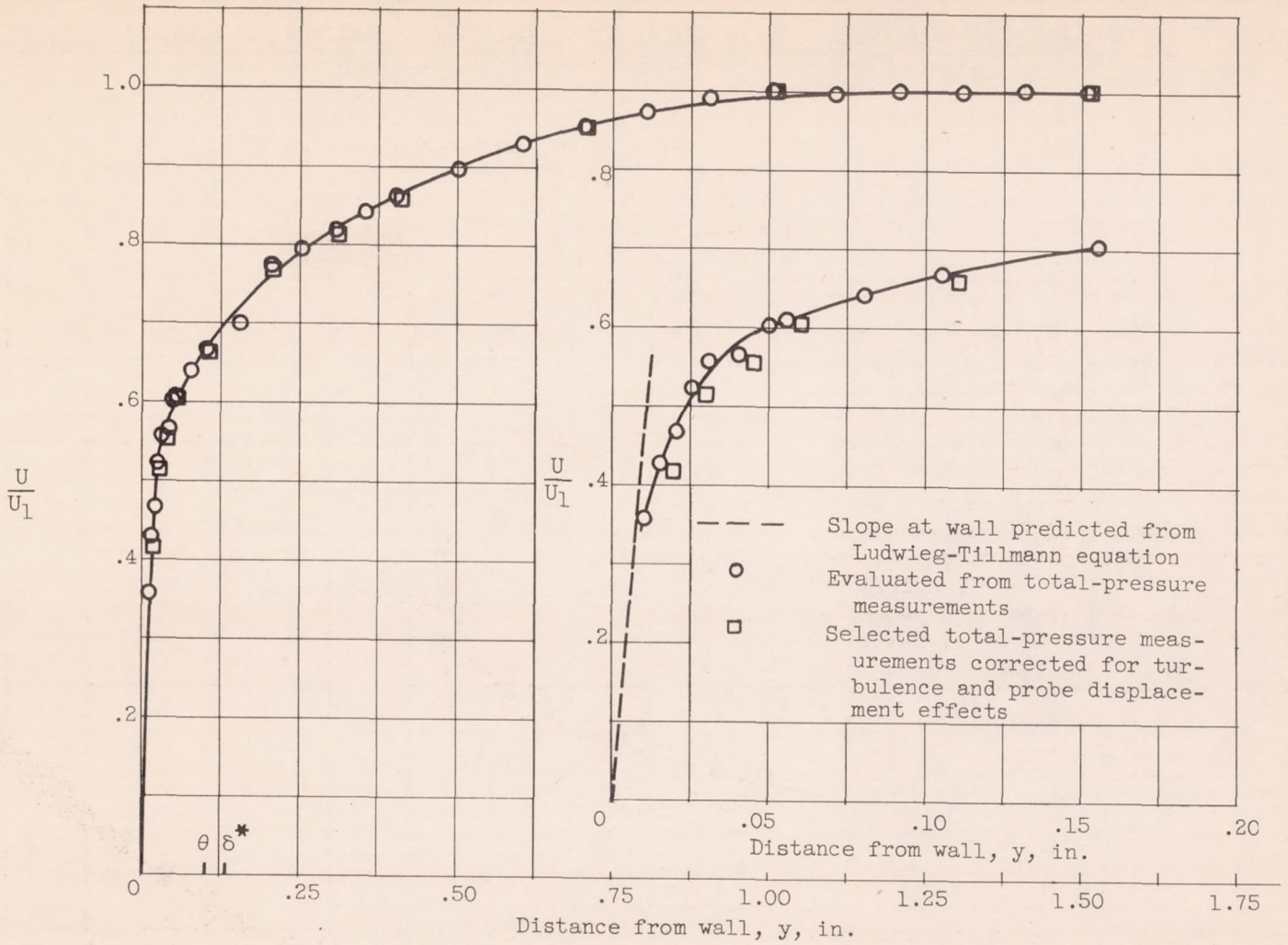

(a) Station 1. $U_1 \approx 54$ feet per second.

Figure 6. - Mean velocity distribution through boundary layer.

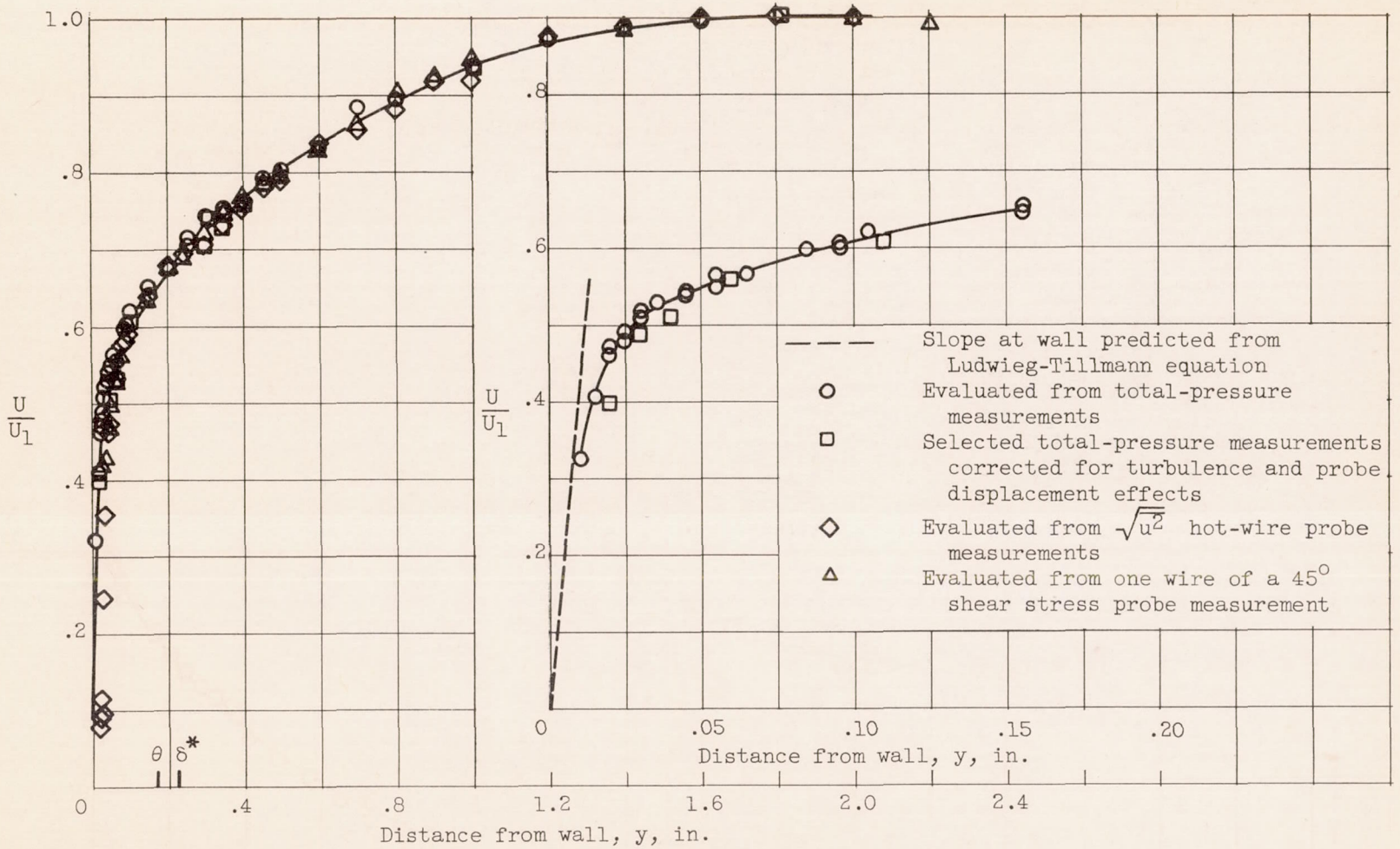

(b) Station 2. $U_1 \approx 52$ feet per second.

Figure 6. - Continued. Mean velocity distribution through boundary layer.

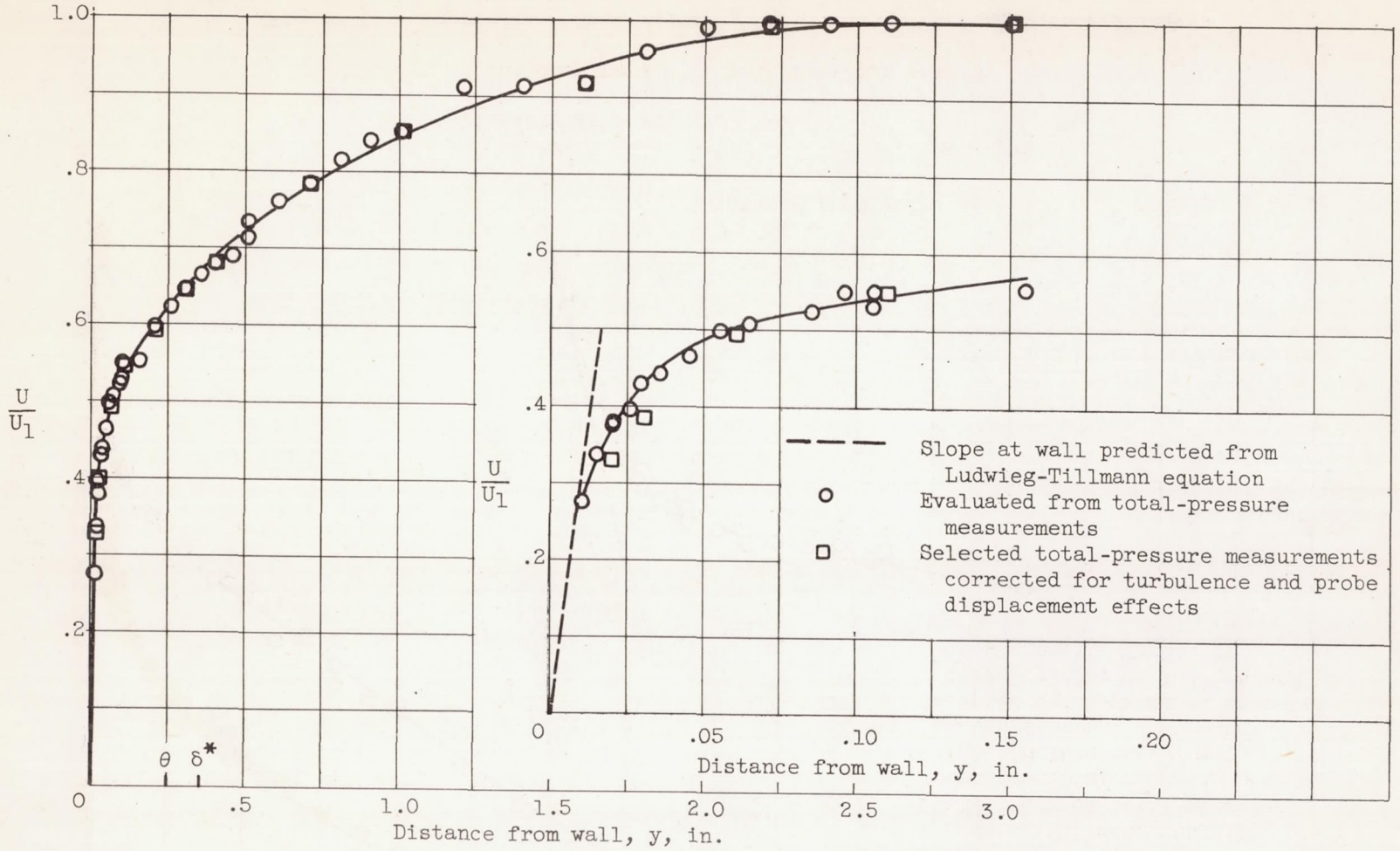

(c) Station 3. U_1 = 48 feet per second.

Figure 6. - Continued. Mean velocity distribution through boundary layer.

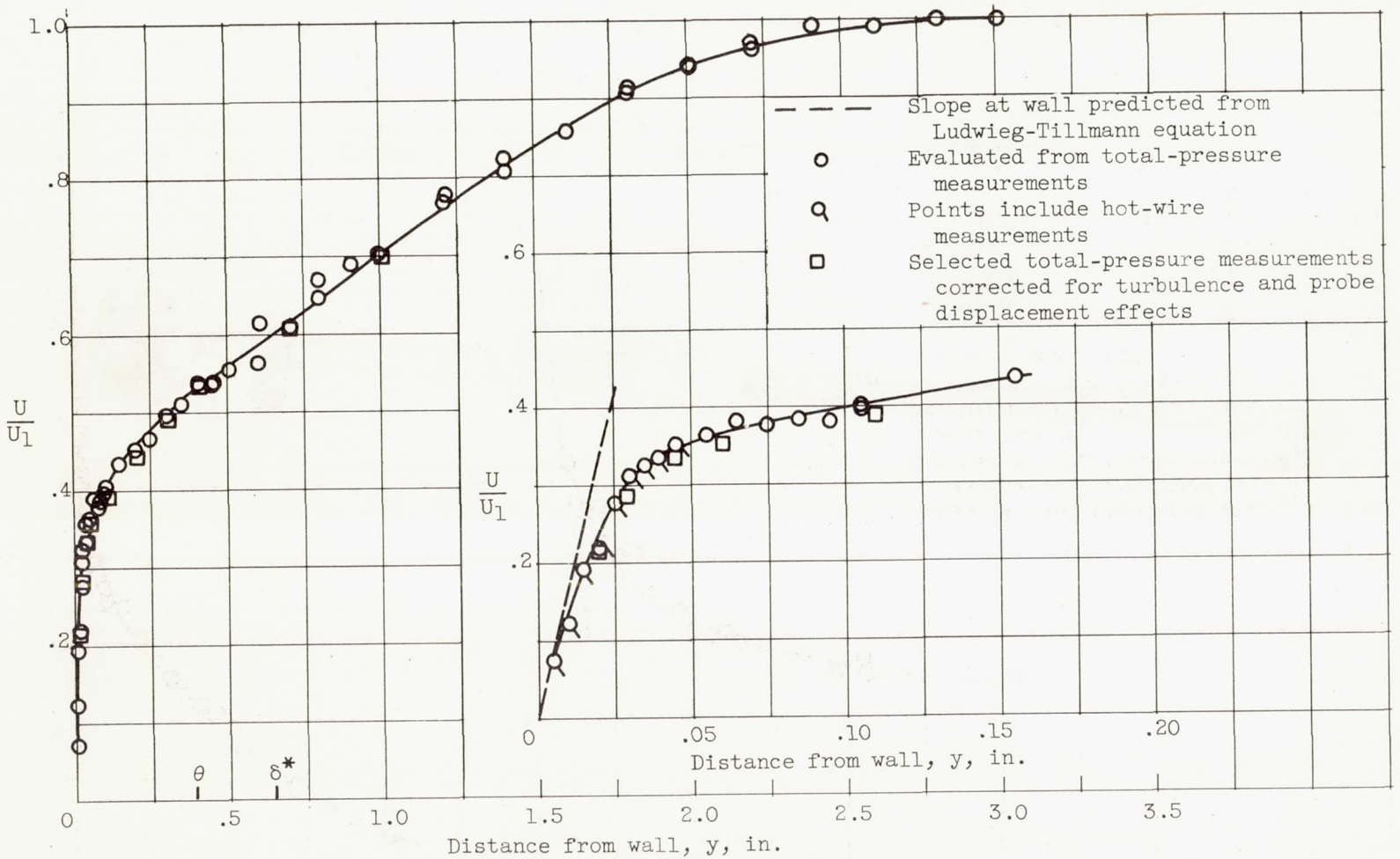

(d) Station 4. $U_1 \approx 43$ feet per second.

Figure 6. - Concluded. Mean velocity distribution through boundary layer.

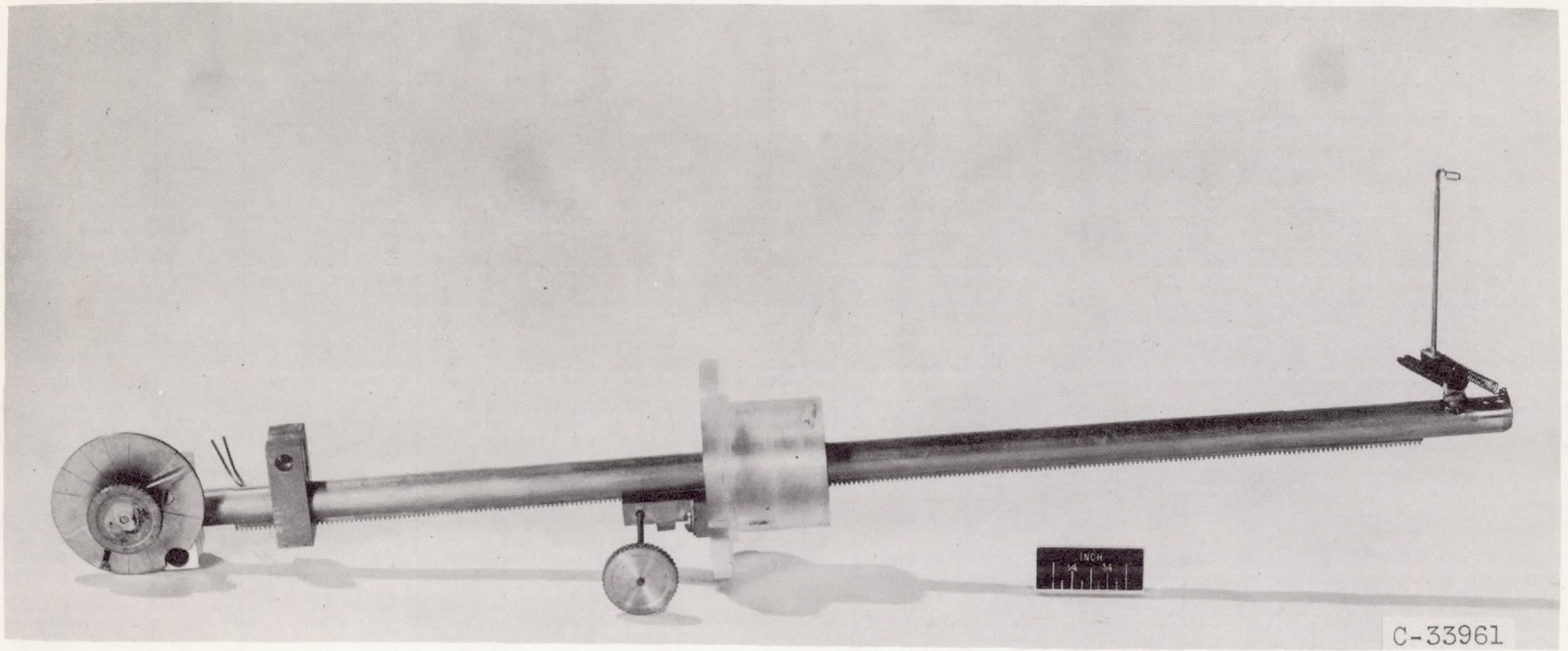

Figure 7. - Boundary-layer flow angle measuring probe.

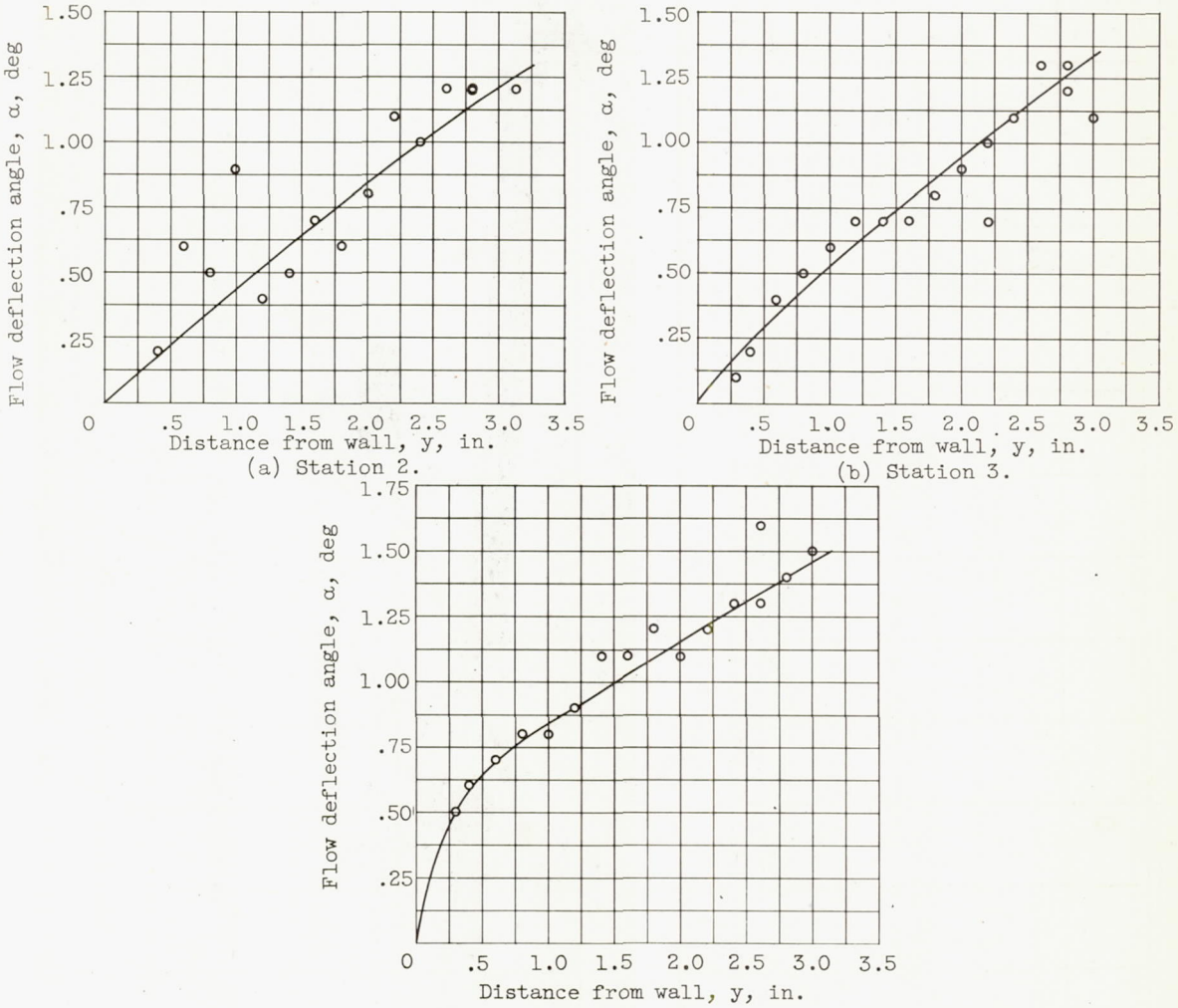

(c) Station 4.

Figure 8. - Mean flow deflection angle through boundary layer.

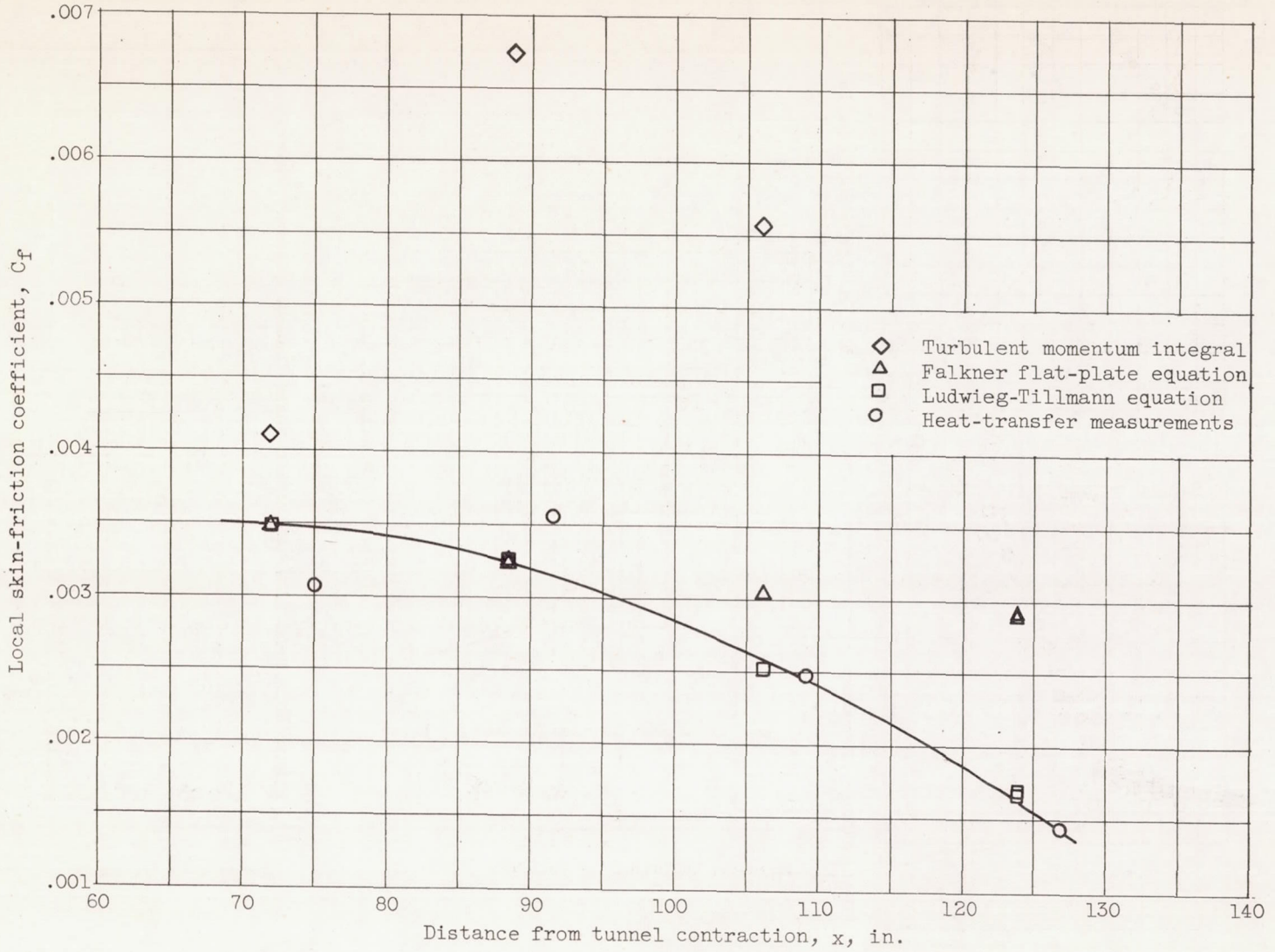

Figure 9. - Variation of local skin-friction coefficient along test wall.

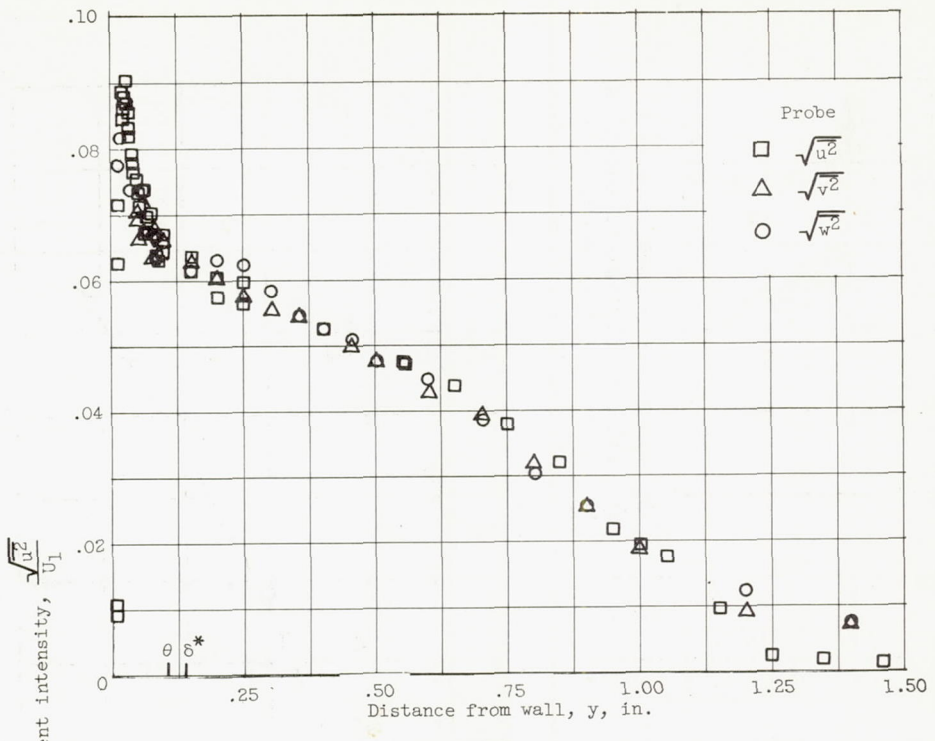

(a) Station 1.

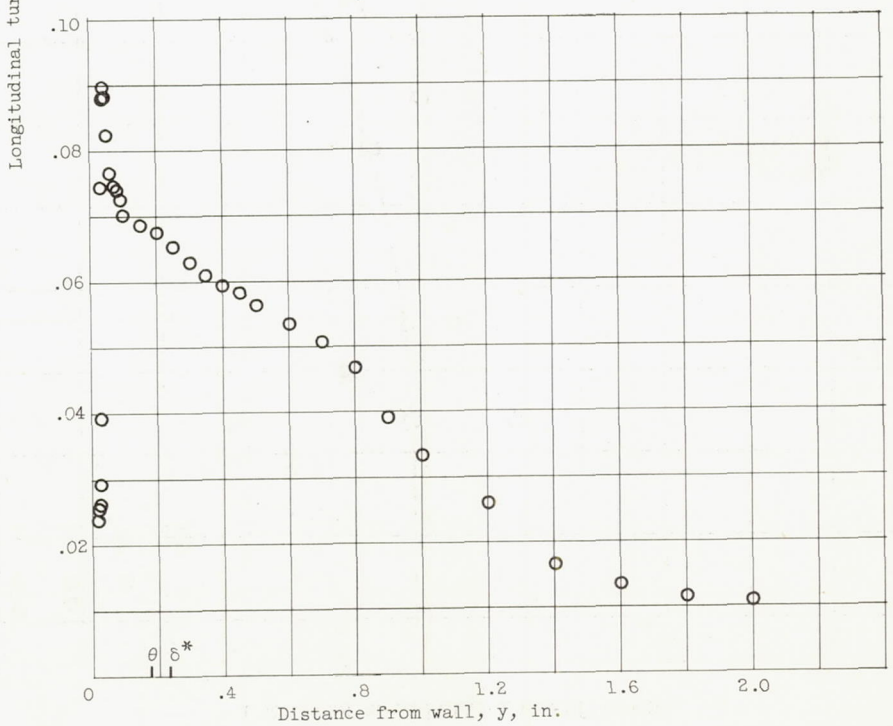

(b) Station 2.

Figure 10. - Distribution of longitudinal turbulent intensity.

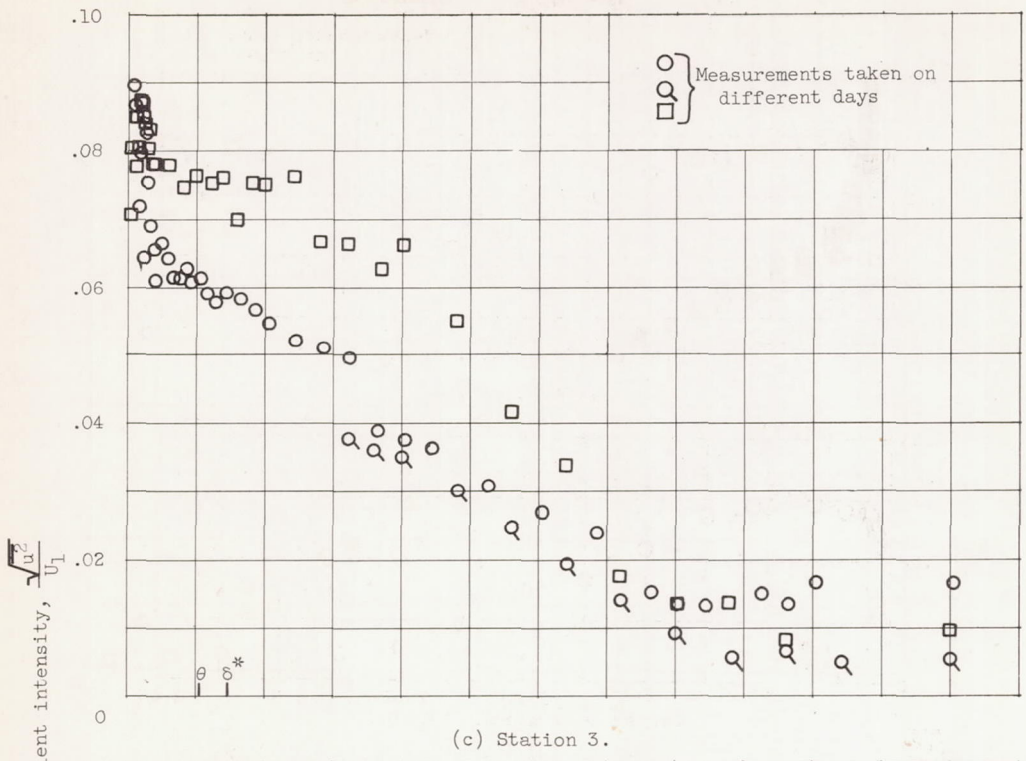

(c) Station 3.

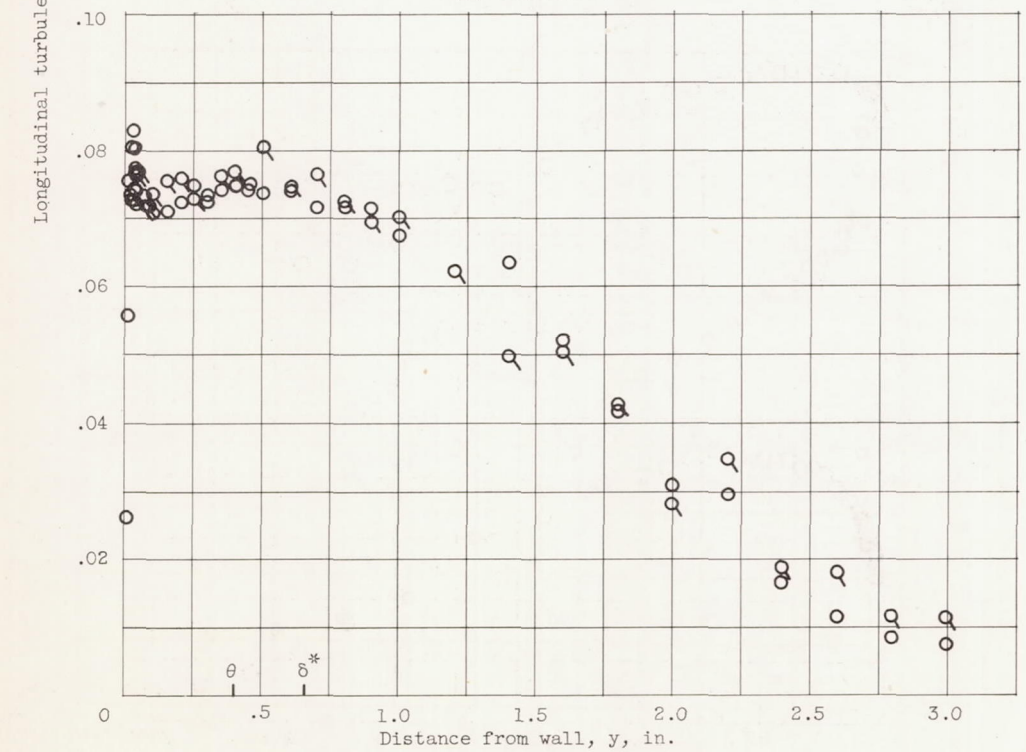

(d) Station 4.

Figure 10. - Concluded. Distribution of longitudinal turbulent intensity.

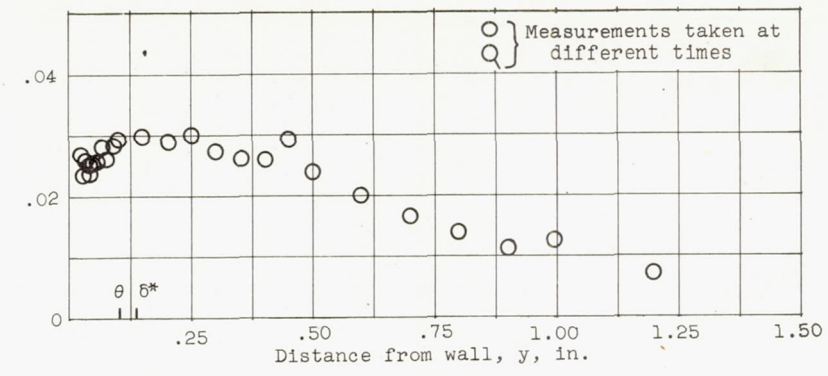

(a) Station 1.

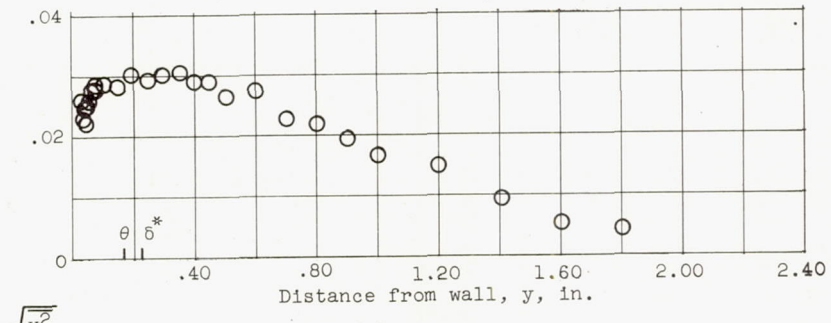

$\frac{\sqrt{\overline{v^2}}}{U_1}$

(b) Station 2.

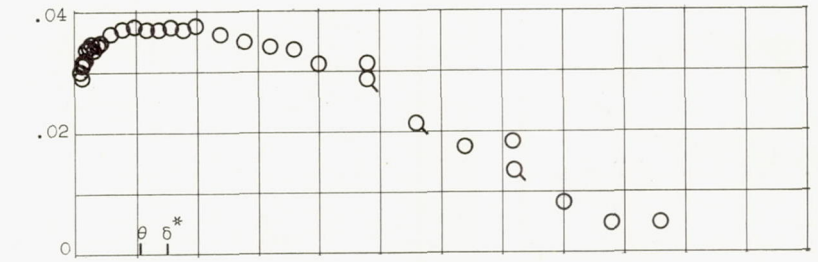

(c) Station 3.

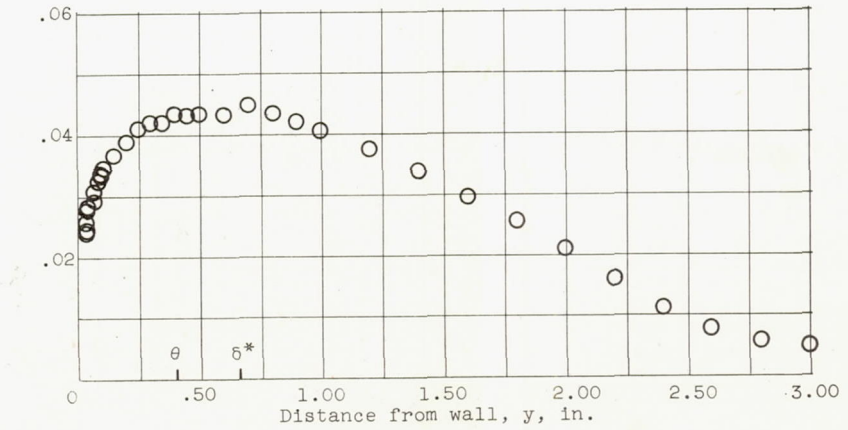

(d) Station 4.

Figure 11. - Distribution of $\sqrt{\overline{v^2}}$ velocity fluctuations through boundary layer.

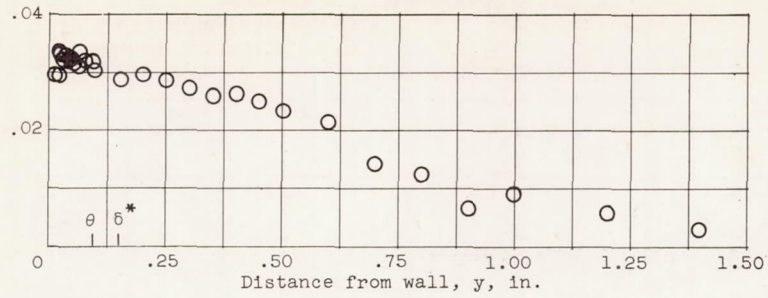

(a) Station 1.

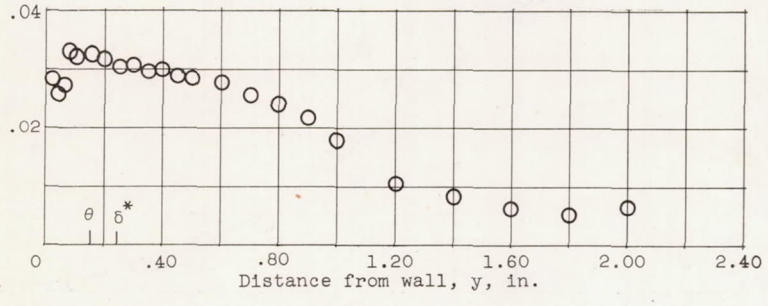

$\frac{\sqrt{w^2}}{U_1}$

(b) Station 2.

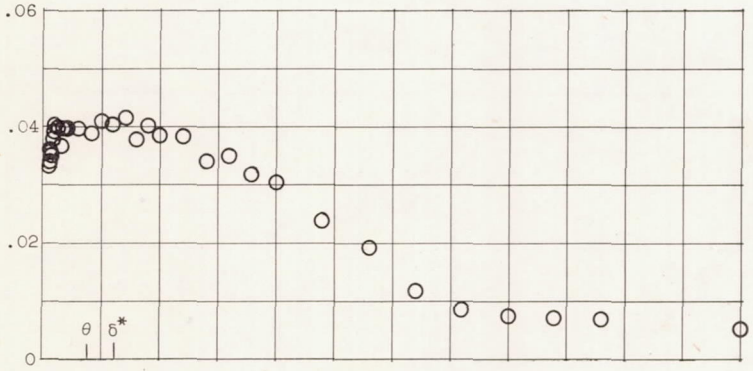

(c) Station 3.

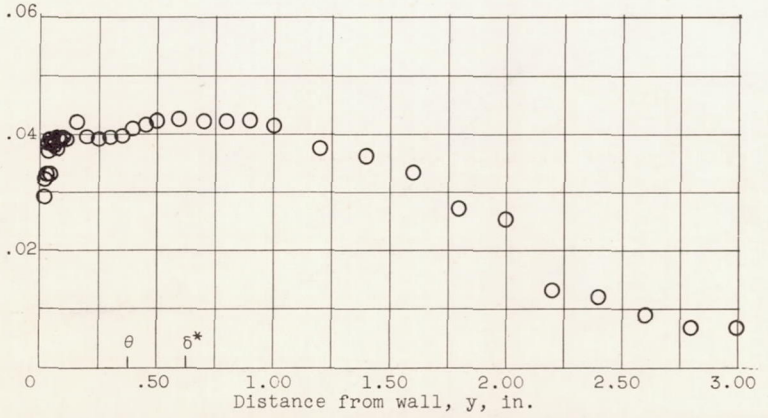

(d) Station 4.

Figure 12. - Distribution of $\sqrt{w^2}$ velocity fluctuations through boundary layer.

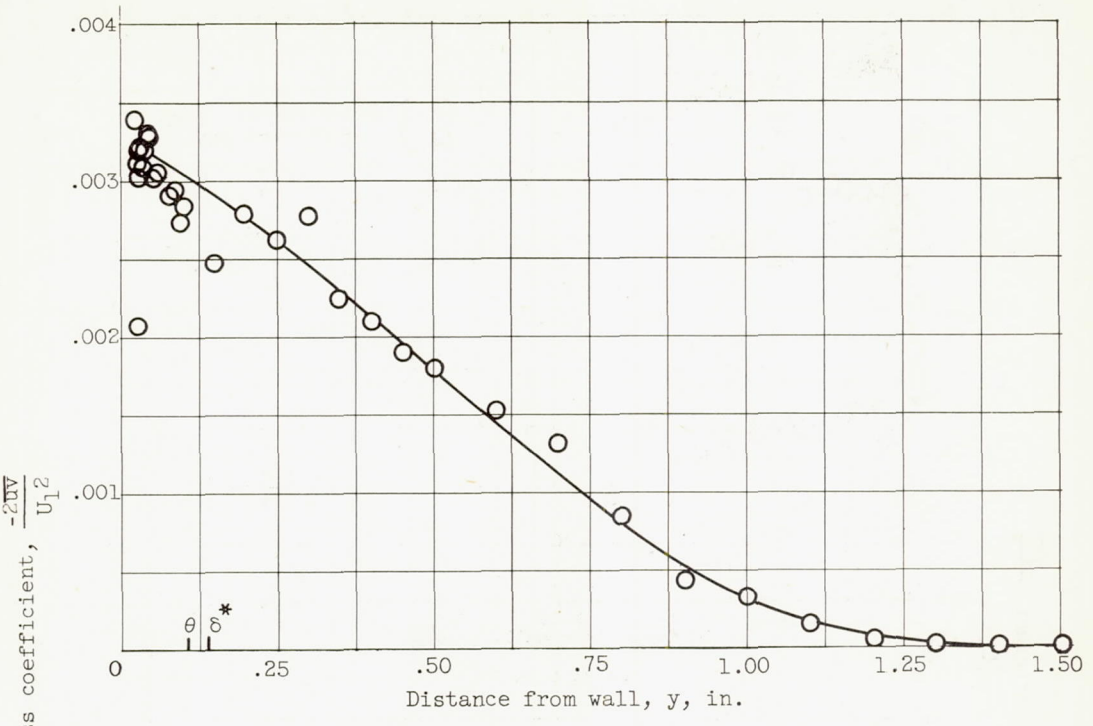

(a) Station 1.

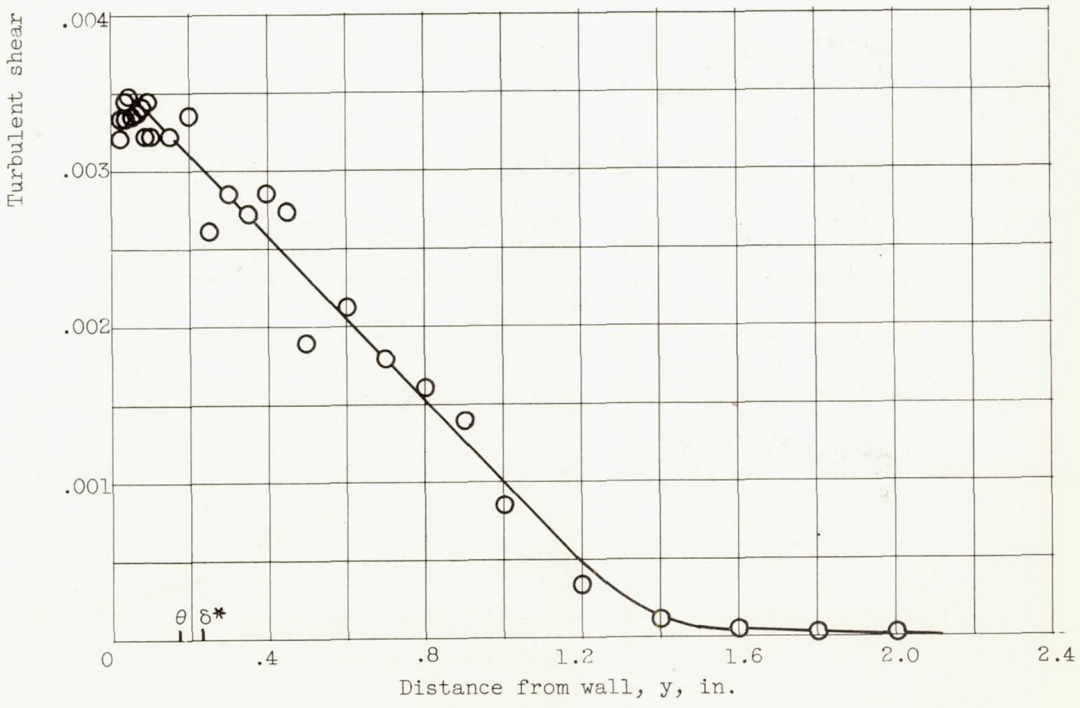

(b) Station 2.

Figure 13. - Turbulent shear stress distribution through boundary layer.

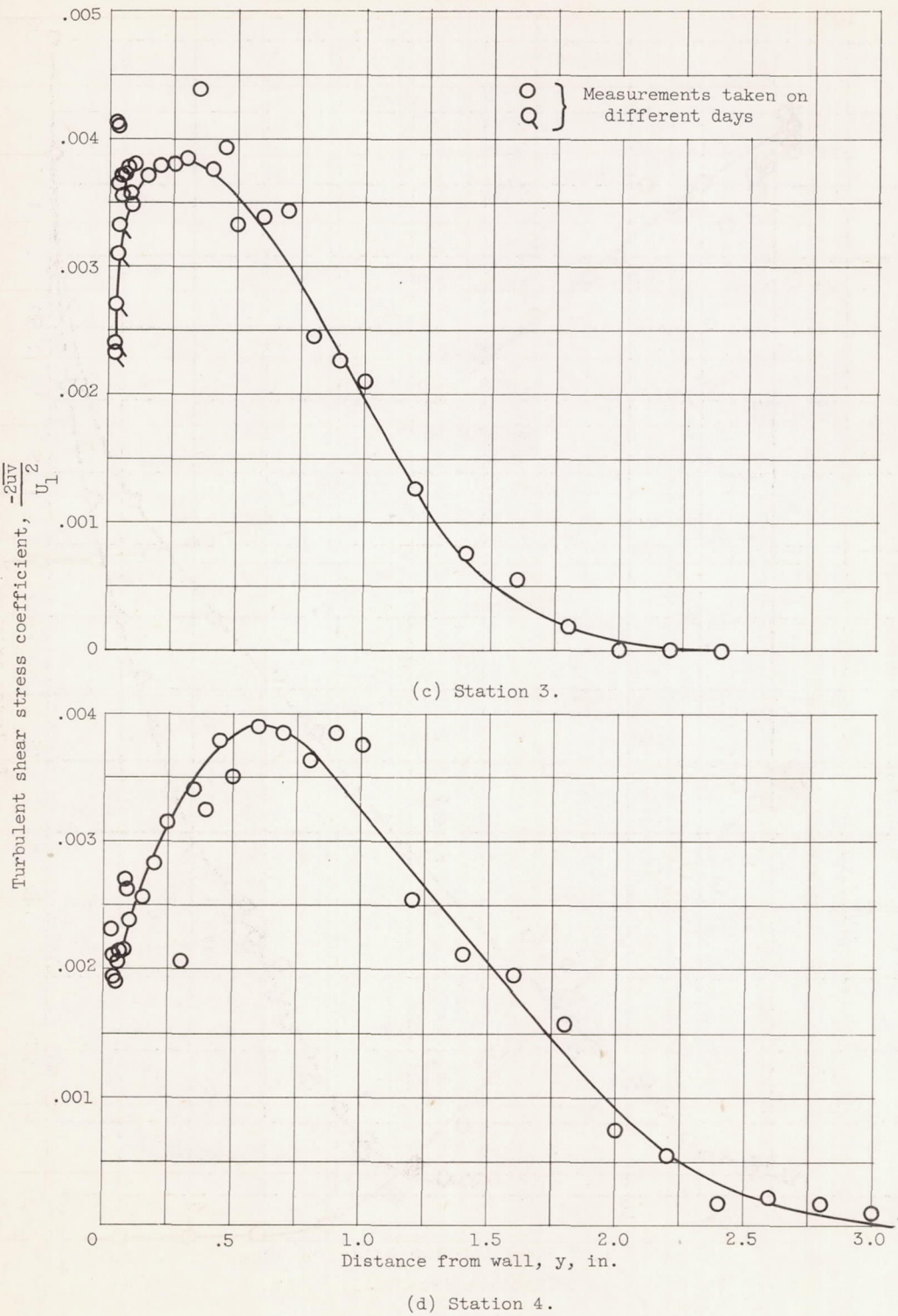

Figure 13. - Concluded. Turbulent shear stress distribution through boundary layer.

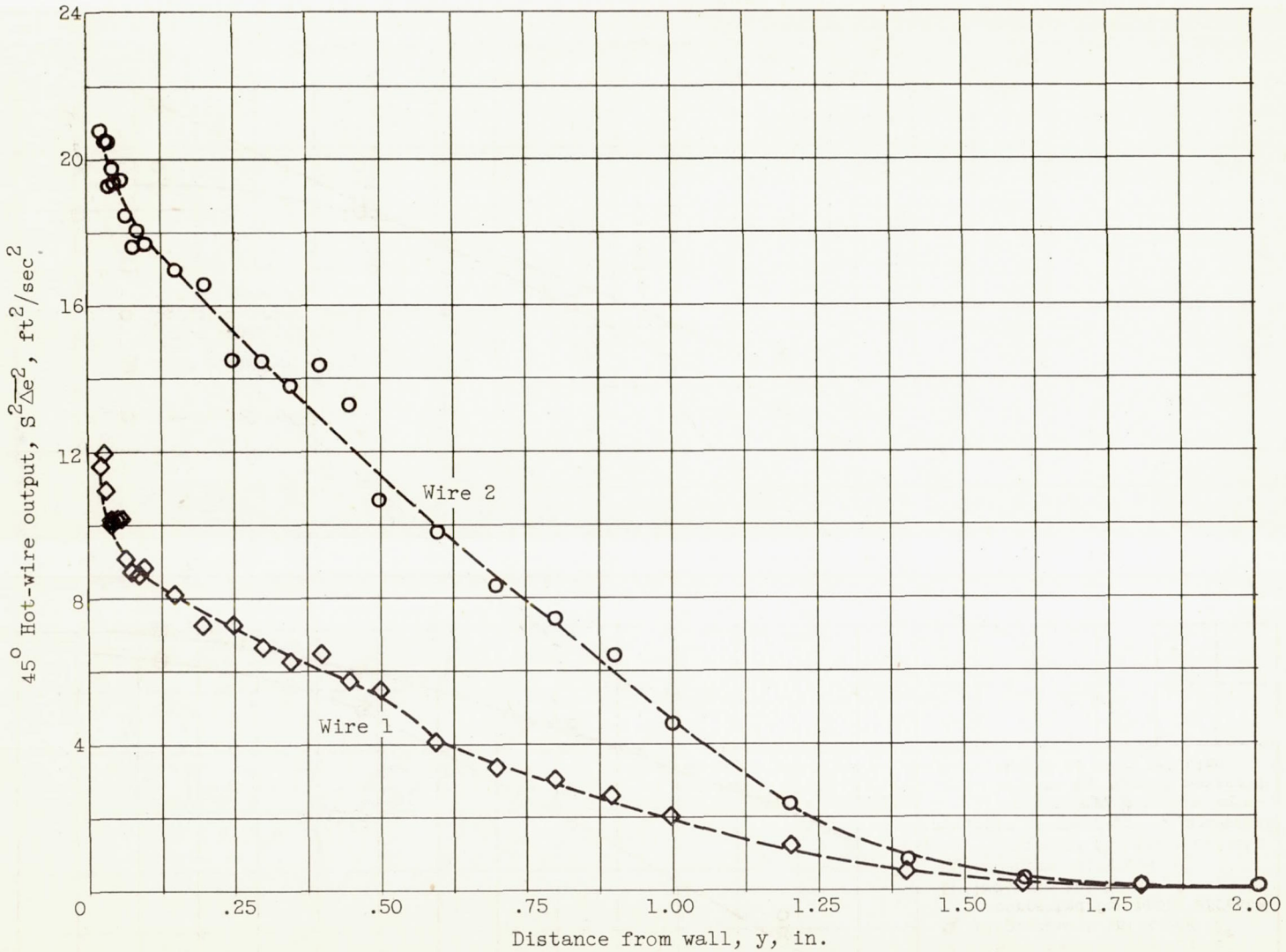

Figure 14. - Determination of $\overline{uv}$ from outputs of two hot wires at 45° to mean flow. Station 2.

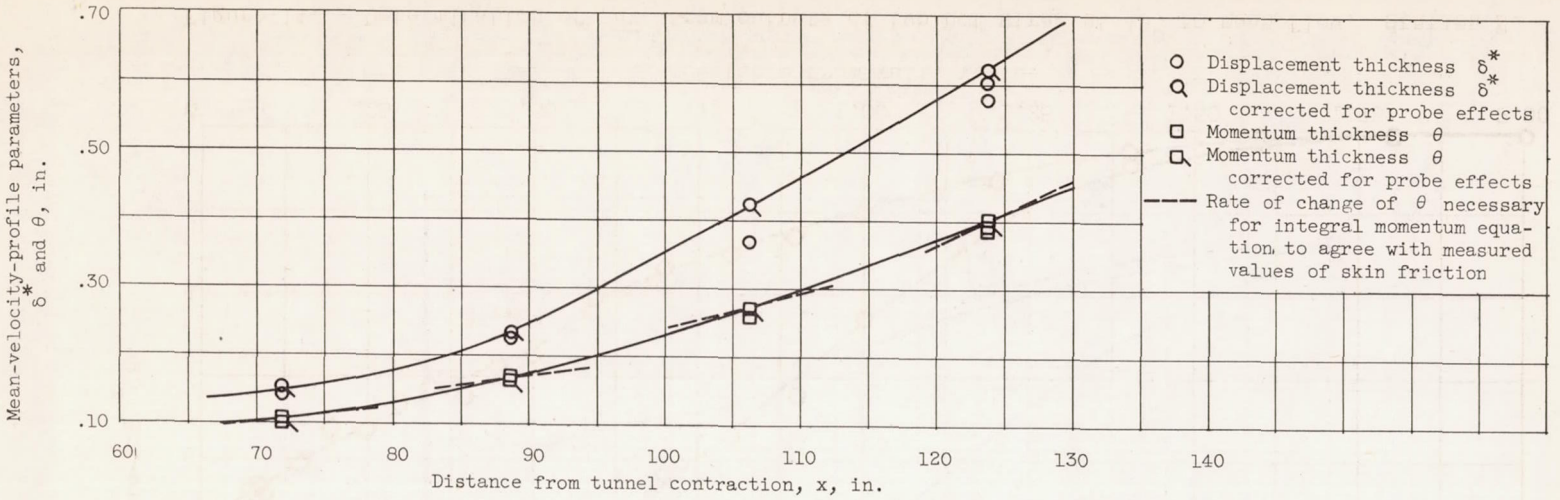

Figure 15. - Variation of mean-velocity-profile parameters along test wall.

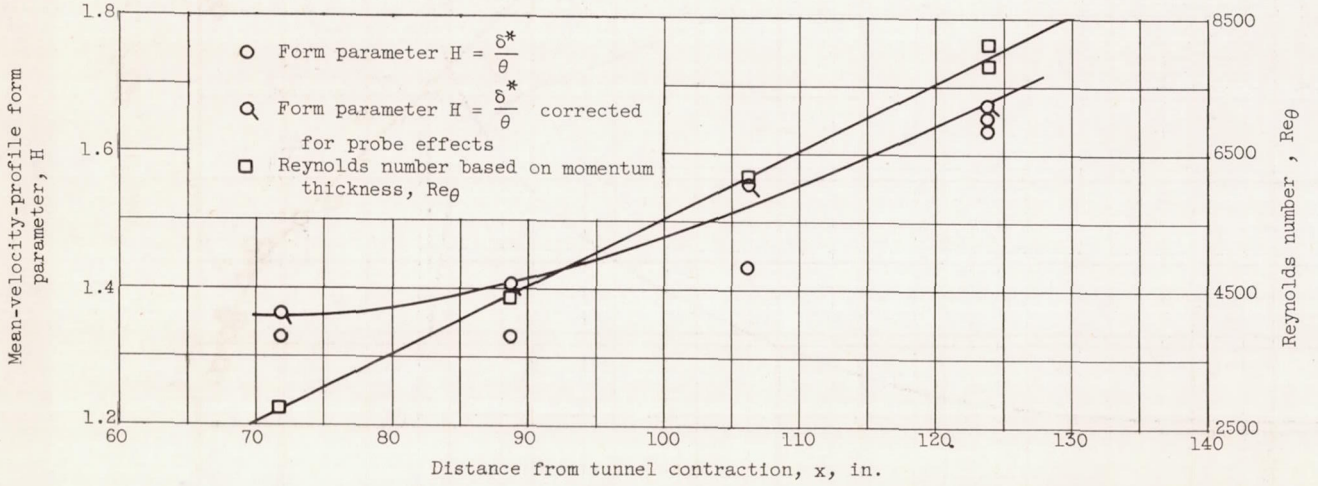

Figure 16. - Variation of mean-velocity-profile form parameter and Reynolds number along test wall.

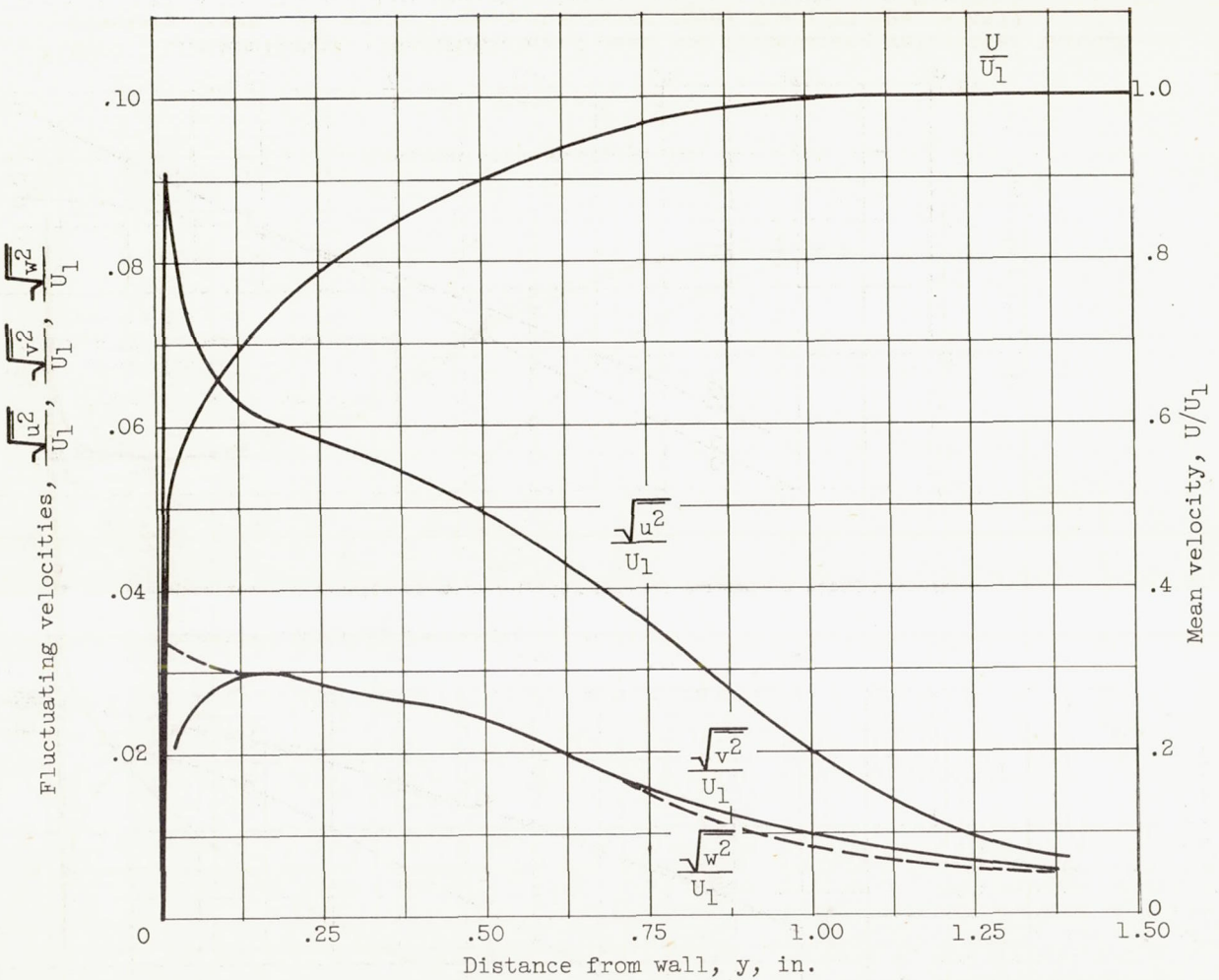

(a) Station 1.

Figure 17. - Distribution of mean and fluctuating velocities through boundary layer. δ^* = 0.136 inch; θ = 0.103 inch; H = 1.32; Re_θ = 2740.

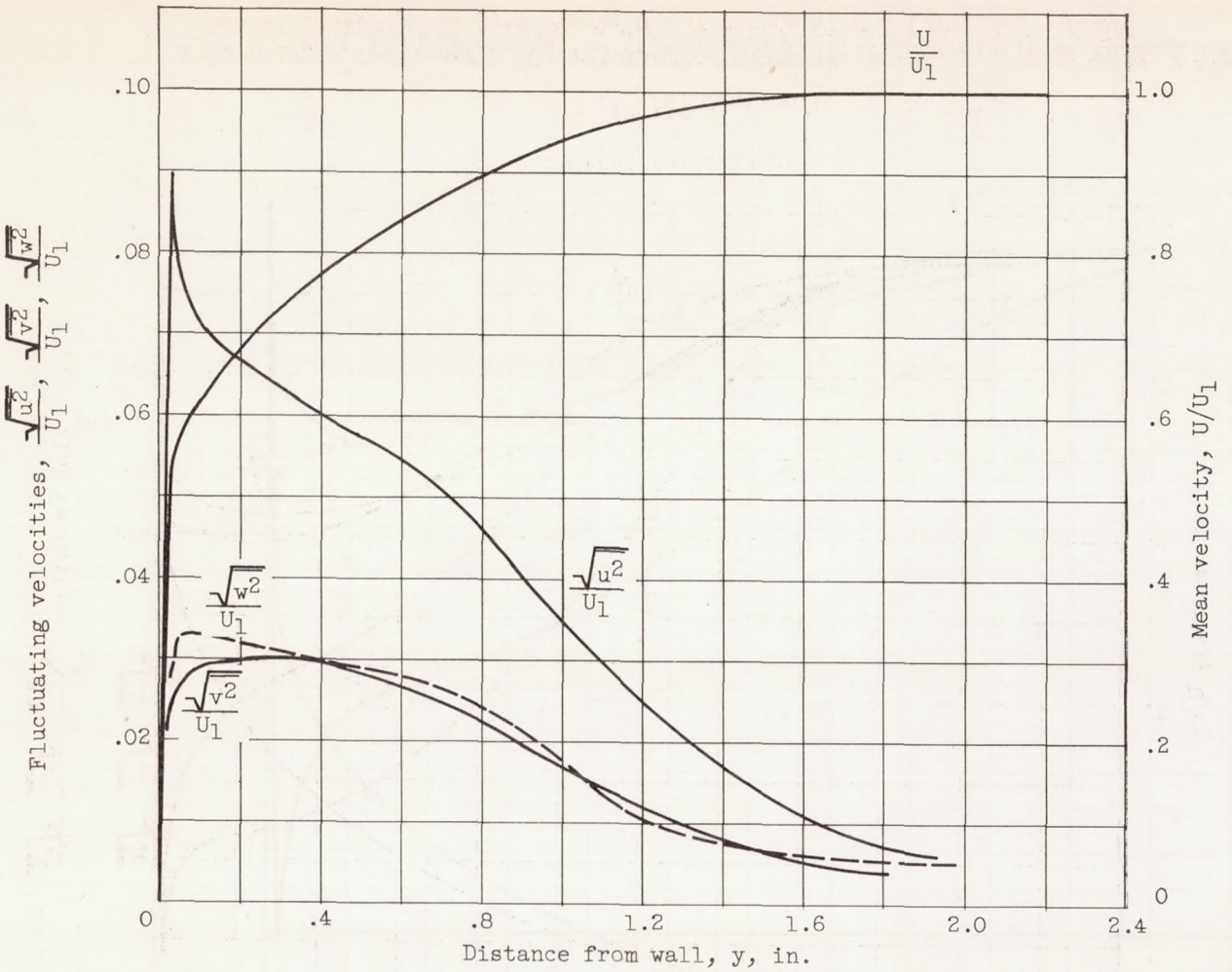

(b) Station 2.

Figure 17. - Continued. Distribution of mean and fluctuating velocities through boundary layer. δ^* = 0.225 inch; θ = 0.169 inch; H = 1.33; Re_θ = 4377.

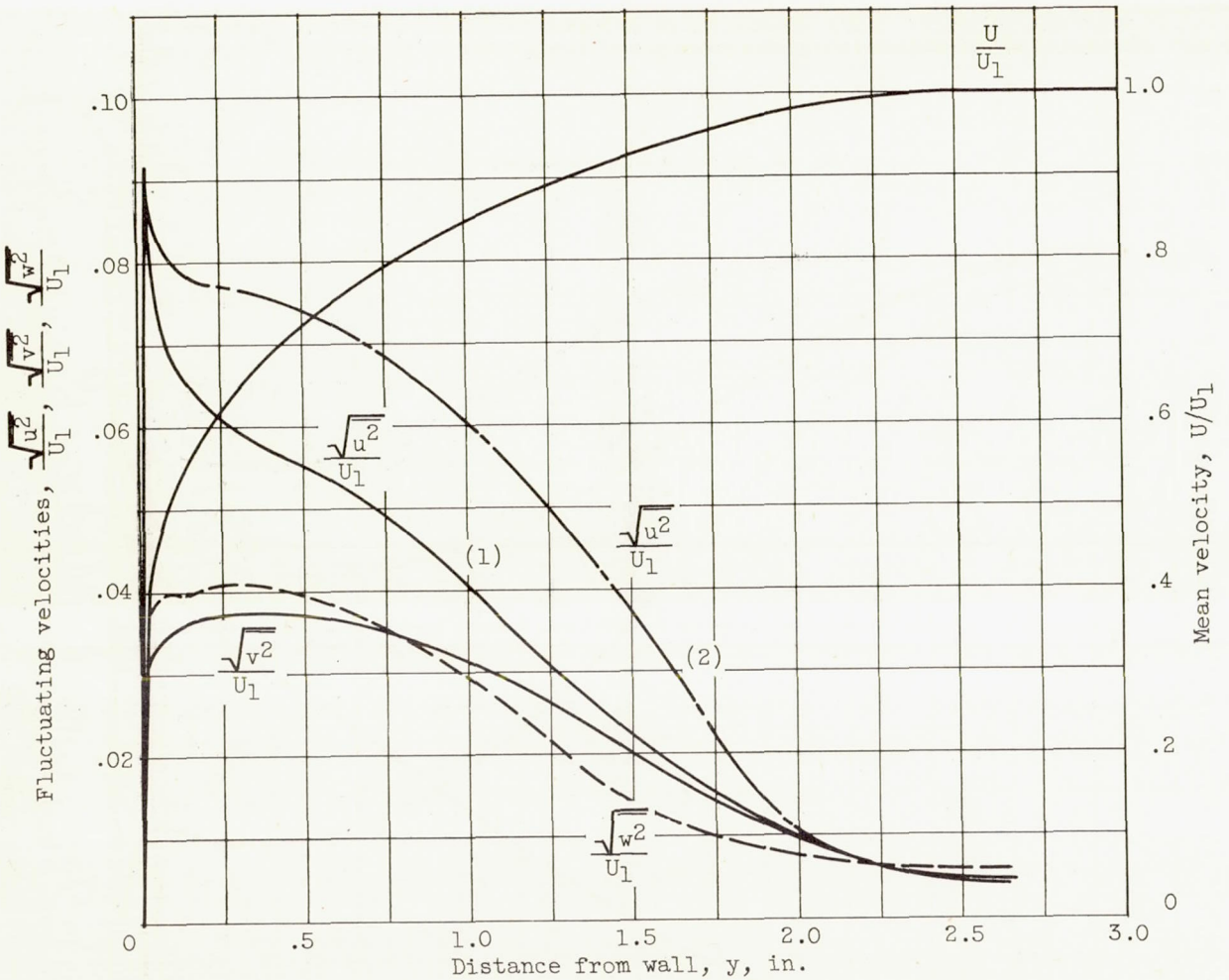

(c) Station 3.

Figure 17. - Continued. Distribution of mean and fluctuating velocities through boundary layer. δ^* = 0.369 inch; θ = 0.257 inch; H = 1.43; Re_θ = 6146.

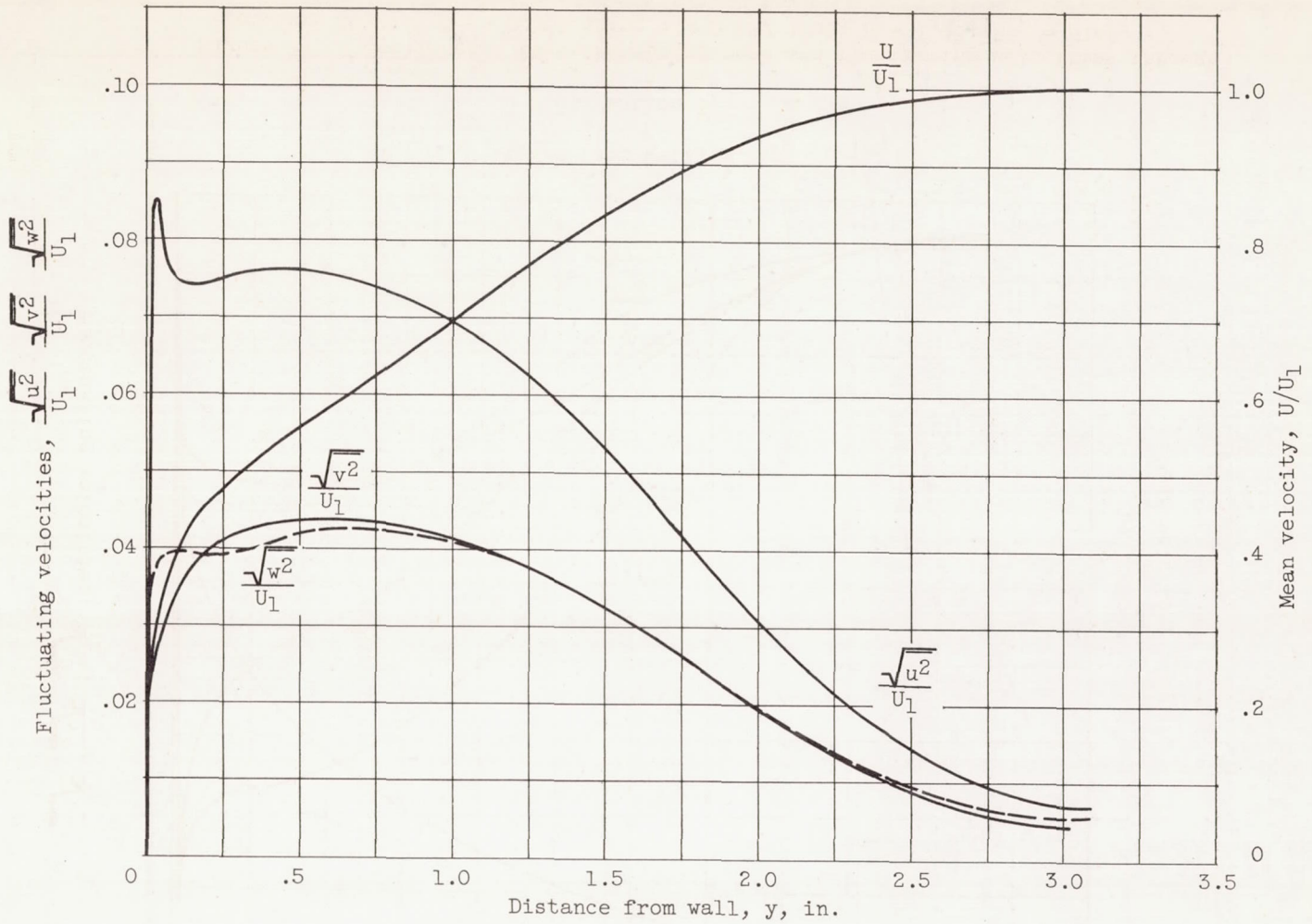

(d) Station 4.

Figure 17. – Concluded. Distribution of mean and fluctuating velocities through boundary layer. δ^* = 0.652 inch; θ = 0.393 inch; H = 1.65; Re_θ = 7800.

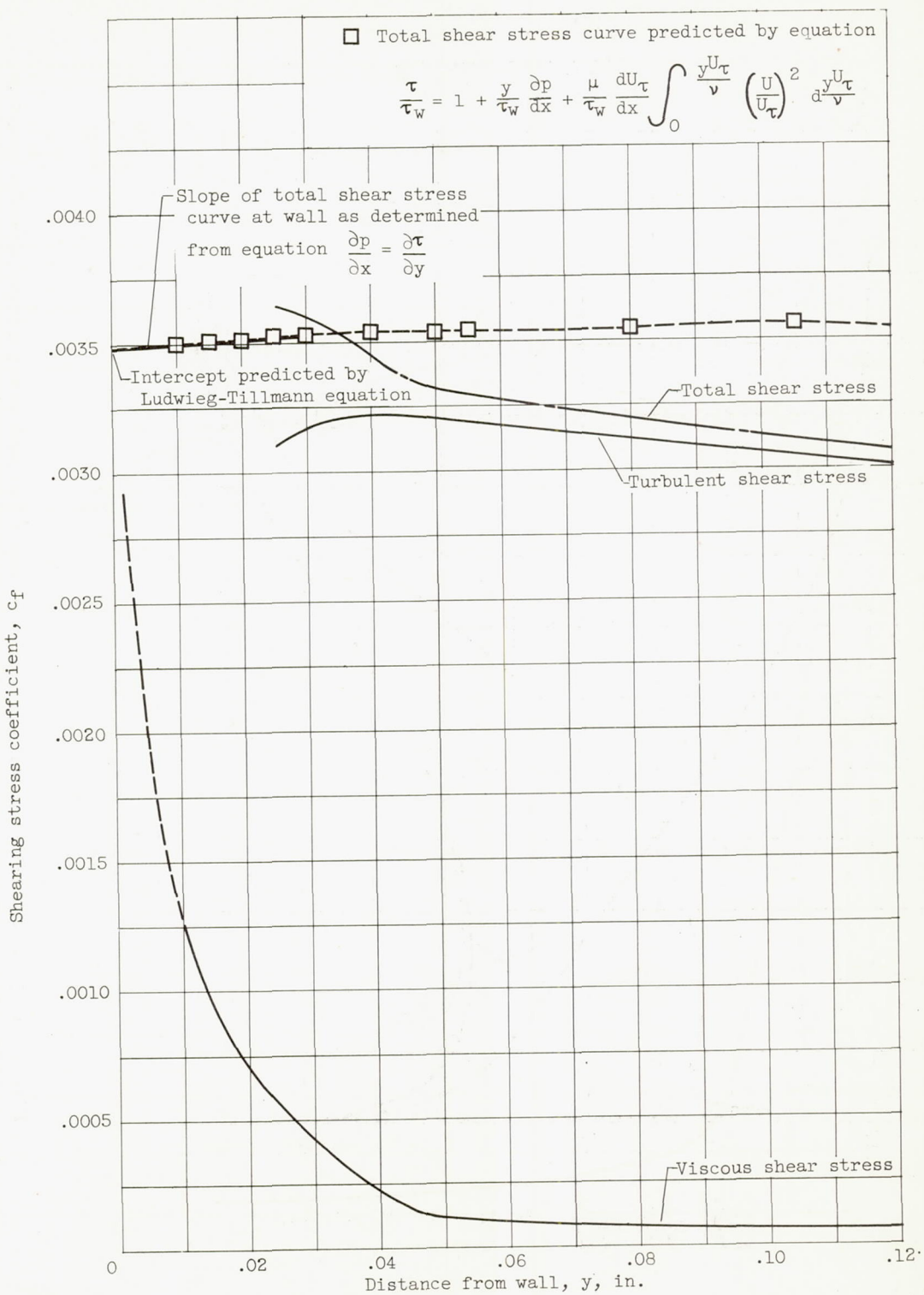

(a) Station 1.

Figure 18. - Shear stress distribution near wall.

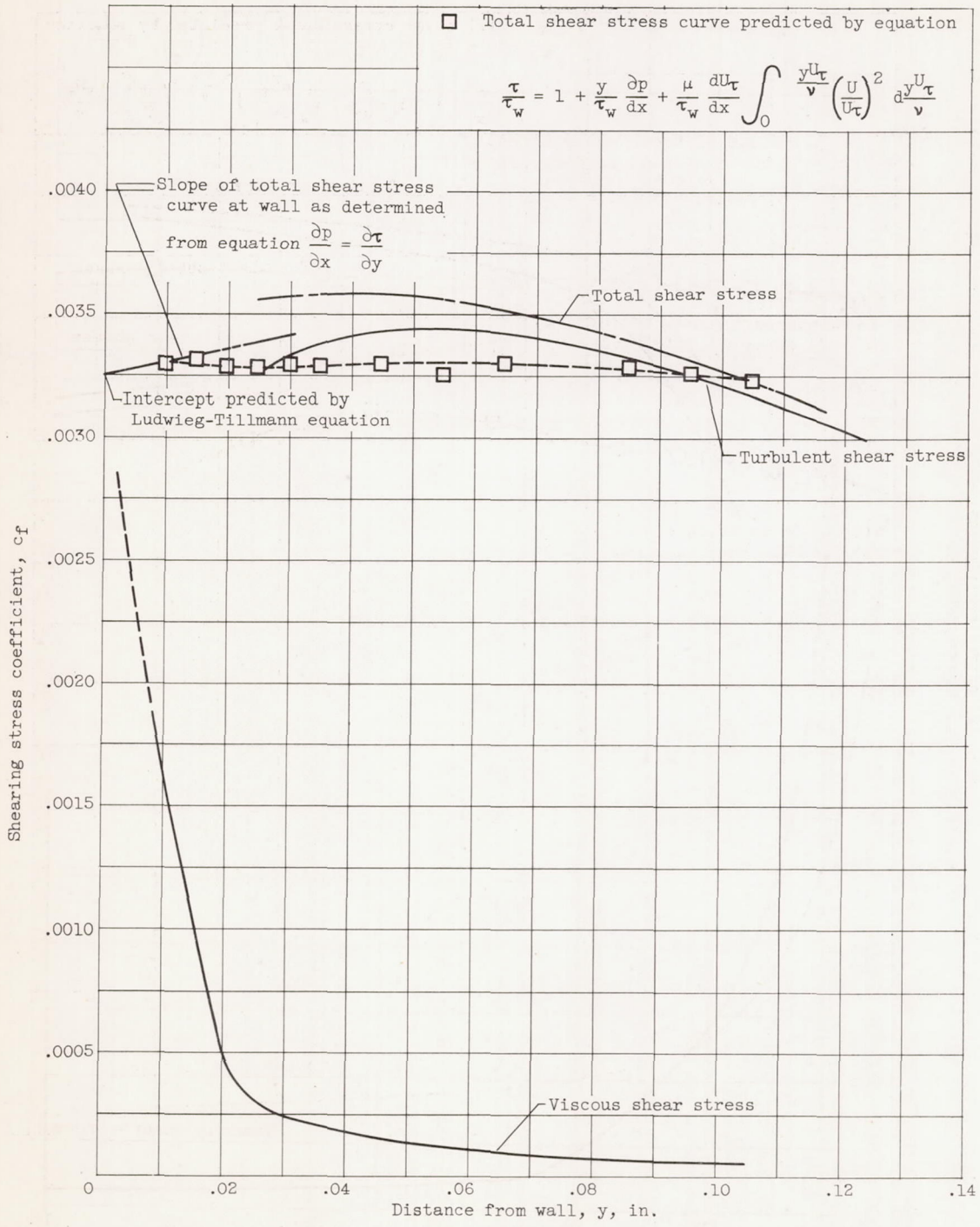

(b) Station 2.

Figure 18. - Continued. Shear stress distribution near wall.

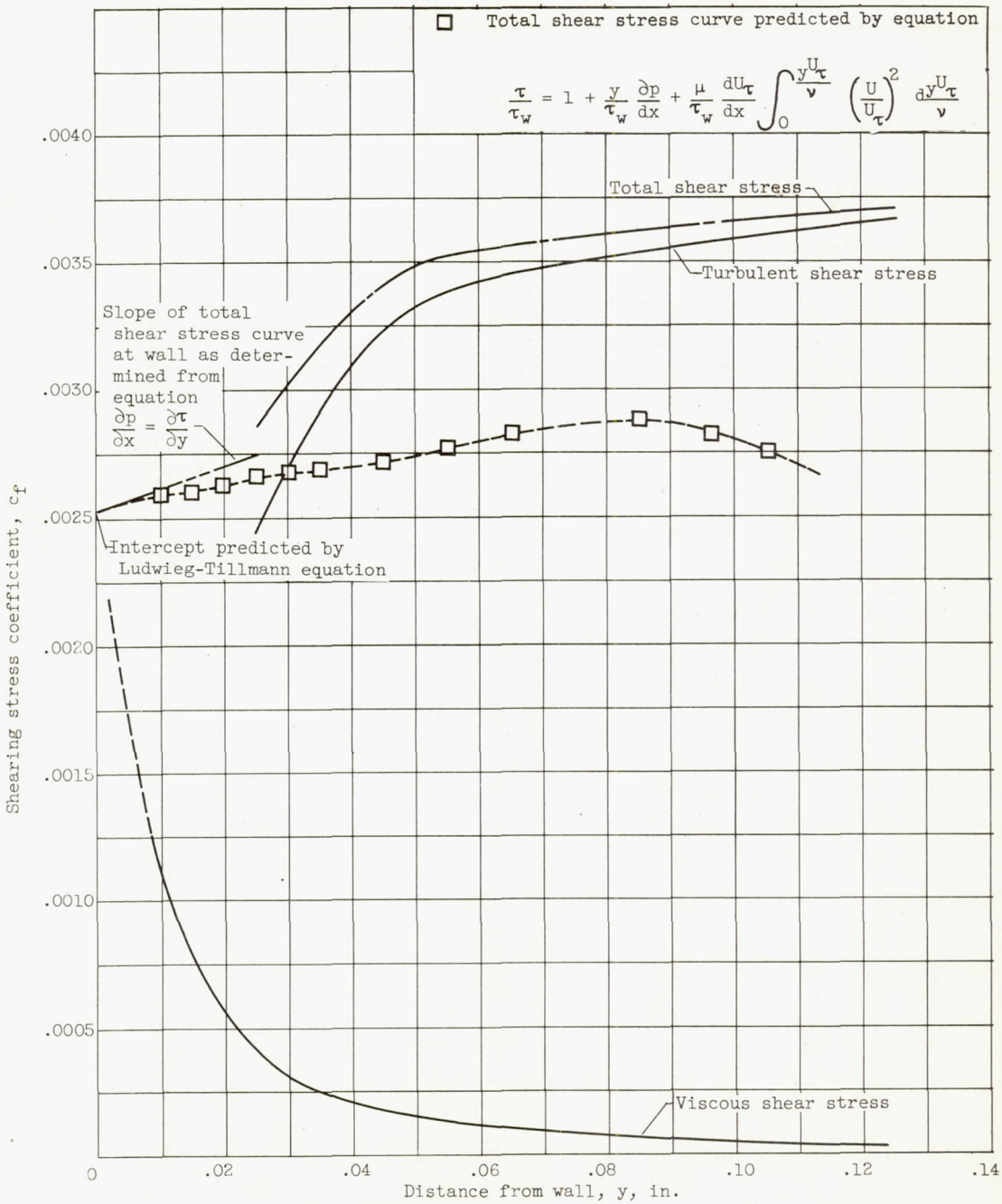

(c) Station 3.

Figure 18. - Continued. Shear stress distribution near wall.

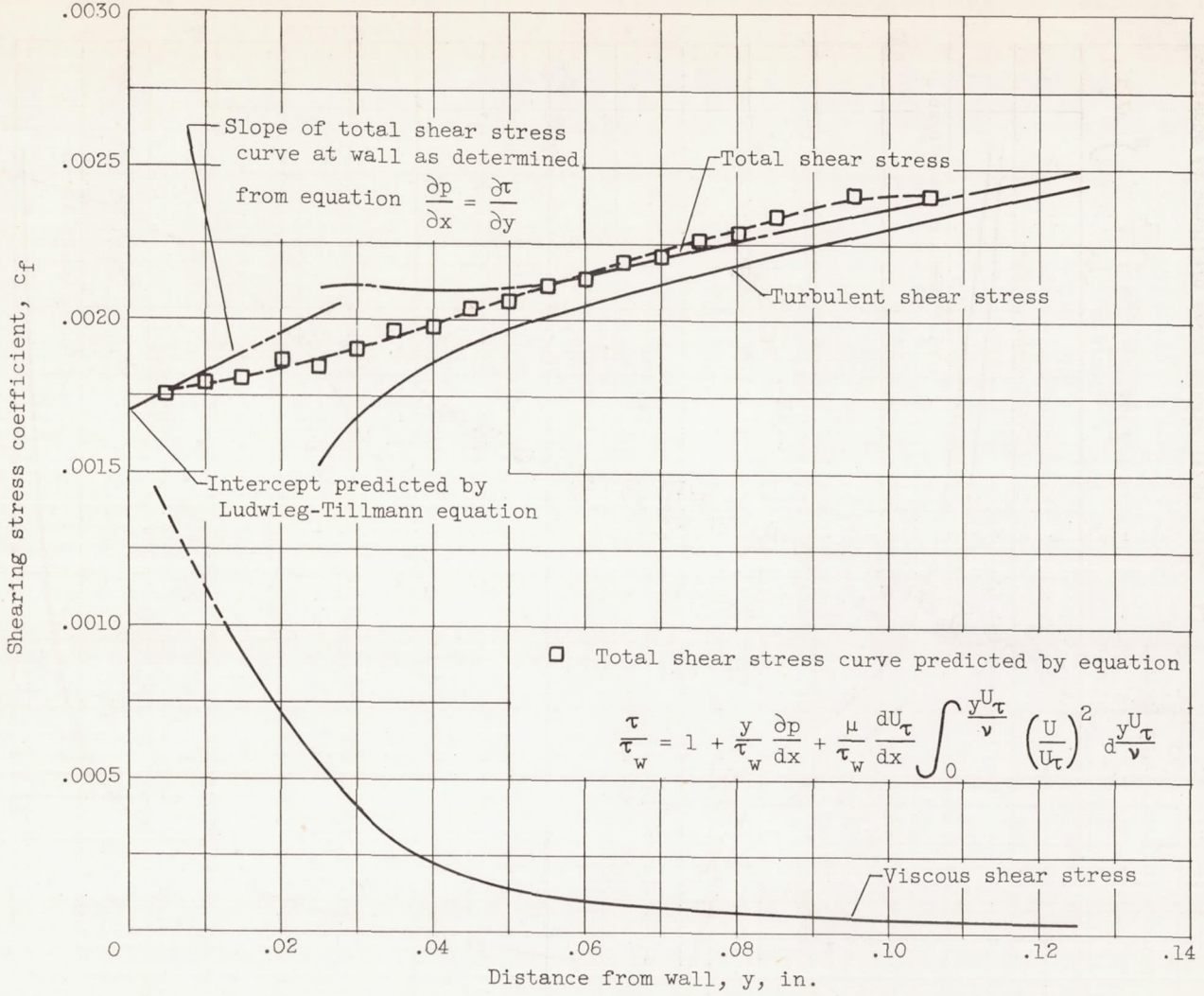

(d) Station 4.

Figure 18. - Concluded. Shear stress distribution near wall.

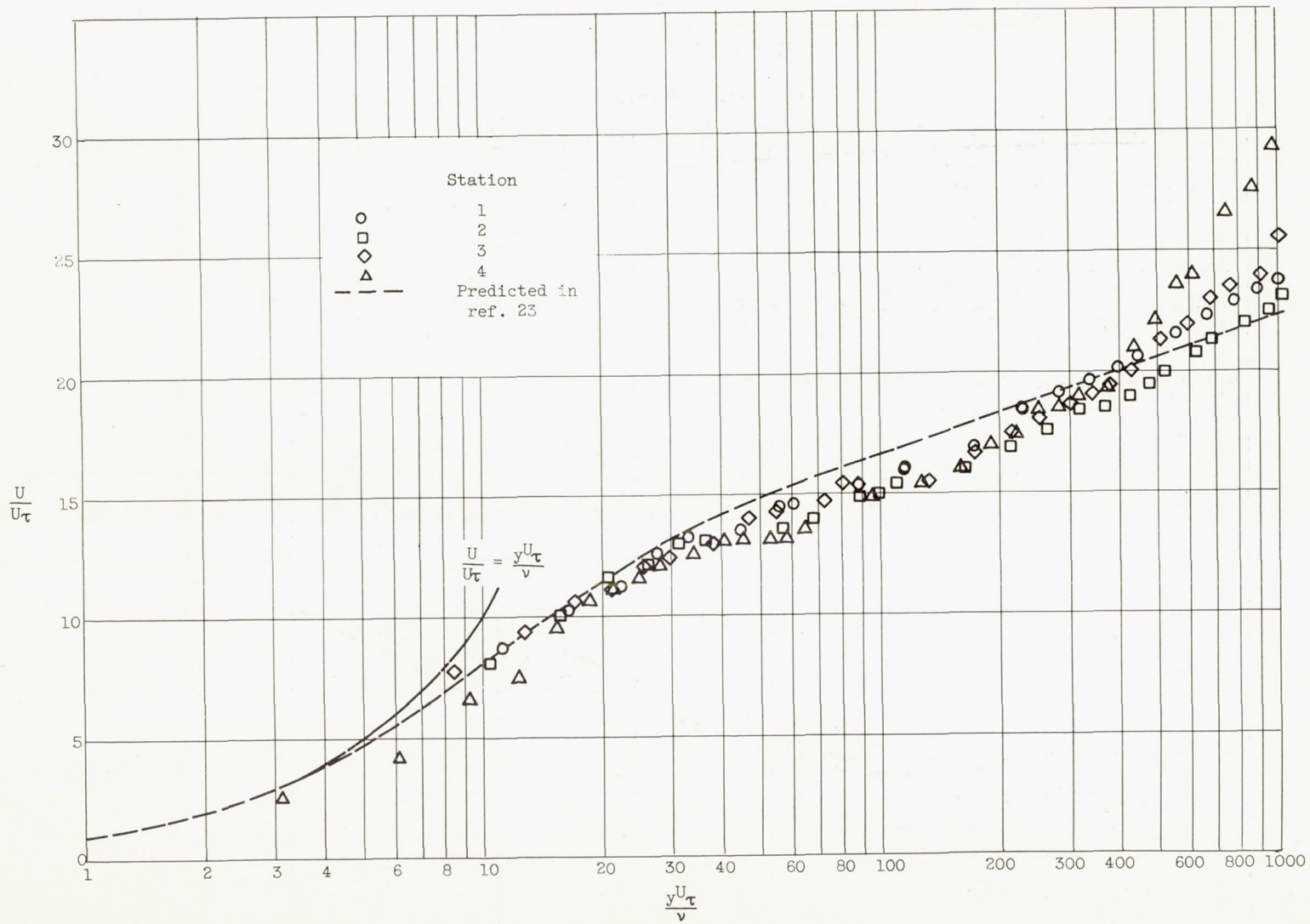

Figure 19. - Semilogarithmic plot of mean velocity distribution near wall.

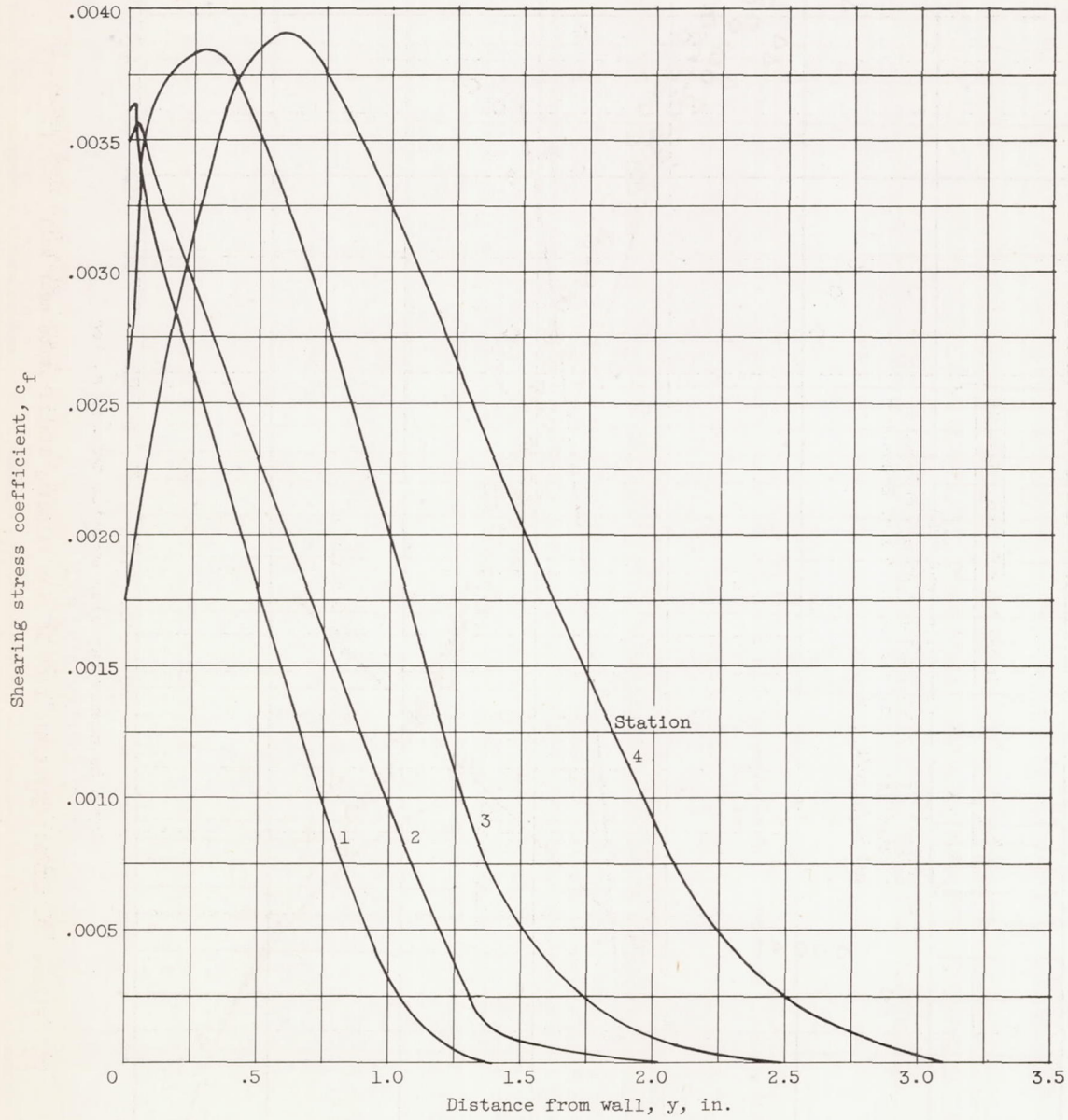

Figure 20. - Total shear stress distribution through boundary layer.

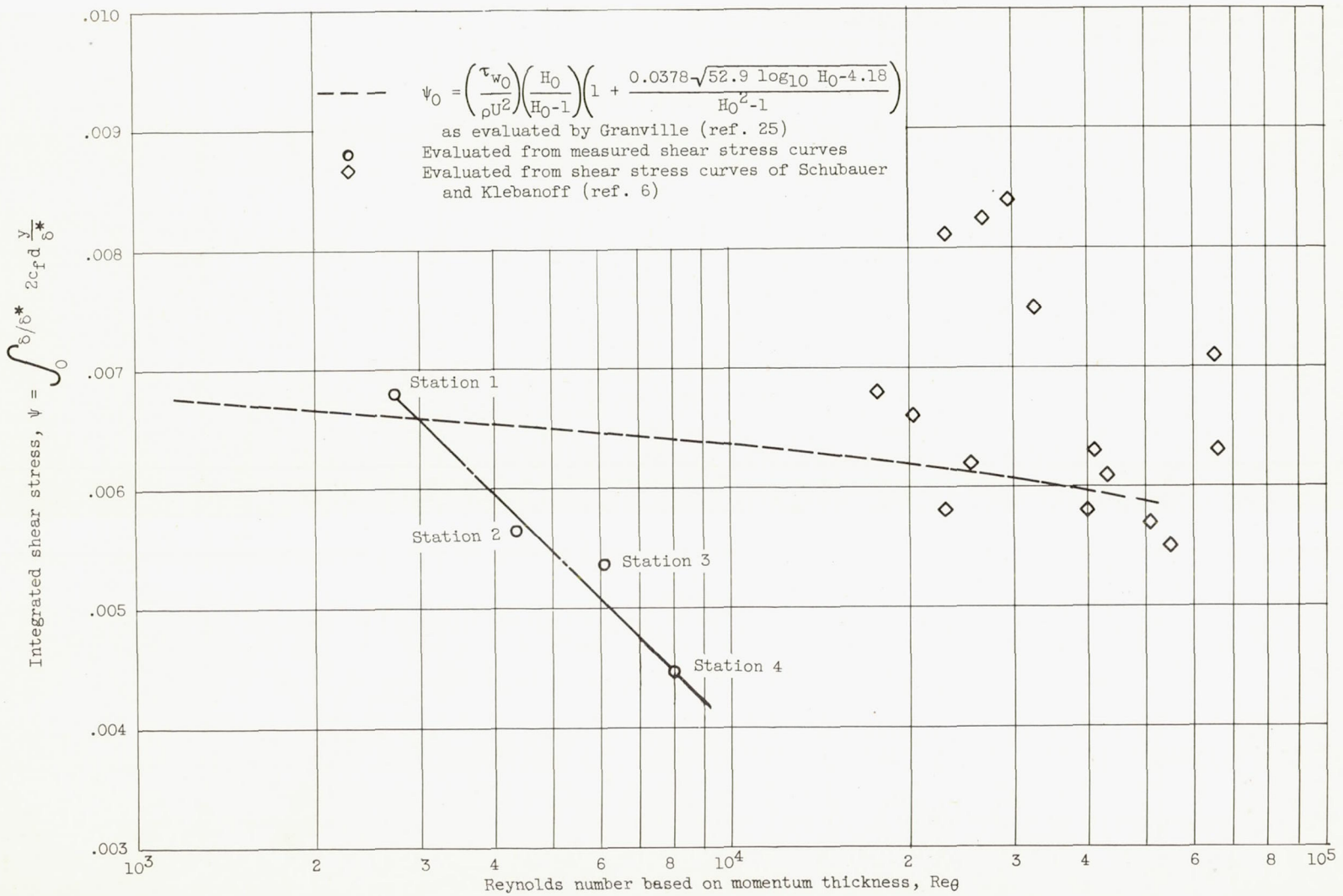

Figure 21. - Semilogarithmic plot of variation of shear stress integral with Reynolds number.

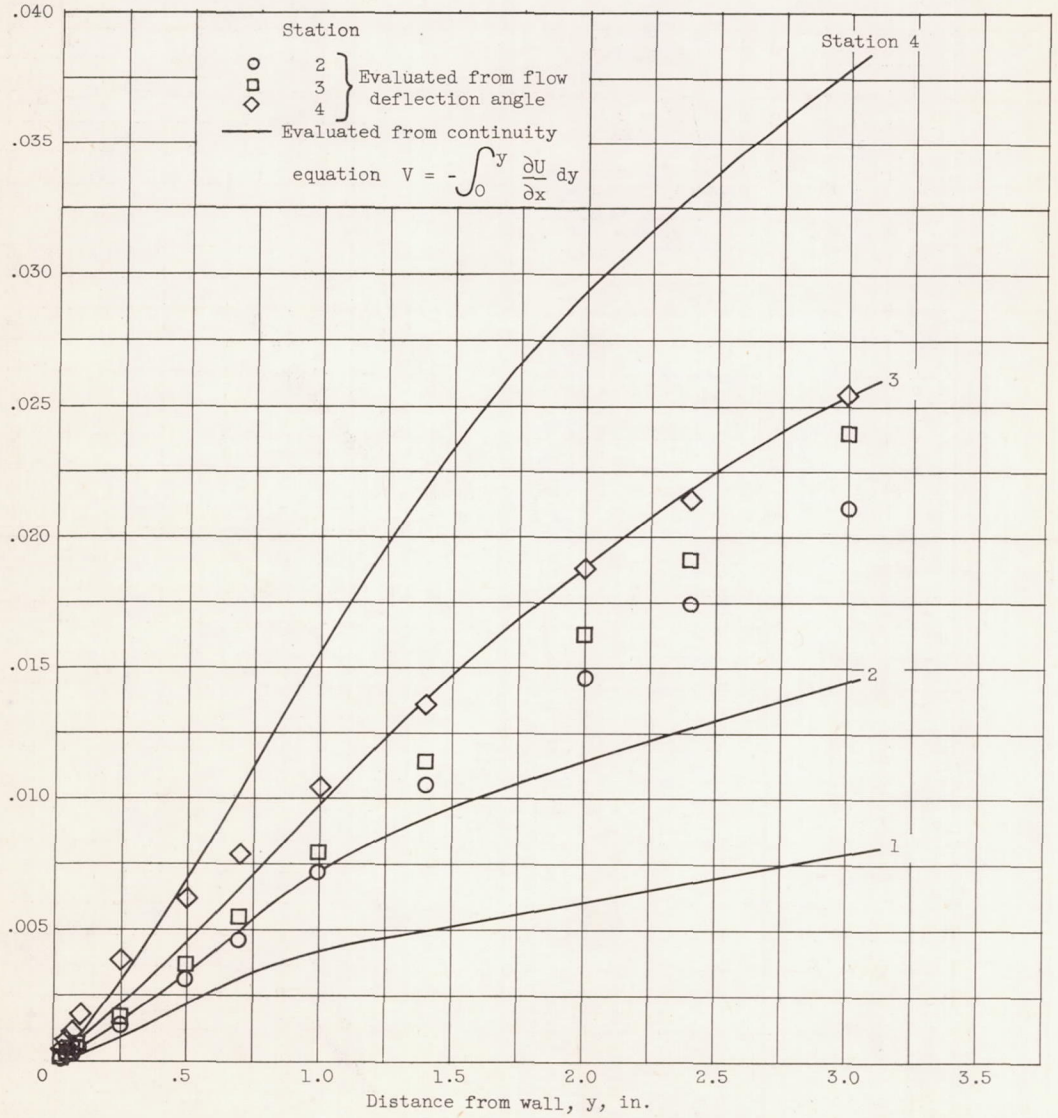

Figure 22. - Variation across boundary layer of mean velocity component normal to boundary.

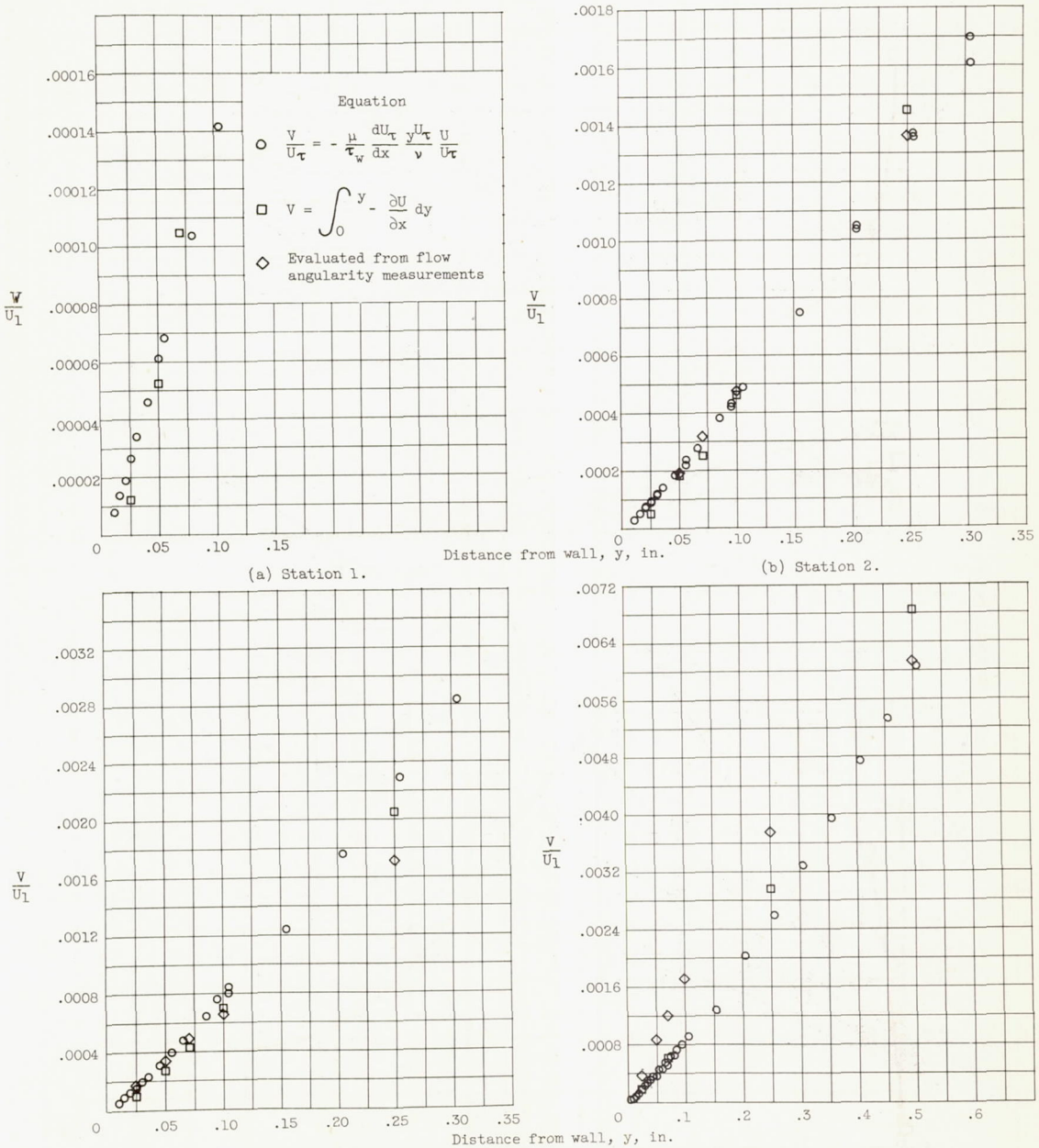

Figure 23. - Predicted values of mean V velocity near wall.

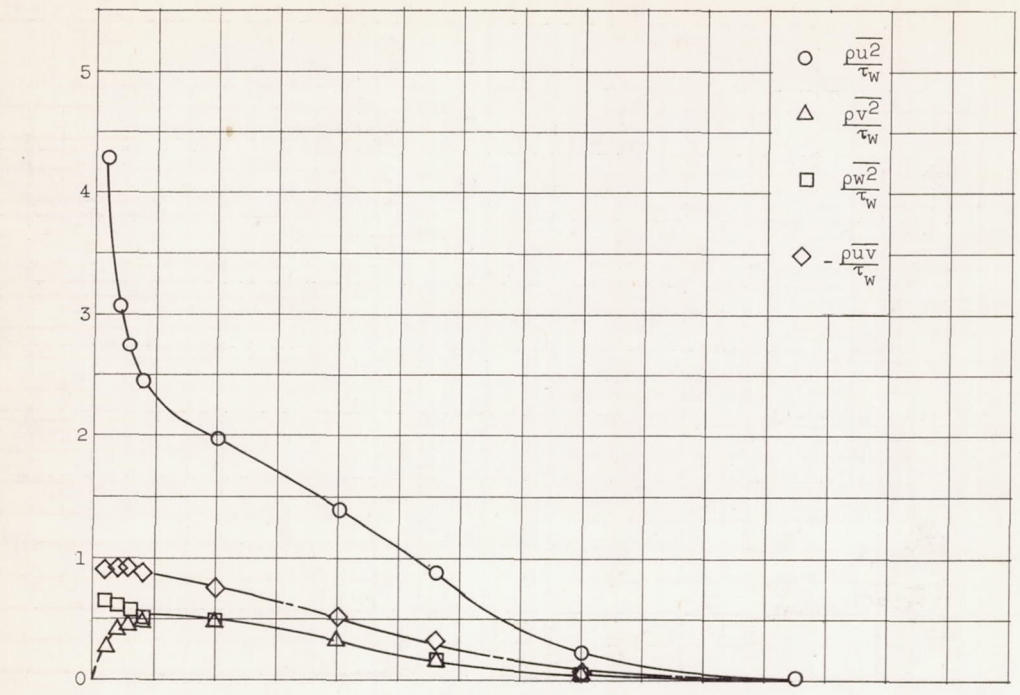

(a) Station 1; turbulent motion.

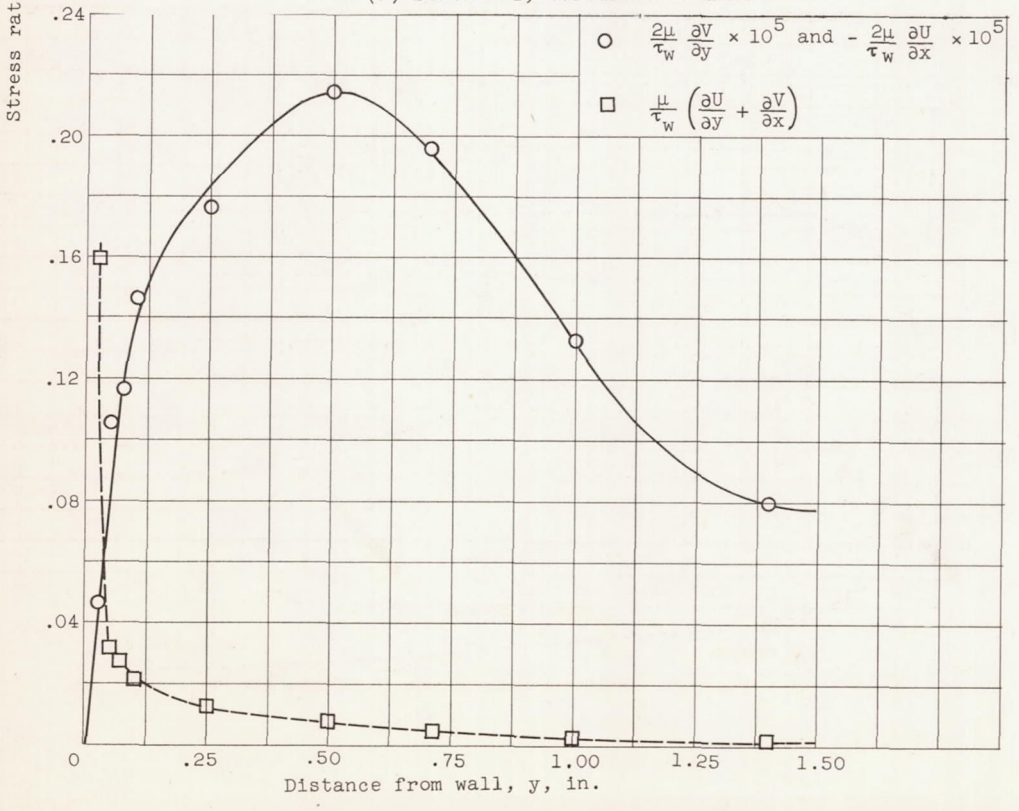

(b) Station 1; mean motion. $\frac{p}{\tau_w} = 178{,}700$

Figure 24. - Distribution of stress terms through boundary layer.

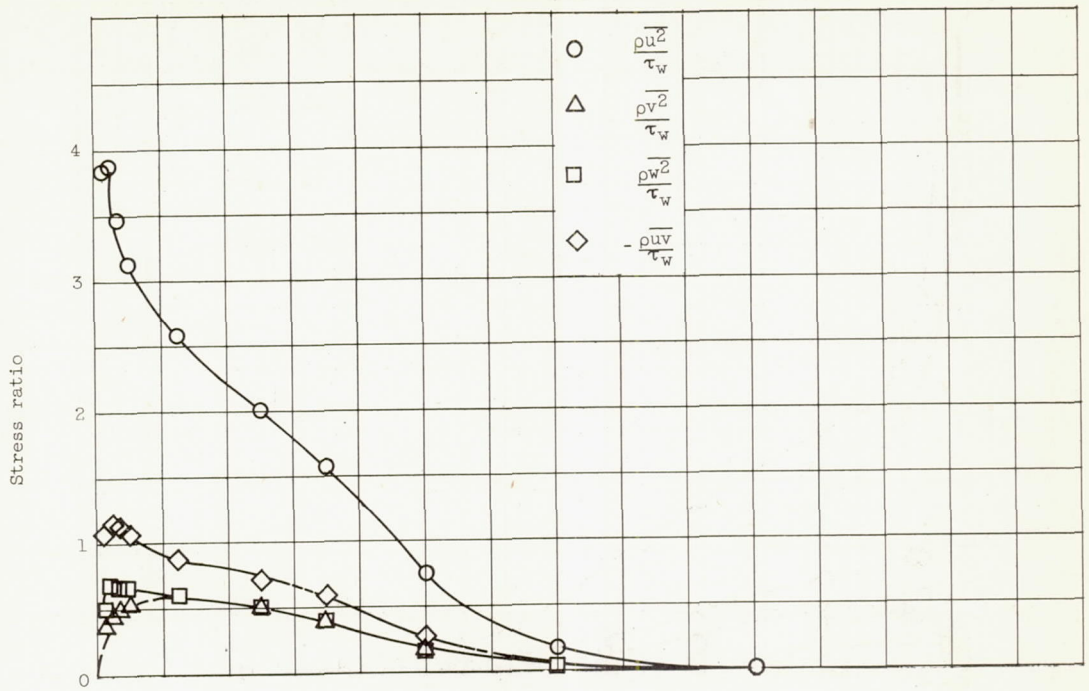

(c) Station 2; turbulent motion.

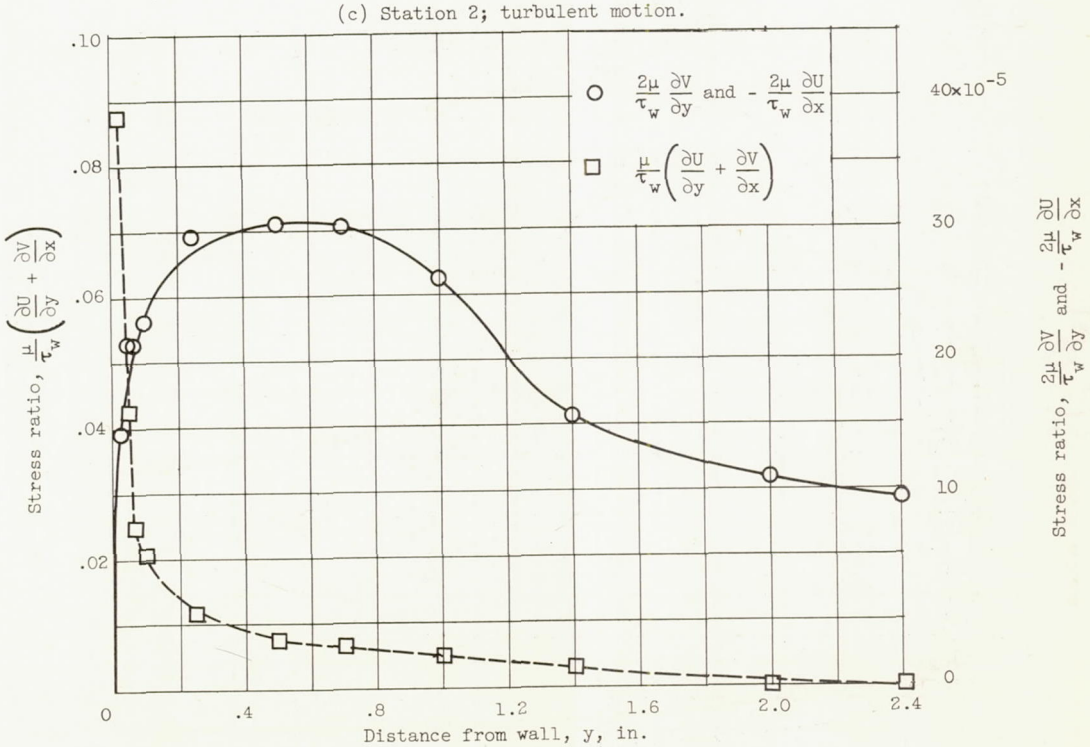

(d) Station 2; mean motion. $\frac{p}{\tau_w} = 203{,}400$

Figure 24. - Continued. Distribution of stress terms through boundary layer.

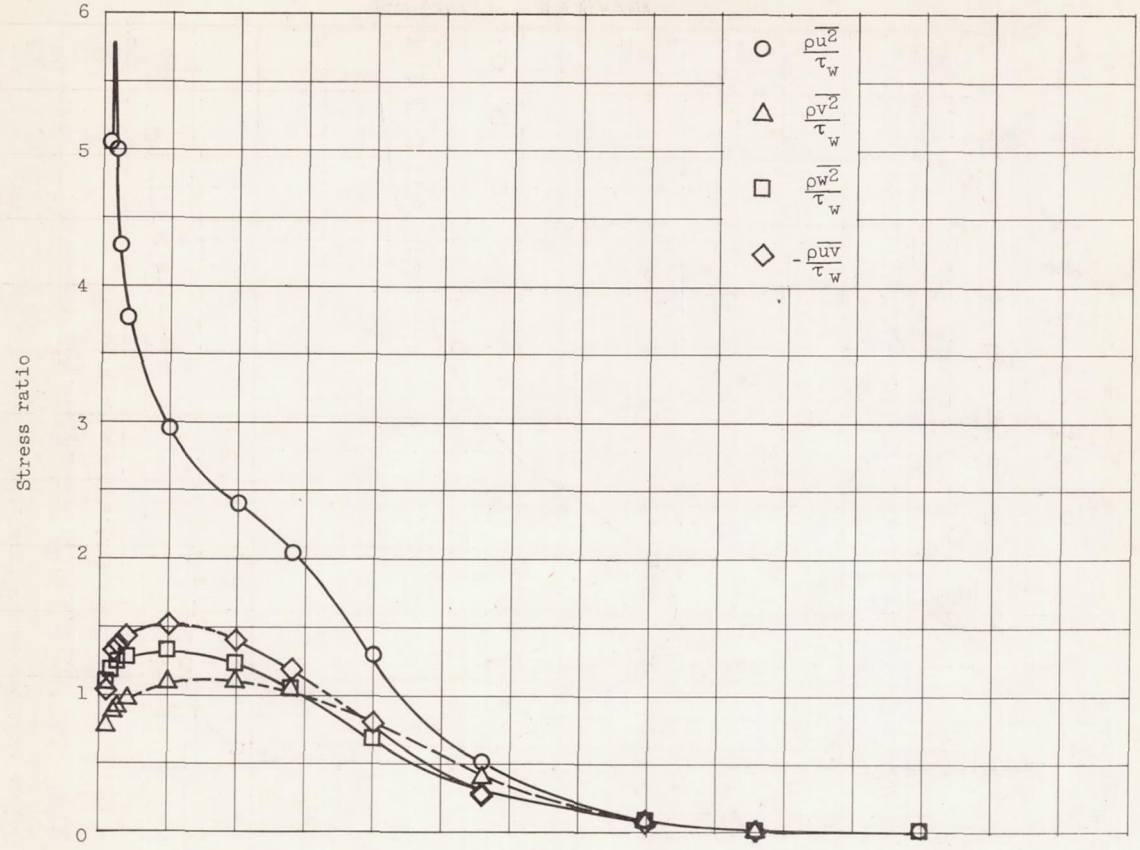

(e) Station 3; turbulent motion.

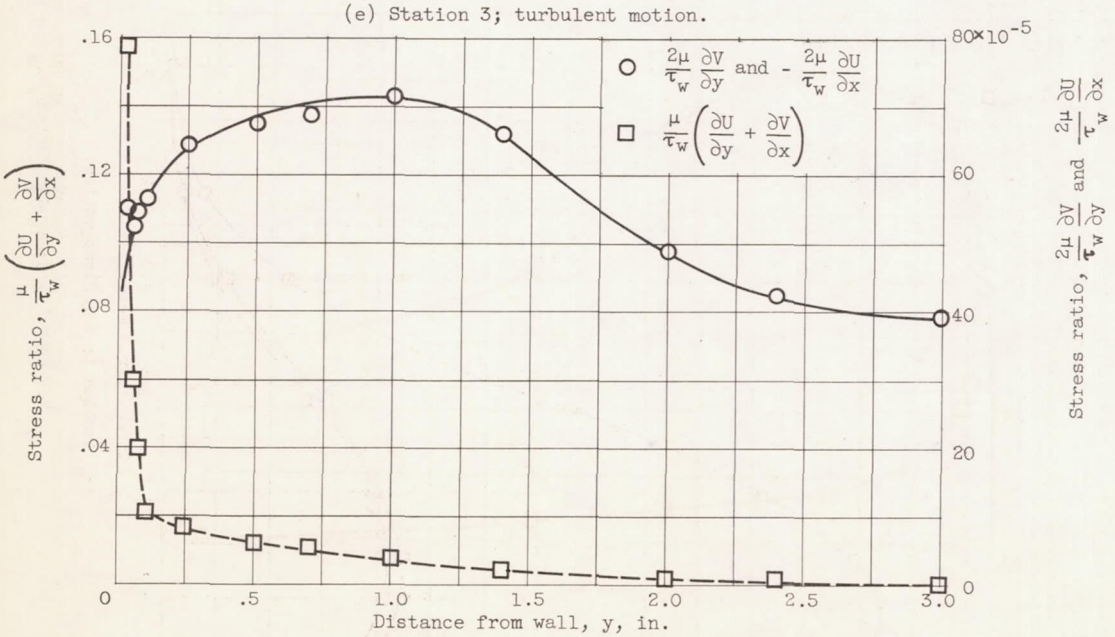

(f) Station 3; mean motion. $\frac{p}{\tau_w} = 308{,}900$

Figure 24. - Continued. Distribution of stress terms through boundary layer.

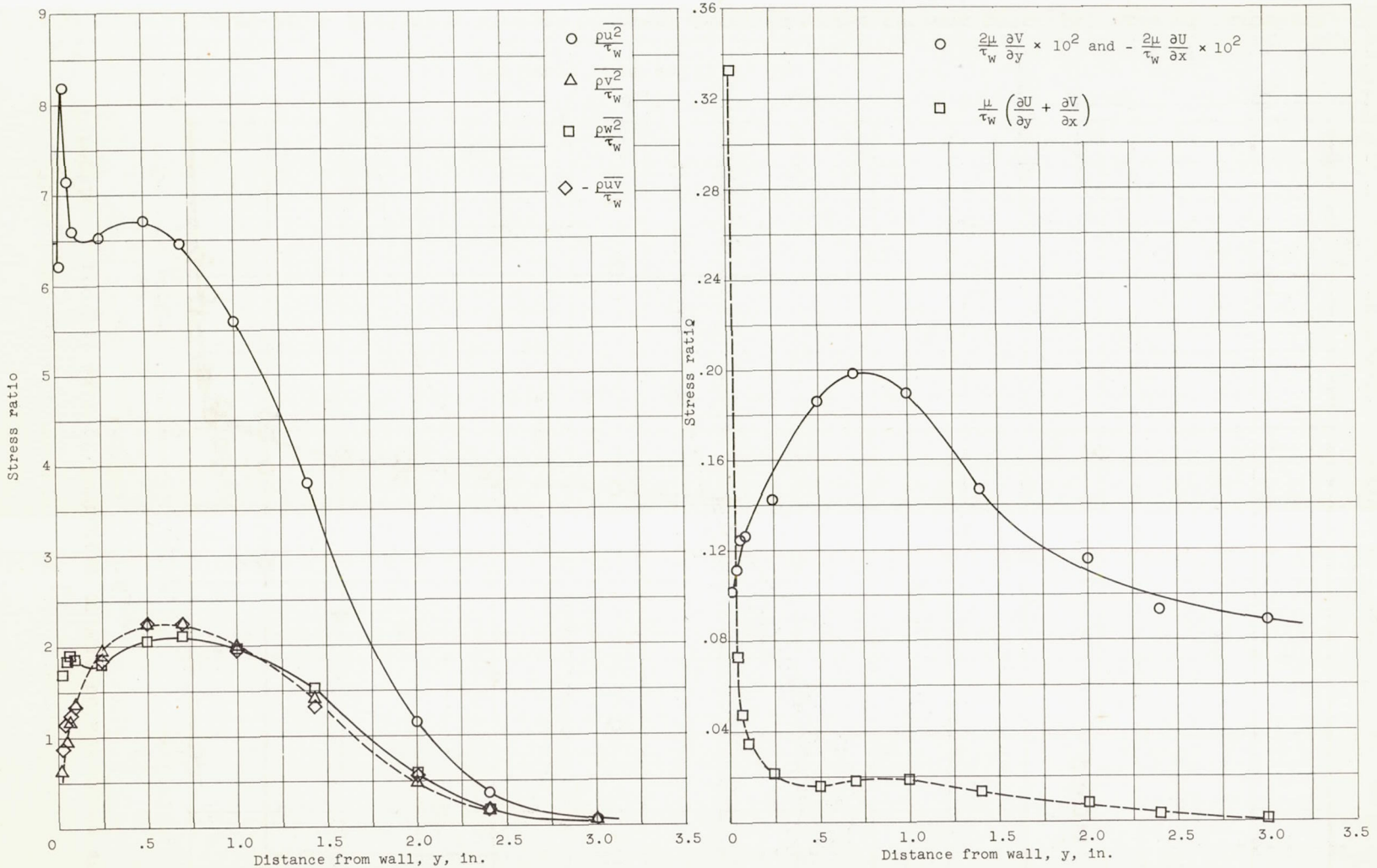

(g) Station 4; turbulent motion.

(h) Station 4; mean motion. $\frac{p}{\tau_w} = 579{,}800$

Figure 24. - Concluded. Distribution of stress terms through boundary layer.

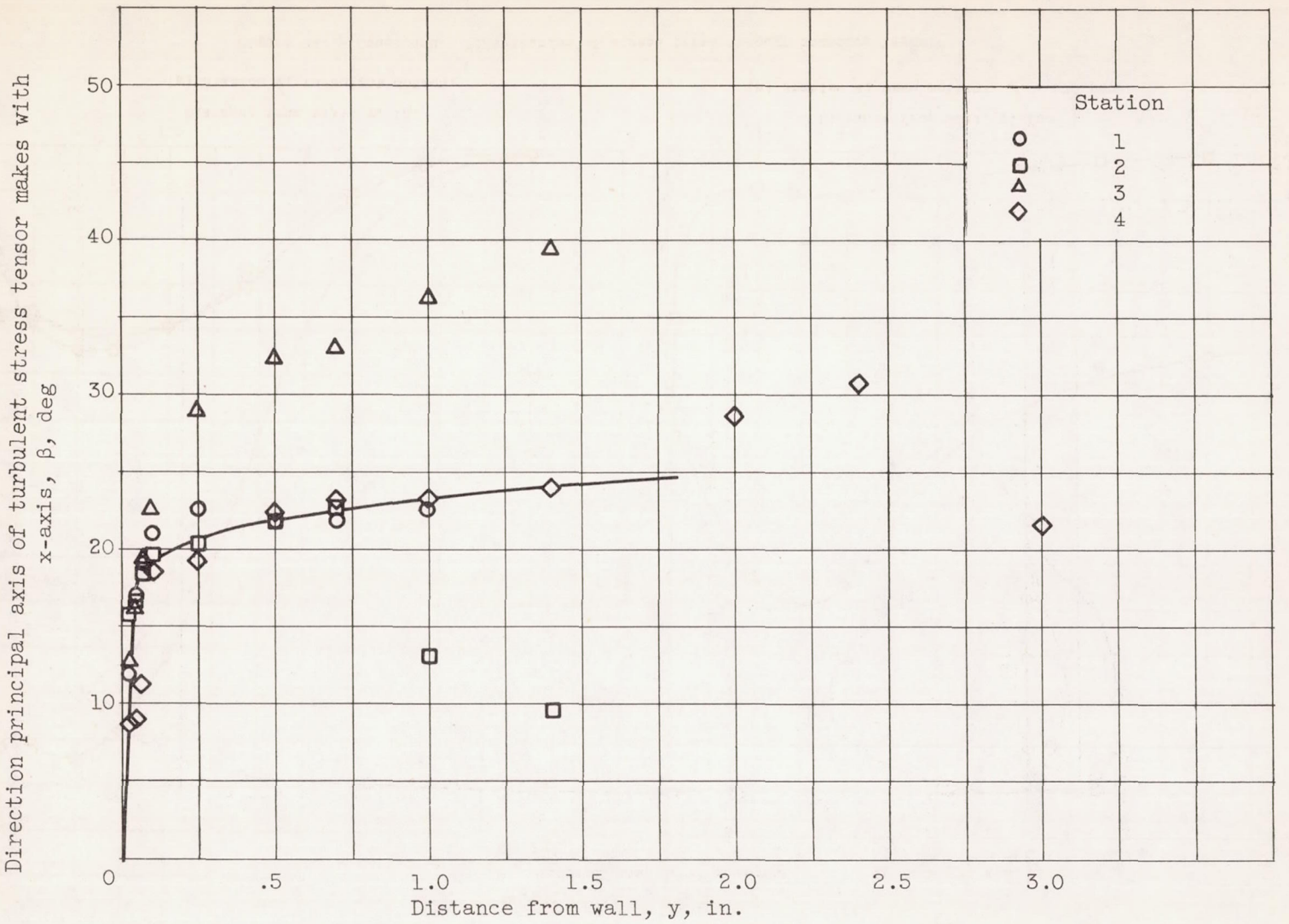

Figure 25. - Variation through boundary layer of angle between principal axis of turbulent stress tensor and x-axis.

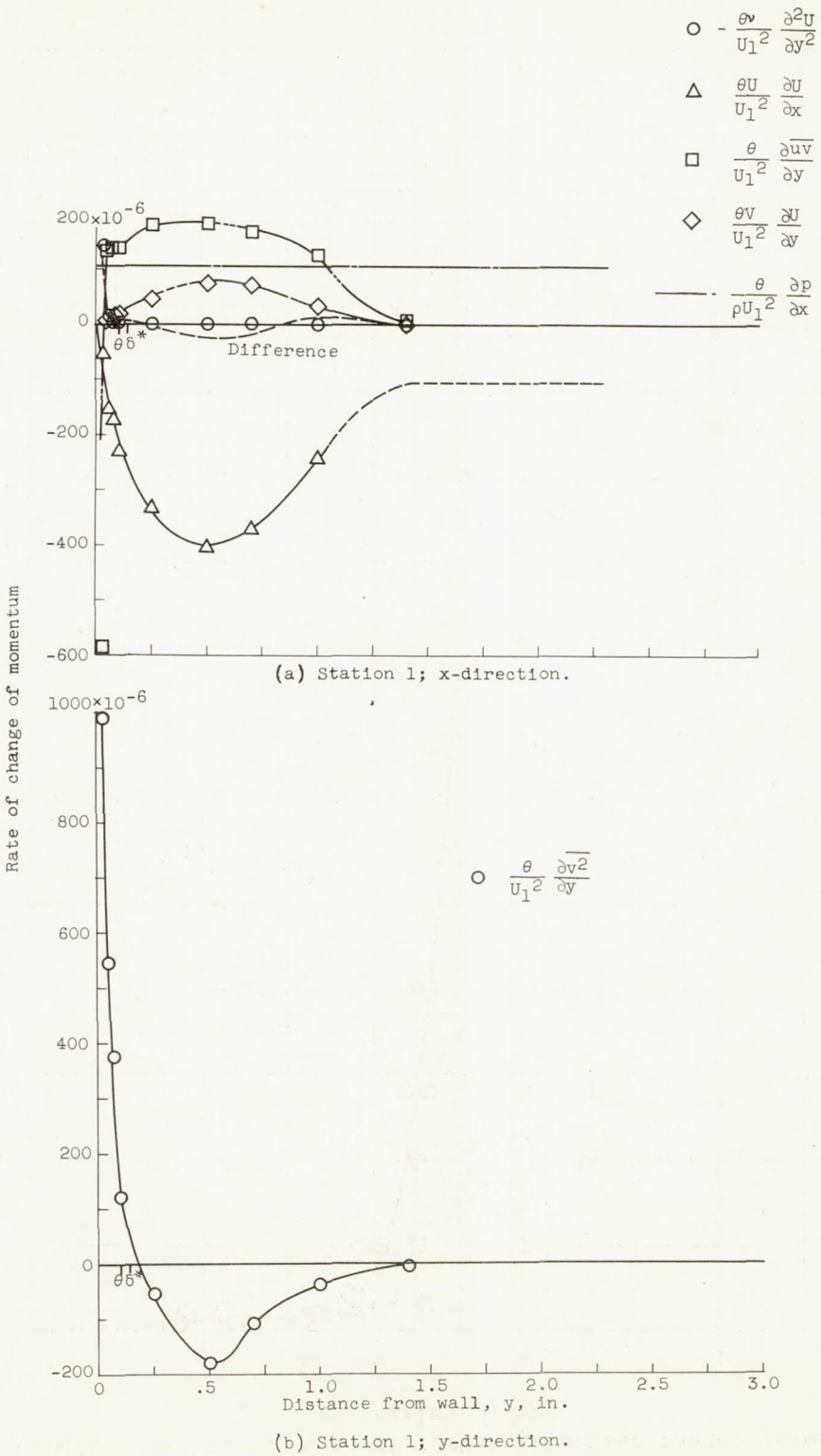

Figure 26. - Distribution of momentum terms through boundary layer.

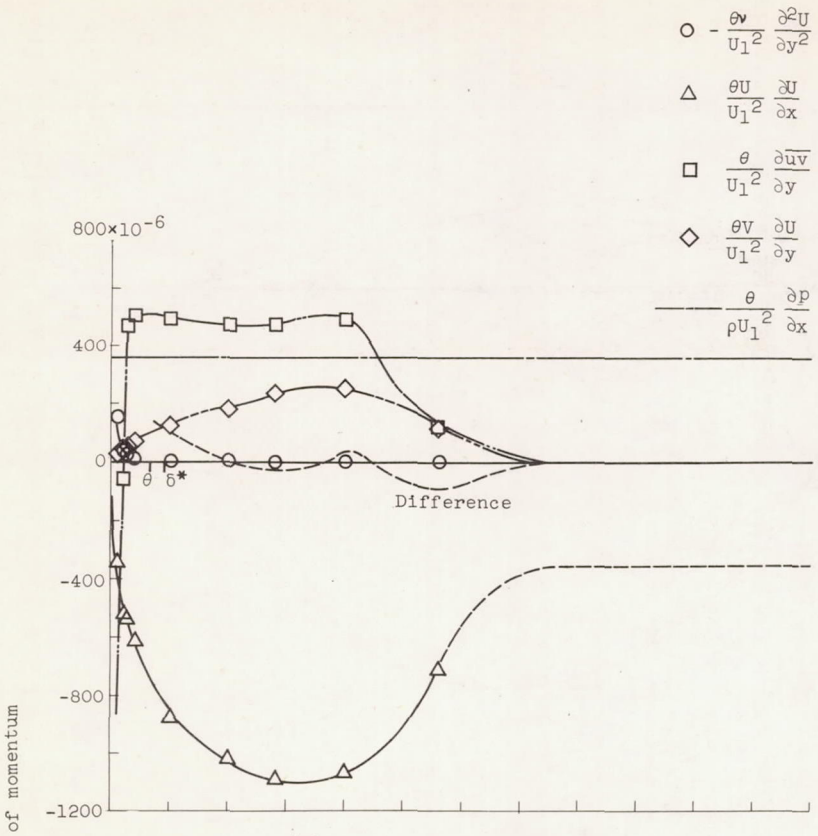

(c) Station 2; x-direction.

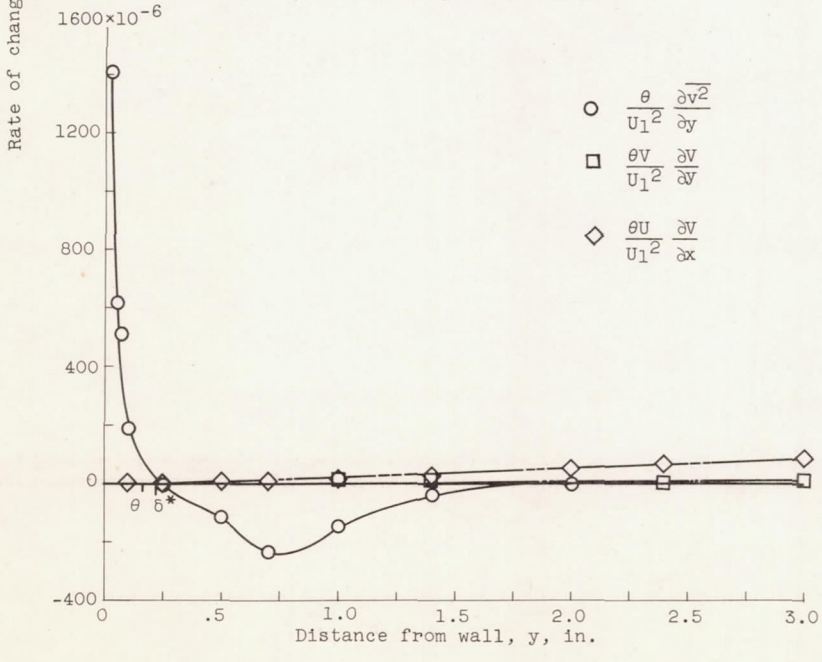

(d) Station 2; y-direction.

Figure 26. - Continued. Distribution of momentum terms through boundary layer.

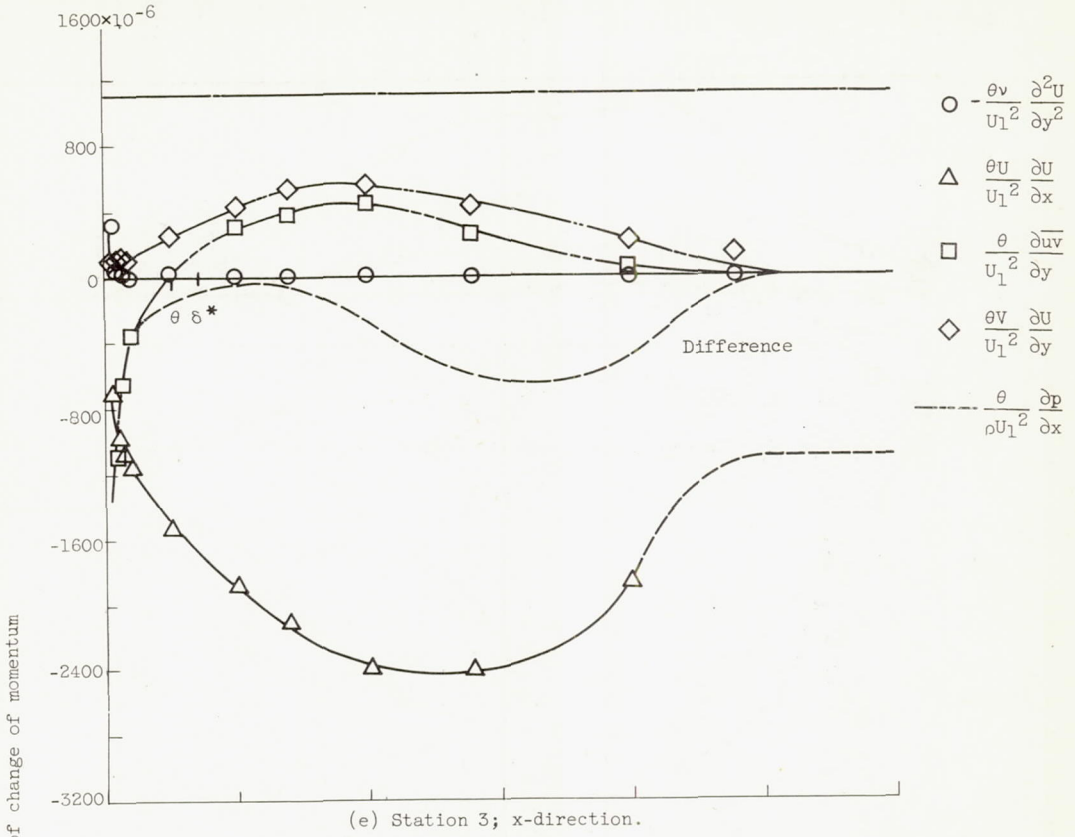

(e) Station 3; x-direction.

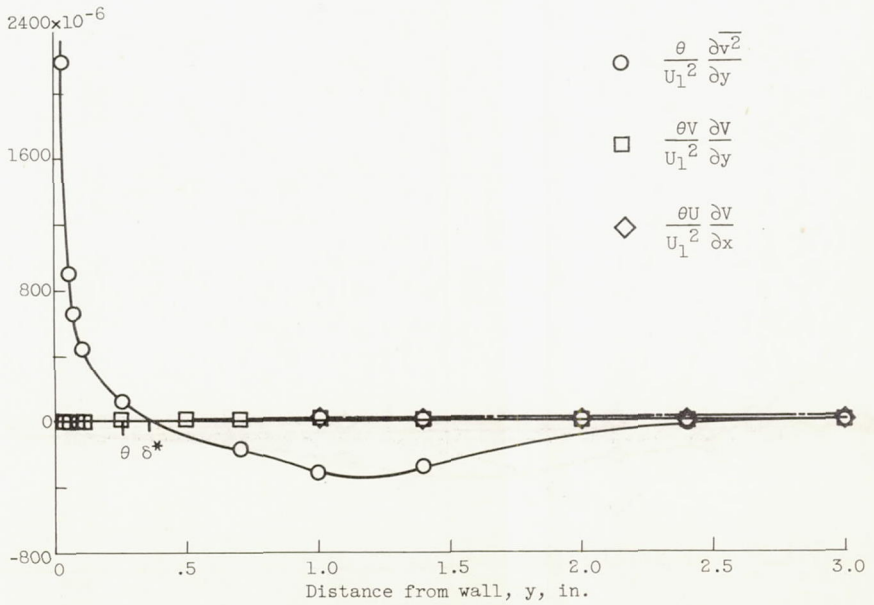

(f) Station 3; y-direction.

Figure 26. - Continued. Distribution of momentum terms through boundary layer.

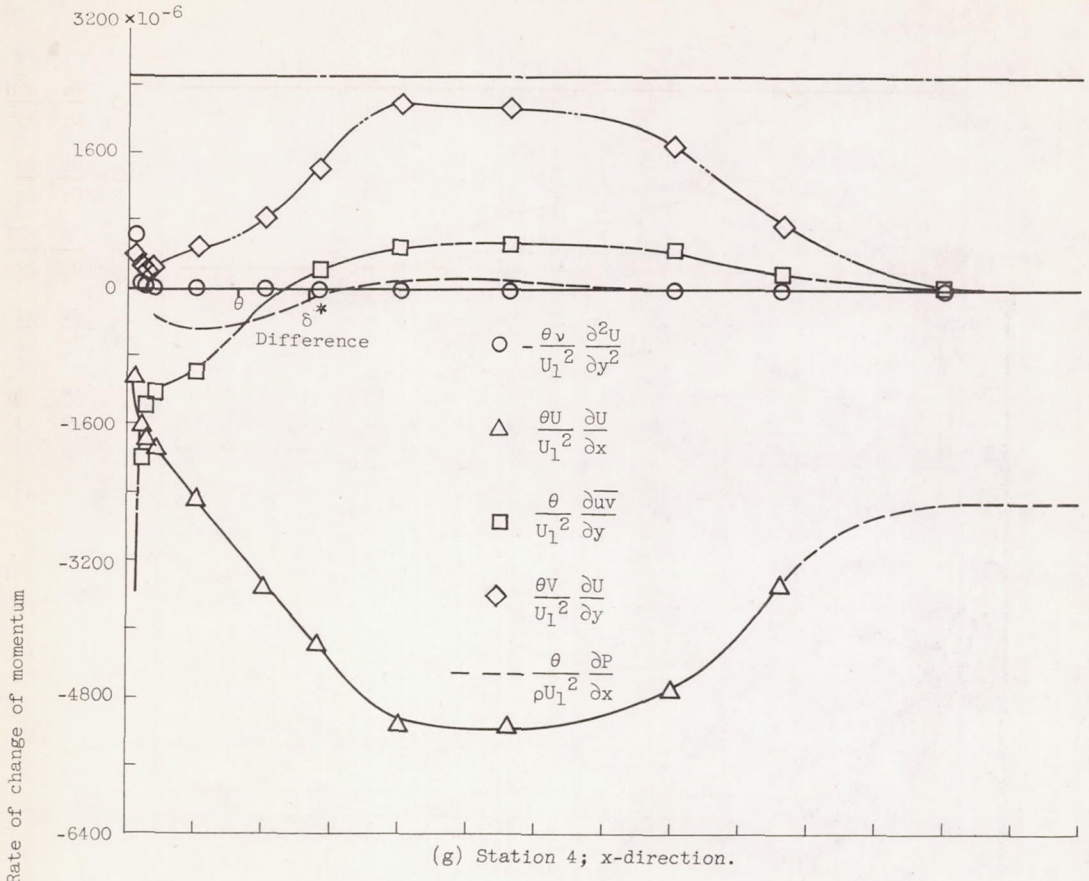

(g) Station 4; x-direction.

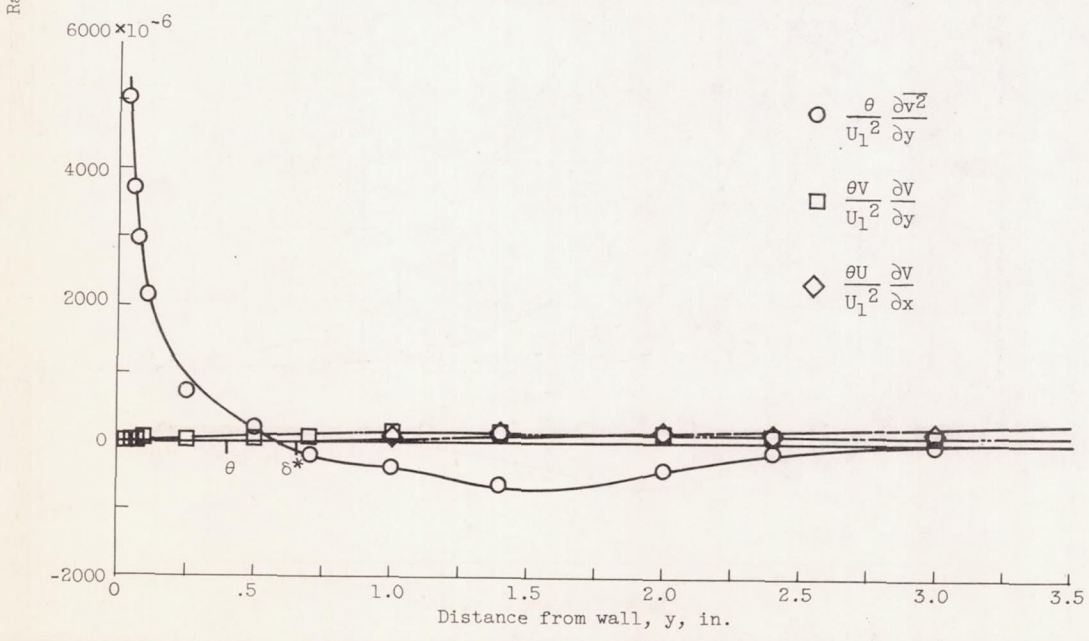

(h) Station 4; y-direction.

Figure 26. - Concluded. Distribution of momentum terms through boundary layer.

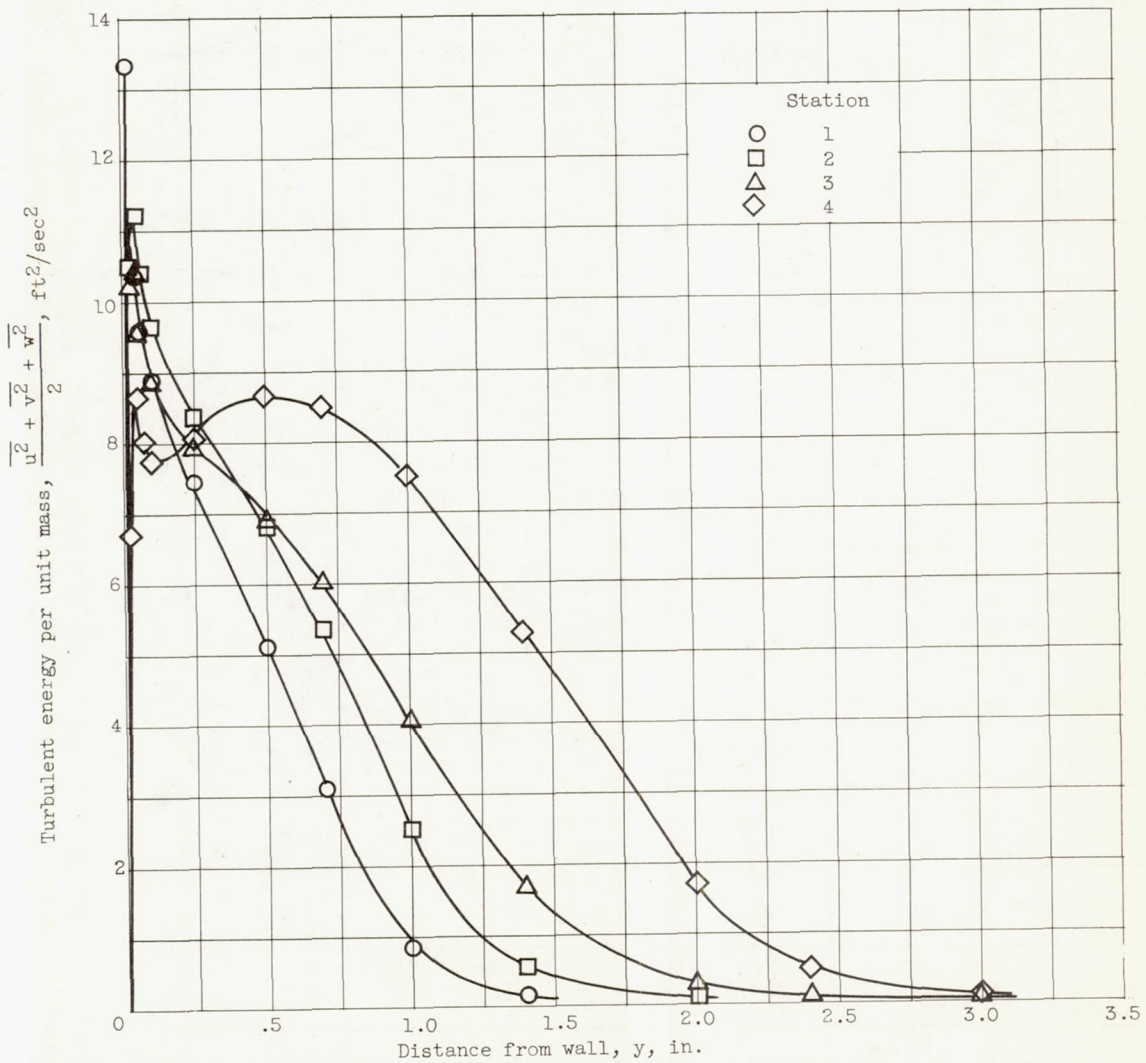

Figure 27. - Turbulent energy distribution through boundary layer.

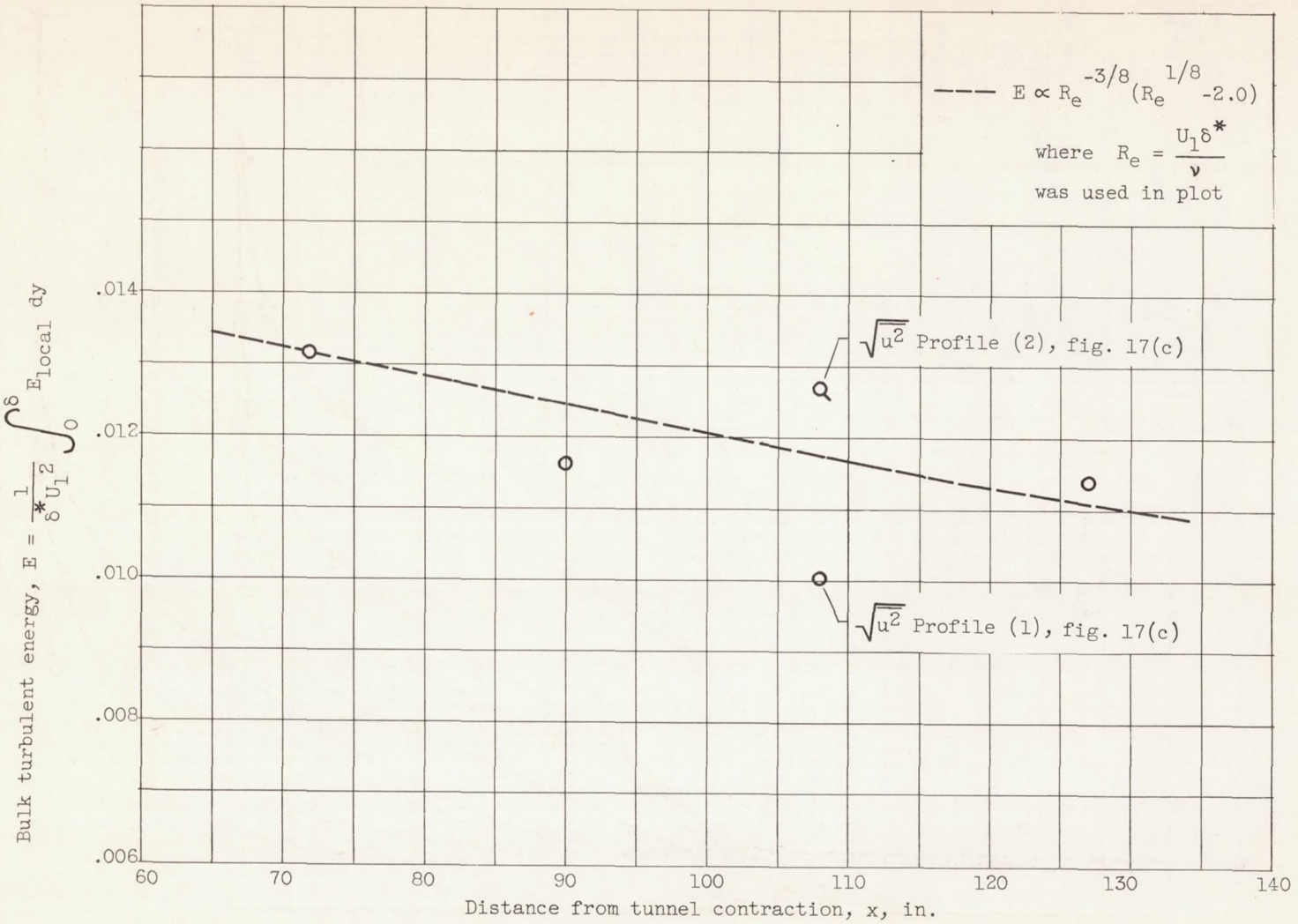

Figure 28. - Variation of bulk turbulent energy along test wall compared with prediction of Corrsin for a fully developed channel flow.

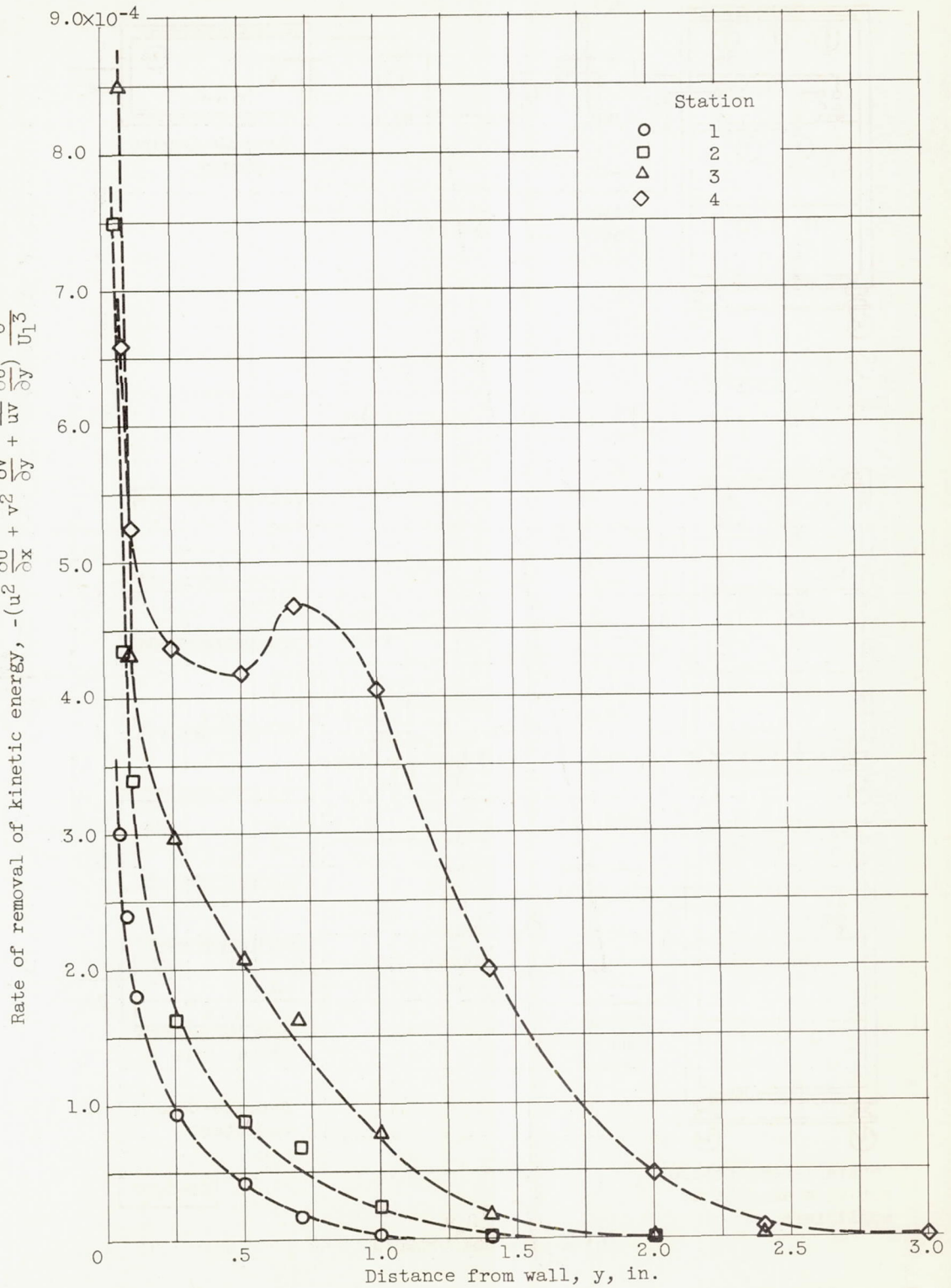

Figure 29. - Rate at which kinetic energy of mean flow is transformed into turbulent kinetic energy.

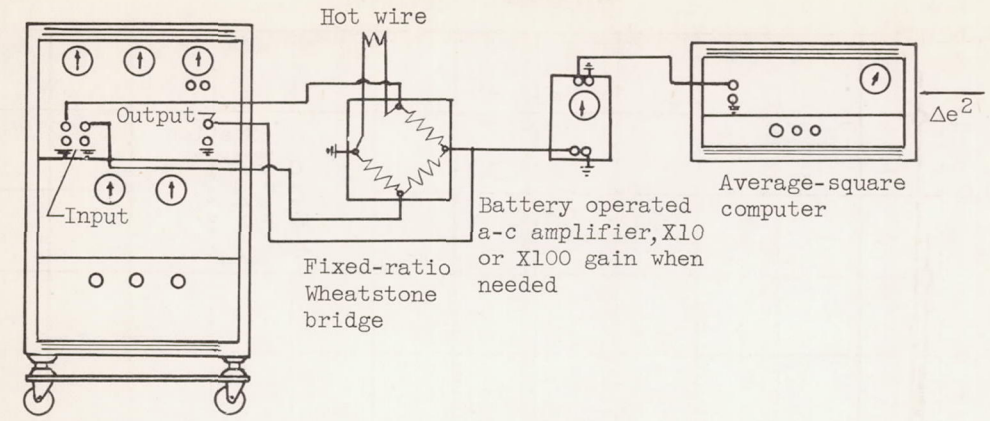

(a) $\sqrt{\overline{u^2}}$ Measurement.

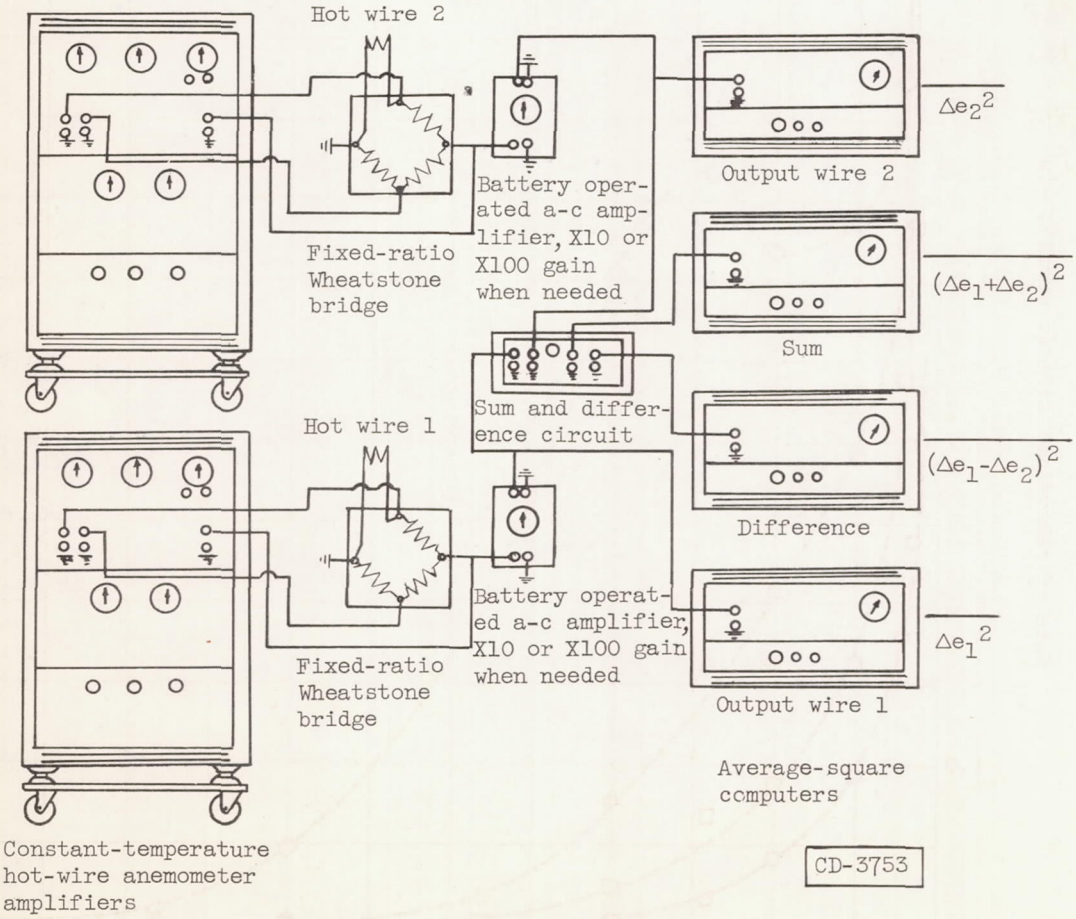

(b) X-wire measurments.

Figure 30. - Block diagram of instrumentation hookup. All connecting cables are of the coaxial type.